Material properties and cover options using HYDRUS (2D/3D) for a large undrained sand tailings dam in northern Alberta, Canada

by

Marie Laura Goddard

Southwest Sands Storage facility on September 1, 2009. (Google Earth)

A thesis presented to Universiteit Utrecht in partial fulfillment of the requirements for the degree Masters of Geoscience

37.5 ECTS

External Supervisor: Carl Mendoza, University of Alberta

Internal Supervisor: Majid Hassanizadeh, Universiteit Utrecht

Faculty of Geosciences

Earth Surface and Water, Hydrology

Utrecht, The Kingdom of the Netherlands

August 2017

Universiteit Utrecht

UNIVERSITY OF ALBERTA

EDMONTON·ALBERTA·CANADA

Statement of originality of the MSc thesis

I declare that:

1. this is an original report, which is entirely my own work,

2. where I have made use of the ideas of other writers, I have acknowledged the source in all instances,

3. where I have used any diagram or visuals I have acknowledged the source in all instances,

4. this report has not and will not be submitted elsewhere for academic assessment in any other academic course.

Student data:

Name: Marie Laura Goddard

Registration number: 4258797

Date: August 21, 2017

Signature: 

ABSTRACT

A flow and transport model was built to simulate the Southwest Sands Storage facility, which is a large oil sands tailings dam and impoundment located on the Mildred Lake oil sands lease in northern Alberta, Canada. Studying the flushing behavior and advancing the material characterization was achieved by building a two-dimensional cross section of 3000 m long and 40 m high (approx. 58,500 m^2 in area) using HYDRUS (2D/3D). Building upon more than a decade's worth of data and work by others, this study synthesised the existing material characteristics, corroborated and refined them, and performed future simulations.

The use of a variable (transient) boundary condition was invaluable to gaining insights into the material characteristics of oil sands tailings; a unique material. The horizontal hydraulic conductivity ranged between 0.137 m/d to 1.27 m/d and the anisotropy ratio was restrained between 1 and 20, in line with reference values. The porosity ranged between 0.35 and 0.40 which was also inline with previous works. The residual saturation ranged between 0.13 and 0.2 which was double to triple the reference values, however an evaluation of the reference Soil Water Characteristics Charts revealed curves without distinct inflection points and therefore difficult to determine a precise residual saturation value. These tailings curves start to break between 0.05 and 0.15 then gradually decline with increasing suction. The van Genuchten unsaturated parameters (alpha = 1.24, n = 1.7) were unique in comparison to those in the agricultural soils databases but within the range of previously reported values for dyke and tailings sand.

The parallel use of both a constant and a variable water flux boundary condition allowed for comparison of the future simulation results, which were of high fidelity. Under the as-is scenario (Future I) the TDS concentration of the dam will be greater than 1000 mg/L until around 2075, but because of the presence of the pond, two-thirds of the model section does not attenuate. Future simulations with remedial covers and landscaping (Futures II and III) had more holistic TDS attenuation distributions with dilution proportional to the amount of recharge. However, even the most restrictive recharge produces TDS concentrations of less than 1000 mg/L at the perimeter ditch after about 60 years due to the local flow system on Benches B and A and the influence of the Toe C ditch.

Recharge rates are very important to reclamation success with topography and vegetation playing key roles. The competition for precipitation, which averages between 450 mm and 500 mm per year, in an area with high evaporation rates, means that the ideal cover should capture and transmit as much precipitation as possible. The transmissivity of the cover will be key to meeting the specific remedial goals and timelines.

Table of Contents

List of Figures

List of Tables

List of Photographs

List of Charts

1. INTRODUCTION

The Athabasca oil sands are an important source of crude oil and a key driver of the Alberta and Canadian economies. Canada ranks as the world's fifth largest oil producer and has the world's third largest oil reserves (173 billion barrels) with the oil sands comprising approximately 97 % of those reserves (CAPP, 2015). The oil sands deposits are located in northern and central Alberta and are exploited in three ways (depending upon the thickness of the overburden and the bitumen viscosity): open-pit mined; in-situ extraction with Steam Assisted Gravity Drainage (SAGD); and traditional wells fitted with screw pumps. Approximately 3 % of the deposits are accessible near the surface (Alberta Government) and open-pit mining has been the dominant process since commercial production started in 1967, however in-situ production has now overtaken mining production. In 2016, open-pit mining produced 1.1 million barrels per day and in-situ produced 1.3 million barrels per day (CAPP, 2017).

Oil sands are strip mined using the truck-and-shovel method as the first step in a process involving both physical (steam, tumblers, screens, crushers) and chemical (caustic soda) methods to separate the bitumen from the host sands (Fig. 1) (Syncrude, 2008; Chalaturnyk et al., 2002).

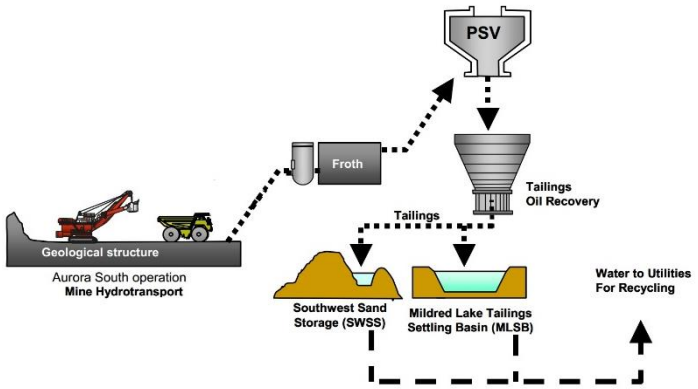

Figure 1**.** Simplified oil sands mining process flow diagram, Syncrude (2010). (PSV – Primary Separation Vessel)

Strip mining of oil sands results in a high waste to oil ratio and is a large consumer of water. For every 0.16 m^3 (1 barrel) of oil produced, about 1 m^3 of sand and 0.25 m^3 of Mature Fine Tailings[1] (MFT) are also produced (Beier et al., 2008). In addition, the total volume of tailings (solids plus water) can be 40 % greater than the volume of mined raw product (Chalaturnyk et al., 2002). Bitumen extraction is also a water intensive process using about 1.9 m^3 (12 barrels) of water[2] for every 0.16 m^3 (1 barrel) of oil, hence for environmental reasons as much process water is recovered and recycled as possible (approx. 75 %) with the remainder (approx. 25 %) entrained within the waste stream (Kasperski and Mikula, 2011). To aid in breaking the bonds between the oil and the solids, sodium hydroxide[3] (NaOH) is added to the hot wash

[1] Fine tailings (water and suspended clay) that have separated into a sediment layer of clay and silt and an upper layer of clarified water (Alberta Energy). Fine tailings are defined to contain particles less than 44 µm in size (Syncrude, 2010).
[2] A mix of fresh and recycled water. Fresh water withdrawals from the Athabasca River are approx. 2 m^3 per 1 m^3 of produced oil (Syncrude, 2017).
[3] Also called caustic soda.

water (Chalaturnyk et al., 2002). The process spoils are piped as a slurry to constructed facilities for settling and eventual long-term storage within a reclaimed landscape. Given the large scale of the mining operations, along with the above described expansion factor and water entrainment, these storage faculties are large features on the landscape. As of 2010, there was a total of around 840 million m^3 of fine tailings that required long term containment, and approximately 170 km^2 of tailings ponds (ERCB, 2010). To put this in perspective, this volume of fine tailings would cover Sea Island, Richmond[4] (location of Vancouver International Airport) to a depth of about 55 m, and the areal extent of the ponds are the same as the City of Regina, Saskatchewan or Salt Spring Island, British Columbia.

These facilities are regulated by provincial authorities who have mandated that the land be reclaimed to a "resilient and functional boreal forest ecosystem" (Alberta Environment and Parks, 2017, p. 7). As these facilities will exist on the landscape for millennia or longer, it is important that the reclamation be self-sustaining with limited risks to human health or the environment. For the purposes of this thesis, the risks can be simplified into two associated types: physical; and chemical. The physical risks are addressed with sound engineering and construction practices that reduce the likelihood of structural integrity problems (slope failure and/or mass movement). The depth of the water table is an example of a physical risk. The chemical risks are based on the properties of the contents (chemical elements, state, concentration, toxicity) of the facility, how they interact with each other, how they migrate within the facility, and minimizing their impacts if/when discharged into the environment. The discharge of groundwater with elevated sodium concentrations is an example of a chemical risk.

The Southwest Sands Storage (SWSS) facility is an oil sands storage facility built by Syncrude Canada Ltd. (Syncrude) to serve its Mildred Lake operations. The practice of recycling the process water has led to a tripling of the Total Dissolved Solids (TDS) concentrations since the facility became operational in the early 1990's. Analyses of the water in 2012 reported a TDS concentration of 5700 g/m^3 (ppm) (Syncrude, 2012) which classifies it as brackish and not suitable for human consumption nor agricultural use[5]. This raises questions about the impacts this water will have on the reclamation efforts, specifically the rate of TDS discharge, in the near and long terms. Research to answer these questions has been ongoing for over a decade and this thesis is a continuum of those works.

1.1 Objectives

The main goal of this research was to advance the numerical modelling begun by McKenna (2002) and expanded upon by Price (2005) for the SWSS. Specifically, the research goals were to:

- Refine and advance the material characteristics of tailings sand
- Determine TDS flushing times and loading rates
- Predict the future TDS distribution
- Evaluate the impact of reduced recharge covers
- Evaluate the impact of remedial topography

[4] Areal extent of approx. 15 km^2
[5] Limit of 500 g/m^3 TDS concentration (Alberta Environment and Parks, 2016).

These objectives were accomplished by employing the software package HYDRUS (2D/3D) (HYDRUS, 2017), which simulates water, heat, and solute movement in variably saturated media in either two or three-dimensions. For this project, the water flow and solute transport modules were employed in a two-dimensional cross-section with unsaturated and saturated soils. The starting point for the model was the condition in the year 2003, with the subsequent seven years of field data (until 2009) used to evaluate and calibrate the model. While additional data were available for the year 2010 and beyond, they were not used because the installation of perimeter drains in 2010 caused a decline and stabilization of the water-table. The simulation of the drained scenario was outside the scope of this project.

1.2 Thesis Outline

The current chapter introduces the research subject, its provenance, and the objectives of this thesis. Chapter 2 acquaints the reader with the research site including a detailed account of the previous research. Chapter 3 presents the conceptual models for flow and solute transport, which sets the scene for the numerical model presented in Chapter 4. The model calibration and sensitivity analysis, are detailed in Chapter 5 leading up to its employment in predictive simulations detailed in Chapter 6. Finally, Chapter 7 rounds out the thesis with the discussion, followed by Chapter 8 with the conclusions and recommendations for future research. In addition to these seven chapters, there are eight appendices (A through H) which present additional background data, precipitation records, groundwater calibration charts, additional sensitivity analyses information, future simulation data tables and figures, and a piezometer location plan with labelled photographs. This last attachment (Appendix H) nicely illustrates the vegetation, bare tailings, and topography.

2. RESEARCH SITE BACKGROUND

2.1 Location and Dimensions

The study site (56°58', 111°45') was located approximately 40 km northwest of the town of Fort McMurray, Alberta in the southwest corner of Syncrude Mildred Lake oil sands lease (Fig. 2). As of 2008, the Southwest Sand Storage (SWSS) facility stored about 390 Mm^3 of tailings and 60 Mm^3 of fluids (450 Mm^3 in total) and had a footprint of approximately 23 km^2 (Syncrude, 2008). It was approximately four kilometres wide (east-west), seven kilometres long (north-south), up to 40 m high and contained a central impoundment referred to as a tailings pond.

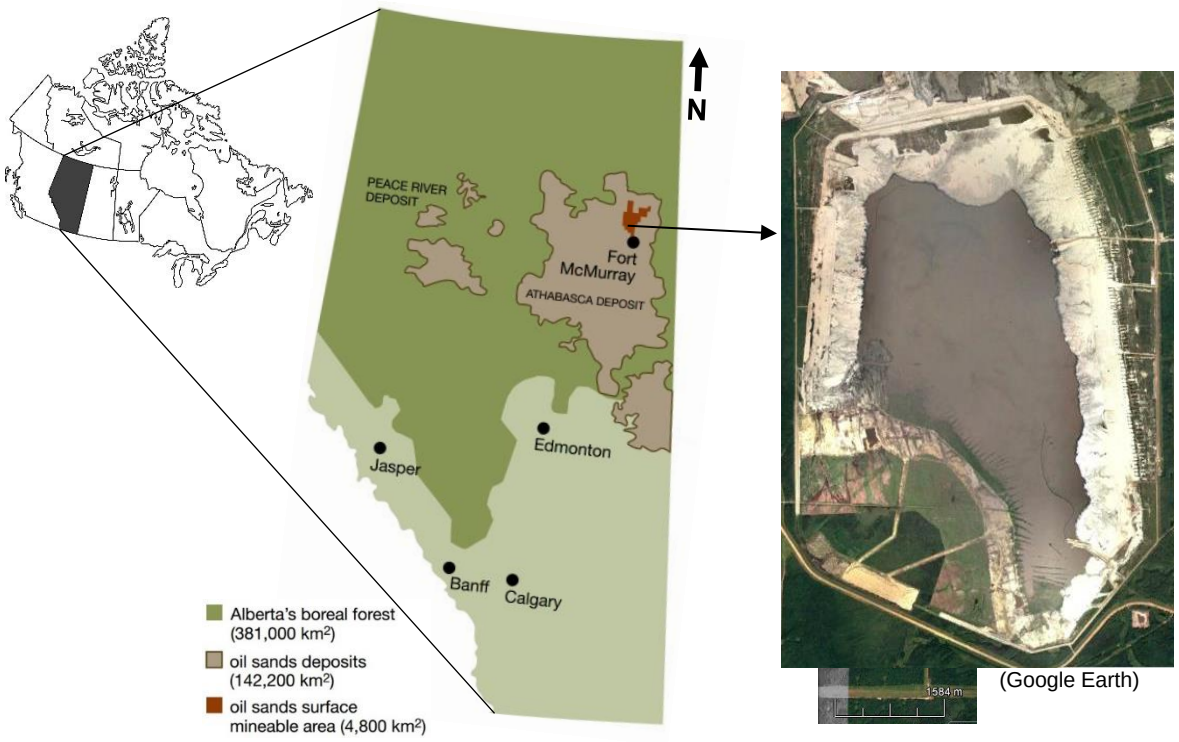

(modified from Government of Alberta, 2016)

Figure 2. Location of Southwest Sand Storage facility in Alberta, Canada.

2.2 Tailings Material Properties

The tailings are what remains after the valuable bitumen has been stripped from the host sand. The reservoir facies of the host formation (McMurray Formation) are coastal plain fluvial-estuarine and estuarine channel complex deposits which are composed of unconsolidated micaceous, fine to medium grained sands, silts, and clays (Hein et al., 2000). The petroleum migrated into the McMurray Formation around 112 ± 5.3 million years ago (Lower Cretaceous Epoch, Aptian and Albian Ages), from older downdip (south to southwest) deposits shortly after deposition (Selby and Creaser, 2005). Barson et al. (2000) inferred that this filling of the reservoir impeded the cementation process leading to its unconsolidated nature and that the original petroleum was microbially degraded during the late stage of migration and/or after emplacement due to its proximity and outcropping at the ground surface.

The SWSS tailings slurry was composed of about 55 weight percent (wt %) solid materials (Chalaturnyk et al., 2002) of which 81 wt % is sand, 10 wt % is silt, 4.4 wt % is clay and 0.5 wt

% is bitumen (Table 1) (McKenna, 2001). The sand is mostly fine-grained sand with a d_{50} of 150-200 µm and is composed almost entirely of quartz (McKenna, 2002). The weight percent of the finer fractions is highly variable ranging from 100 % to 180 % (McKenna, 2001). The properties of the silt and clay fractions have been a topic of extensive research for many decades as the clay water slurry flocculates poorly resulting in suspended fines which can delay consolidation and water release (Chalaturnyk et al., 2002). This behavior makes this material unique and interesting to study.

Table 1**.** Material properties of tailings by weight percent (wt %) (McKenna, 2001). (CV - Coefficient of Variation).

Sand	Silt	Clay	Bitumen
81	10	4.4	0.5
CV 20	CV 100	CV 180	CV 150

2.3 Geology, Depositional History, and Reclamation Efforts

Construction of the facility began in 1991 with two parallel starter dykes in the northeast corner, between which tailings were piped to form the main dam (Price, 2005; Liggett, 2004). The facility was extended over time into 21 operational areas, called Cells (numbered 31 through 51) into the current footprint (Fig. 3) (Liggett, 2004). The facility grew most significantly between 1991 and 2003, such that at the end of 2003 it held approximately 285 Mm^3 of solid materials and 120 Mm^3 of water (Chart 1), for a total of 405 Mm^3. After 2003, deposition volumes were reduced, such that for the purposes of this study, the configuration of the pond, beach, and dam were considered to be static.

Chart 1**.** Annual and cumulative sand and net water deposited 1991 to 2003 (modified from Liggett, 2004)

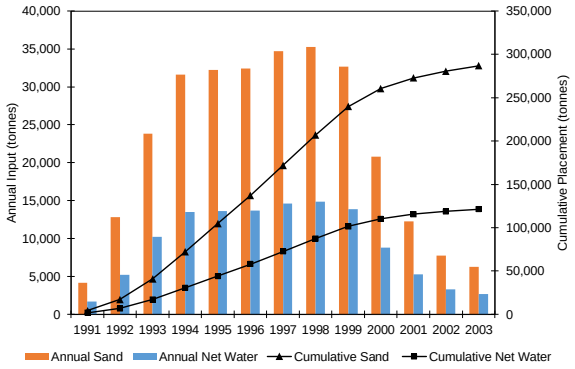

Chart 2**.** Annual TDS of tailings water 1991 to 2002 (Liggett, 2004)

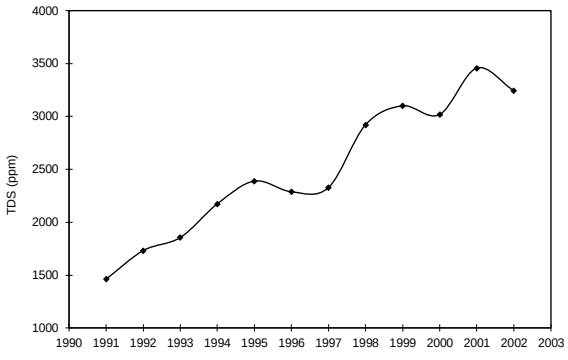

The slurry was deposited via three pipelines which were moved periodically to evenly distribute the tailings. The sands fell out of suspension first and were reworked with heavy equipment to construct the series of dykes, slopes, and benches. The dam was built with a shallow slope (20H: 1V), as measured from the perimeter ditch to the highest point, in a series of benches and slopes named A through E (Fig. 4). Individually, the Slopes range between 5 % to 6 % incline, and Bench C also slopes outwards (approx. 2 % tilt) to mitigate ponding of water (Price, 2005). Both Benches A and B were constructed with inward sloping surfaces (< 1 %) and water collecting berm channels at the bench/slope boundaries (Price, 2005). The excess

material was discharged behind the highest point of the dam, forming the beach area. The finer particles (MFT) migrated towards the central pond as they took longer to settle out of suspension than the sands (Price, 2005).

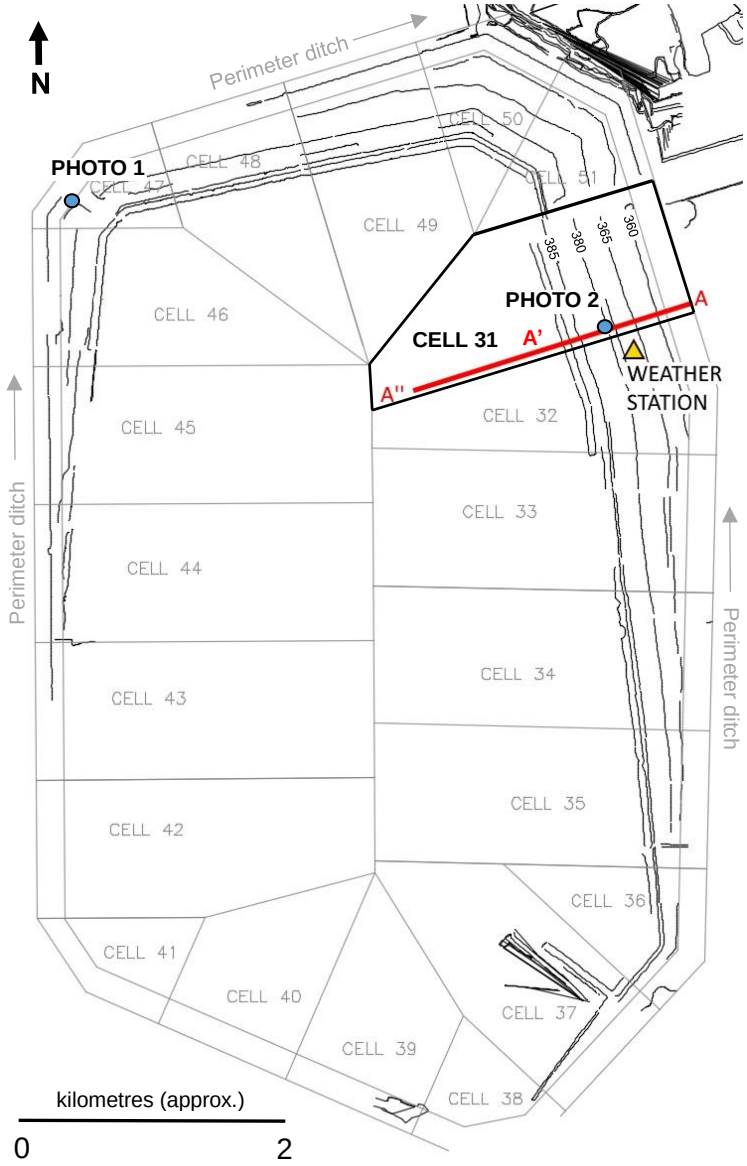

Figure 3**.** SWSS cell configuration and elevation contours showing locations of cross-section A'' to A and A' to A (red line), weather station (yellow triangle), Photographs 1 and 2 (blue dots), perimeter ditch and flow direction. (modified from Syncrude).

The original ground surface beneath the SWSS gently slopes towards the northeast and consists of Pleistocene glacial till and lacustrine deposits and Clearwater Formation shales (Fig. 4) (Price, 2005). The hydraulic conductivity of these units are two to three orders of magnitude lower than the tailings sand (Price, 2005; Esford, 2003; Klohn Leonoff, 1990).

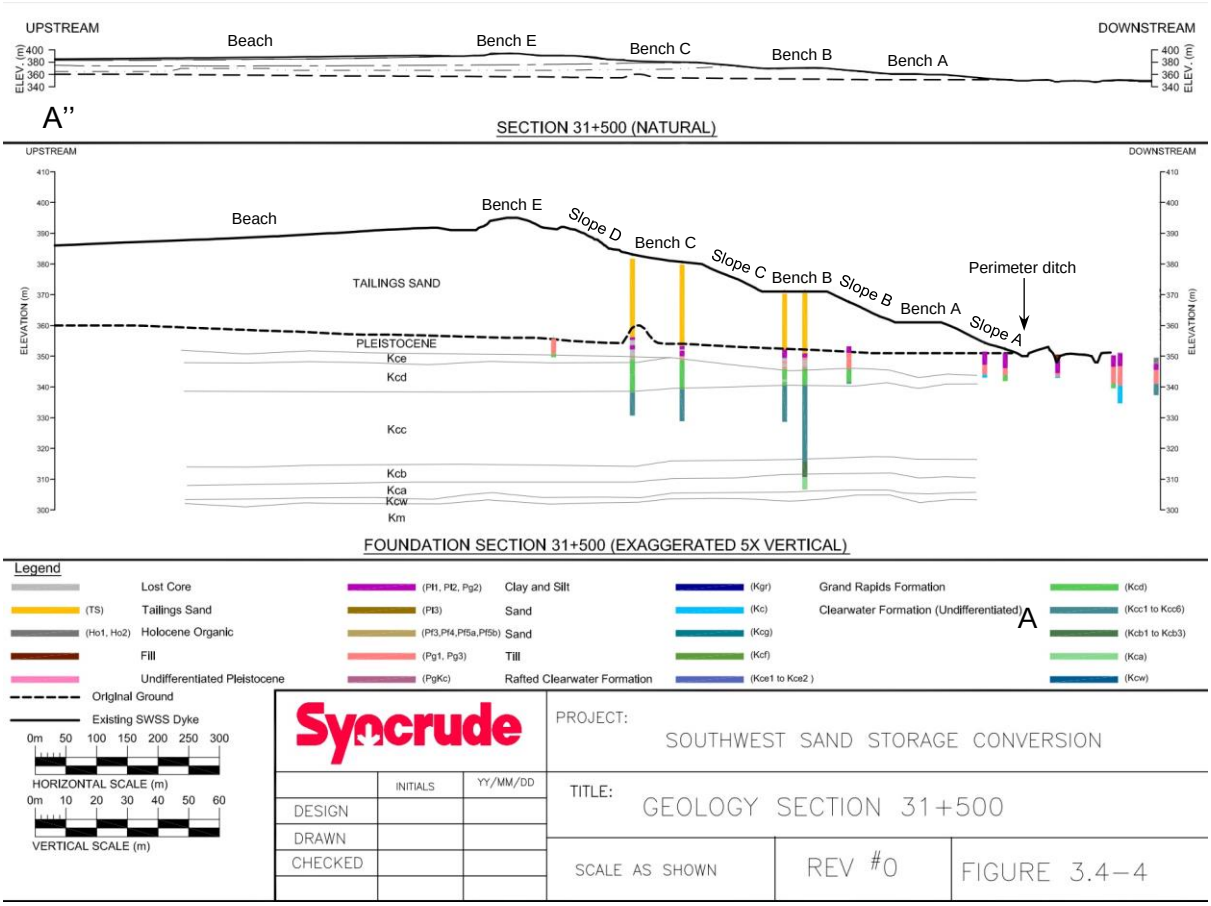

Figure 4**.** Cell 31 geological cross-section A'' to A, natural and 5x vertical exaggeration (modified from Syncrude, 2008).

The water level in the pond was kept to a depth of one to three metres via a decant dredge which transfers fluids to a nearby storage facility for eventual recirculation. Runoff was collected in a perimeter ditch and was also recycled. This recycling of this process water has, over the years, led to an increase in the concentration of salts (reported as TDS concentration) from about 1500 g/m^3 [6] in 1991 to approximately 3200 g/m^3 in 2002 (Chart 2). Recent porewater TDS concentrations collected from the fine tailings beneath the pond at around 380 m elevation (circa 2001 dam ground surface) were 5000 g/m^3 in 2011, 5700 g/m^3 in 2012 and 4500 g/m^3 in 2013 (Syncrude, 2011, 2012, 2013).

The TDS concentration of the seepage water[7] within the perimeter ditch has doubled over a 17-year period from 1300 g/m^3 in 1996 to 2700 g/m^3 in 2013, with intermittent peaks of around 4000 g/m^3 in 2003, 2010 and 2011 (Syncrude, 2013).

Photograph 1 taken circa 1995 shows the western dam face mid-construction, with the beach and pond behind it. Photograph 2 illustrates the drilling at GW11 cluster of monitoring wells on Slope C (Price, 2005) which shows the shallow slope of the dam face. Additional photographs of the landscape are appended to the Piezometer Location Plan (Appendix H).

[6] g/m^3 = ppm = mg/L

[7] Definition: seepage water – groundwater that leaves the facility by a slow rate of discharge along a seepage face (and in this specific case the water that accumulates in the perimeter ditch).

Photograph 1. Aerial view of SWSS looking south along western flank circa 1995 showing Slopes/Benches C and D (McKenna, 2002)

Photograph 2**.** Drilling at monitoring wells GW11 on crest of Bench C in 2002, looking west towards perimeter road (tree line ~625 m distance) (Price, 2005)

Reclamation efforts began in 1995 by applying a cover onto the slopes and benches of A and B. The cover material ranged in thickness from around 50 cm to around 105 cm and was a mixture of peat and mineral materials salvaged locally during overburden stripping (Naeth et al, 2010). The reclaimed areas were planted with a mix of grasses and deciduous shrubs on the benches and coniferous and deciduous trees on the slopes (C. Mendoza, pers. comm.; Price, 2005). The closure goal is to reclaim the SWSS to an equivalent landscape capability, however there are several challenges with oil sand tailings revegetation efforts such as: highly soluble sodium concentrations; low water storage capacity; high erosion potential; nutrient poor; and the absence of organic matter and microbes (Fung and Macyk, 2000). A study by Burgers (2005) on the neighbouring Cell 32 indicated that sodicity, soil nutrient deficiencies, and a thin cover were affecting revegetation success.

2.4 Climate and Ecosystem

The climate is sub-humid continental characterized by short warm summers, long cold winters, low precipitation and high potential evapotranspiration. Specifically;

- The frost-free period ranges from 105 days to 115 days over the months of June, July and August (Alberta Agriculture and Forestry)
- The mean daily temperature in January is -18°C and in June is 16°C (Carey, 2008)
- The mean annual precipitation (1971 to 2000) is 0.453 m (Environment Canada); general range of 0.450 m to 0.500 m (Alberta Environment and Parks)
- The annual precipitation range (1944 to 2007) is a low of 0.240 m in 1998 to a high of 0.675 m in 1973 (Environment Canada)
- Snow melt accounts for about one quarter to one third of the total precipitation (Carey, 2008; Carrera-Hernandes et al, 2011)
- The total annual potential evapotranspiration ranges from 0.450 mm to 0.550 m (Webster et al., 2015)
- Evapotranspiration was measured using the eddy covariance method at the weather station in neighbouring Cell 32 (Fig. 3, Photos 3 to 6) in 2005 and 2006 between the months of May and September (Carey, 2008). The data indicated that an average of 0.325 m of water per year was lost to the atmosphere at this location on Bench B, representing 88 % of the annual averaged total precipitation (0.369 m).

- Snow melts over a short period of less than ten days in April (C. Mendoza, pers. comm.)

The climate is characterized by pronounced seasonal and decadal wet and dry cycles which in combination with the geology have led to a unique ecosystem where runoff is minimal and the water balance is driven by storage (Devito et al, 2012).

The SWSS is located on the western Boreal Plains with the vegetation consisting of coniferous trees (black and white spruce, jack pine, balsam fir, tamarack) and deciduous trees (trembling aspen, balsam poplar, birch)) along with grasslands in drier areas (Brandt et al, 2013). Stands of trees are interspersed with wetlands and peatlands (Webster et al, 2015).

A weather station was installed during the summer of 2001 on Cell 32, on Bench B (455535.00 E, 6316771.00 N) approximately 200 m south of monitoring well GW08-3. A snow depth sensor was added in October 2007. Photographs 3 to 6 show the weather station apparatus and the surrounding vegetation throughout all four seasons between 2001 and 2010.

Photograph 3**.** Bench B in winter looking east. November 9, 2001 (Syncrude)

Photograph 4**.** Bench B in spring looking northeast. May 1, 2006 (Syncrude)

Photograph 5**.** Bench B in summer looking northwest (up at Slope C). August 8, 2006 (Syncrude)

Photograph 6**.** Bench B in autumn looking northwest. September 27, 2010 (Syncrude)

2.5 Previous Research

This study is built upon a large volume of work by four authors whose publications have provided field data for material properties and model calibration (Table 2).

Table 2**.** Summary of previous works

Author	Date	Report Title	Facility	Type	Relevance
Grace Hunter	2001	Investigation of groundwater flow within an oil sand tailings impoundment and environmental implications	Tar Island Dyke and Pond 1*	MSc. Thesis University of Waterloo	Material properties
Gordon McKenna	2002	Sustainable mine reclamation and landscape engineering	SWSS, MLSB	PhD. Thesis University of Alberta	Geostatistical analyses of SWSS tailings; material properties
Jessica Liggett	2004	Water and salt budgets for a sand tailings dam	SWSS	BSc. thesis University of Alberta	Perimeter ditch seepage rates; TDS of annual layers
Adrienne Price	2005	Evaluation of groundwater flow and salt transport within an undrained tailings sand dam	SWSS	MSc. Thesis University of Alberta	Foundation works and instrumentation; key field data

* Located approx. 20 km east of the SWSS on Suncor main mine lease. MLSB – Mildred Lake Tailings Settling Basin

Hunter (2001) studied Tar Island Dyke and Pond 1, another oil sands tailings storage facility located approximately 20 km east of the SWSS, to identify potential contaminant pathways from the facility to the adjacent receiving environment (Athabasca River). This facility stores tailings mined from the same geological formation as the tailings within the SWSS and therefore has a similar material composition as the SWSS with minor differences due to age (it's older) and management (processes and methods). For this reason, the material properties values from Hunter were used as references for the material properties in this study, in particular residual saturation and the unsaturated parameters alpha and n.

McKenna (2002) performed a seepage analyses for Cell 31 using SEEP/W (Geo-slope International Limited, 1998) and calculated a discharge rate of 0.16 m^3/m/d at the perimeter ditch using the following parameters: a single homogenous tailings deposit with a horizontal hydraulic conductivity (K_h) of 0.6912 m/d; a ratio of horizontal hydraulic conductivity to vertical hydraulic conductivity (K_v) (K_h/K_v) of 1/16 (0.0625); a steady state boundary condition 0.090 m/y recharge on the slopes and 0.180 m/y recharge on the beach; and a groundwater divide approximately 500 m down beach.

The Liggett (2004) thesis provided groundwater seepage rates at the toe of the dam (at the perimeter ditch) which were valuable for calibration of the model. Her work also included conceptual diagrams for flow and solute transport which were modified and advanced during this study.

Price (2005) undertook a field campaign in 2002 and 2003 to install instrumentation along transect A' to A[8] in Cell 31 and collect data needed to calibrate a numerical model. This included the construction of: 66 groundwater monitoring wells (at 14 locations); 10 shallow piezometers in the ditches and near the perimeter ditch; staff gauges in the perimeter ditch and at the toes of slopes (Fig. 5, Appendix H). Further work included: the collection and analyses of groundwater from these wells; the measurement of groundwater elevations; slug testing; and seepage measurements at the perimeter ditch. Several rounds of measuring and sampling were performed in 2002 and 2003 to characterize the groundwater. Readers are directed to Price's thesis for details on field methodologies and site characterization.

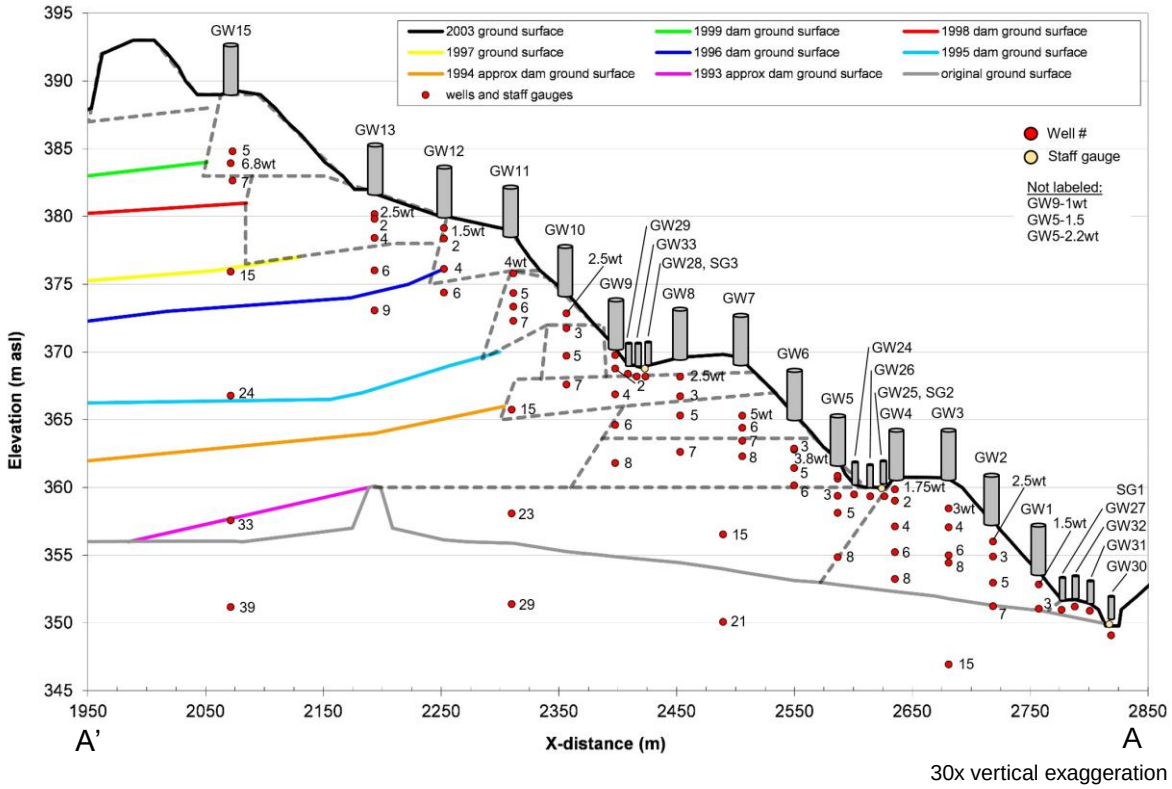

Figure 5. Dam cross-section A' to A illustrating cells, annual layers (1993 to 2003) and monitoring well and staff gauge locations (modified from Price, 2005).

Price (2005) constructed a steady-state numerical flow and transport model with a constant flux boundary using GEO-SLOPE's SEEP/W (Geo-slope International Limited, 2002) program discretized into nine hydrostratigraphic zones based on Fig. 5. The model was calibrated with K_h values between 0.138 m/d to 0.648 m/d, K_h/K_v ranging from 1 to 20, porosity of 0.4, and residual saturation value of 0.07 (Table 3). The alpha and n values were not reported by Price and not readable within the program, so were determined with a web-based program (Seki, 2007) for the KeyIn "Sandy Silt (Coarse Tailings) Ks = 4.8-07m/s" volumetric water content function which was the sole function used for all nine hydrostratigraphic zones. The program calculated an alpha of 5.11 m^{-1} and an n of 3.51 and successfully matched the residual saturation (0.0775) and porosity (0.3996), with a reported a coefficient of determination of

[8] Same transect as A" to A illustrated on Figs. 3 and 4, except truncated near the top of the dam (just west of Bench E)

0.998 (good fit). In additional to modelling the 2003 configuration[9], she applied three different boundary recharge rates to simulate three different covers: 50 mm/y; 24 mm/y; and 5 mm/y.

Table 3**.** Price (2005) material properties

Hydrostratigraphic Zone	Model K (m/d)	K_h/K_v	θ_r	θ_s	α (m^{-1})*	n*
(1) Sand Bench	0.605	10	0.07	0.4	5.11	3.51
(2) Bench A	0.259	10	0.07	0.4	5.11	3.51
(3) Bench B	0.181	20	0.07	0.4	5.11	3.51
(4) Bench's C & D	0.216	5	0.07	0.4	5.11	3.51
(5) Toe B	0.648	1	0.07	0.4	5.11	3.51
(6) Toe C	0.562	1	0.07	0.4	5.11	3.51
(7) Lower Beach	0.138	20	0.07	0.4	5.11	3.51
(8) Upper Beach	0.406	20	0.07	0.4	5.11	3.51
(9) Contained Beaching	0.285	10	0.07	0.4	5.11	3.51

θ_s – porosity θ_r – residual saturation * Seki, 2007

Price's calibrated boundary recharge rates for the 2003 configuration ranged from 0.032 m/y to 0.158 m/y (Table 4), resulting in discharge/seepage values ranging between 0.0095 m/d to 0.053 m/d at four seepage faces along the dam (Table 5).

Table 4. Price (2005) steady state recharge fluxes. Rates and percentages of averaged annual precipitation (0.456 m).

Benches A & B	Slopes A & B	Benches and Slopes C, D, and E	Beach
0.086 m/y	0.032 m/y	0.158 m/y	0.158 m/y
19 %	7 %	35 %	35 %

Table 5. Price (2005) steady state discharge (m/d)

Perimeter Ditch	Toe A	Toe B	Toe C
0.02592	0.00950	0.05098	0.05356

[9] The state of the facility in the year 2003

Price (2005) concluded the following:

- The flow model results were sensitive to recharge rates
- As local flow systems extend from the benches to the adjacent slope toes, there is a dilution and downwards salt migration in the shallow groundwater on Benches A, B, and C due to local recharge
- Groundwater discharge was focused at the toes of the slopes
- The backward-sloped benches have large local flow systems and promote deeper and faster flushing of the process water by recharge
- In the 2003 configuration:
    - 23% of the water table was within one metre of the ground surface due to the backward sloped bench design and the higher hydraulic conductivity at the dyke toe
    - Local flow systems on the benches and slopes will take decades to flush the process water
    - The intermediate flow systems on the perimeter dyke will take centuries to flush the process water
    - The discharge of process water with a TDS concentration greater than 1000 g/m^3 will continue for longer than 25 years

2.6 Data Sets

Since the original work by Price (2005), sets of groundwater and climate data has been collected providing the foundations for this project and allowing for improved calibration of the previous numerical model (Table 6). The groundwater data have been collected as part of ongoing University of Alberta research under the supervision of Carl Mendoza. Precipitation data was generally provided by the on-Site weather station, with gaps filled by the Environment Canada Mildred Lake weather station, located nearby. Annual snow surveys on Cell 31 were undertaken either by University of Alberta staff/students or by O'Kane Consultants Inc. in partnership with The Society of Canadian Limnologists.

Table 6**.** Utilized data sets

Data	Start Date	End Date	Frequency
Groundwater elevation	August 15, 2002	October 25, 2009	~9 times per year
Groundwater chemistry, Electrical conductivity	October 2002	July 2009	1 to 3 times per year
Precipitation	January 2000	December 2009	Daily
Snow surveys	March 2004	March 2009	Once per year

3. CONCEPTUAL MODELS

Before beginning development of the numerical model, the concepts of water and solute balance within the entire facility, and the concepts of water flow and solute transport within the modelled section were developed and illustrated. The goal of a conceptual model was to represent the system and its relationships in a visual form to guide the research. Liggett (2004) had already developed water and solute balance diagrams which were updated for this thesis. Price (2005) developed a conceptual hydrogeological model that inspired the included illustration (Fig. 7).

3.1 Water and Solute Balance

The water balance consisted of the following elements (Fig. 6 left):

- Inputs
  - process water
  - precipitation (rain and snow) including runoff
- Outputs
  - evaporation (pond and beach only)
  - evapotranspiration (dam only)
  - groundwater seepage

Based on observations, runoff and overland flow was minimal and diverted to the infiltration pathway instead of leaving the system. The solute balance was 1:1 input to output as TDS was transported by advection without adsorption or degradation (Fig. 6 right)

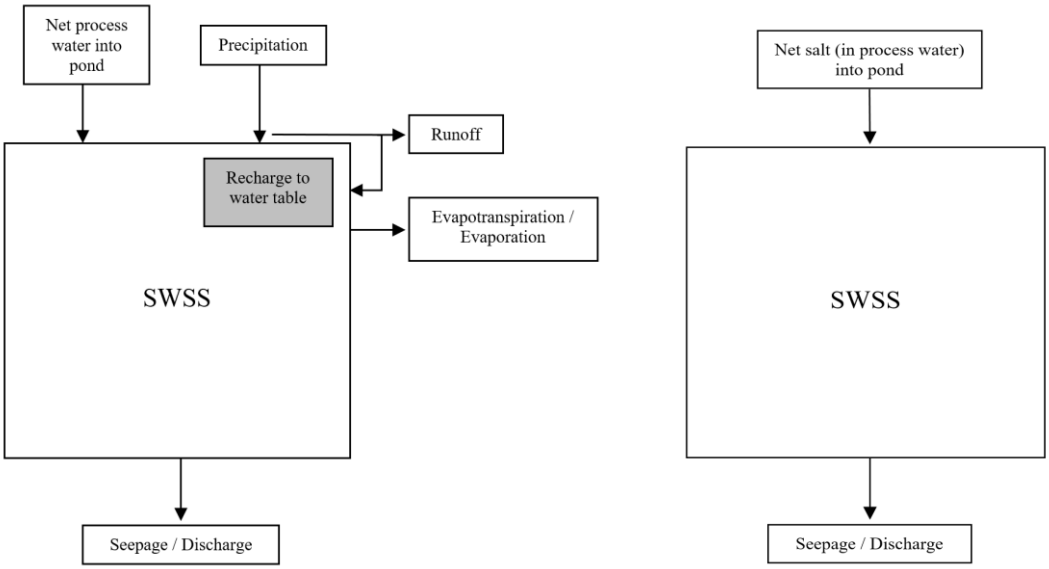

Figure 6. Conceptual diagrams: water balance (left) and solute balance (right) (modified from Liggett, 2004)

3.2 Groundwater Flow and Solute Transport Conceptual Models

The A'' to A transect was classified into three sections based upon the dominant feature: the pond; the beach; and the dam (Fig. 7). The dam was subdivided into cells based on

construction characteristics and for flexibility when modelling smaller scale variations. The water level in the pond was maintained at a constant elevation as part of the water reclamation system and this zone was considered to be static during the calibration phase 2003 to 2009. The beach sloped towards the pond and had both recharge and discharge faces.

The recharge rate along the top of the dam was sufficiently high to form a groundwater mound and divide beneath the upper beach. The water table either sloped shallowly westwards towards the pond, or sloped eastwards roughly following the topography of the dam face. Precipitation, in the form of rain and snow melt, directly recharges the groundwater, which leaves the modelled section at seepage faces located along the dam and lower beach.

A declining water table is a potential result of future reclamation measures (Price, 2005) therefore was also illustrated on the conceptual flow model. The location of the groundwater divide is important to the groundwater velocity and migration direction of the solute. The conceptual model for solute transport (Fig. 8) involves dilution and the movement of TDS by advection and dispersion. The process water (high TDS) mixes with infiltrated precipitation water (low TDS) and migrates with the water flow via advection and dispersion. This mixed water has a TDS concentration between the two end members.

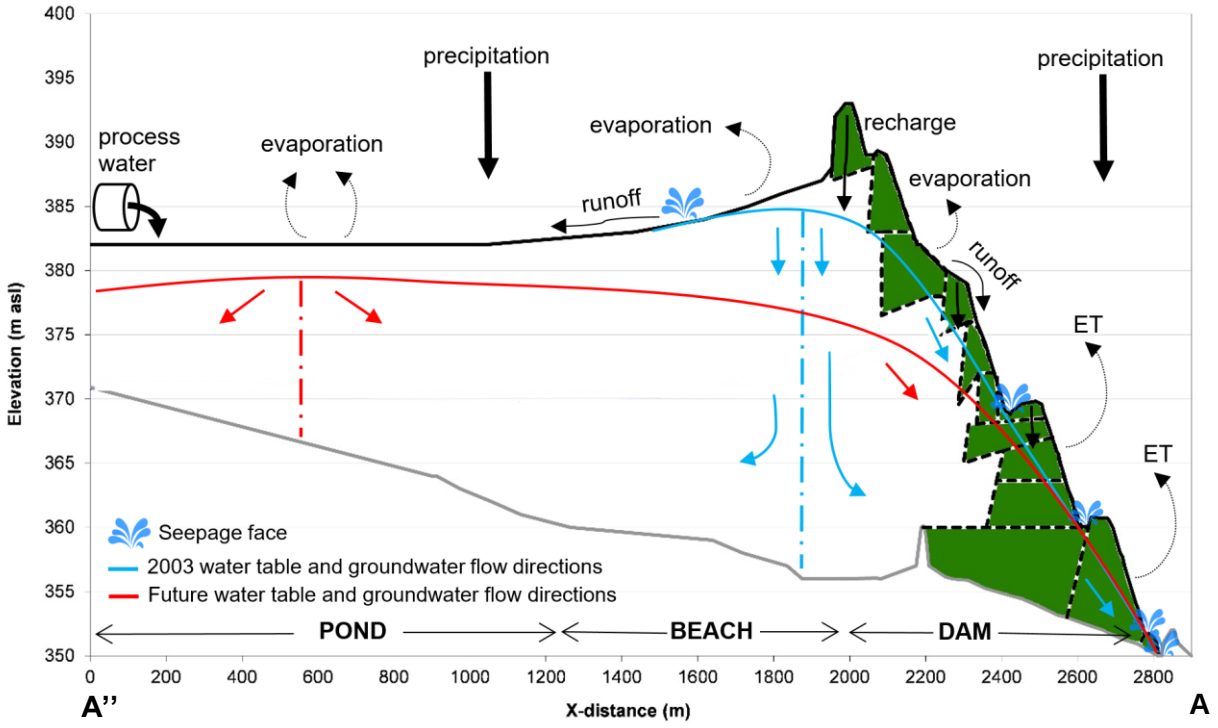

30x vertical exaggeration, ET – evapotranspiration

Figure 7**.** Section A" to A conceptual flow model (modified after Price, 2005). Green filled cells represent "worked" areas where the tailings have been redistributed and compacted due to earthworks by heavy equipment. The colorless space represents areas of passive settlement with little to no earthworks. The seepage faces are boundaries where the water table breaches the ground surface (at atmospheric conditions) and groundwater discharges from the saturated zone as either evaporation or downward flow as a thin film (USGS, 1987). The elevation of the water table is illustrated at the 2003 condition (groundwater divide beneath the beach) and at a future (lower) elevation (Price, 2005).

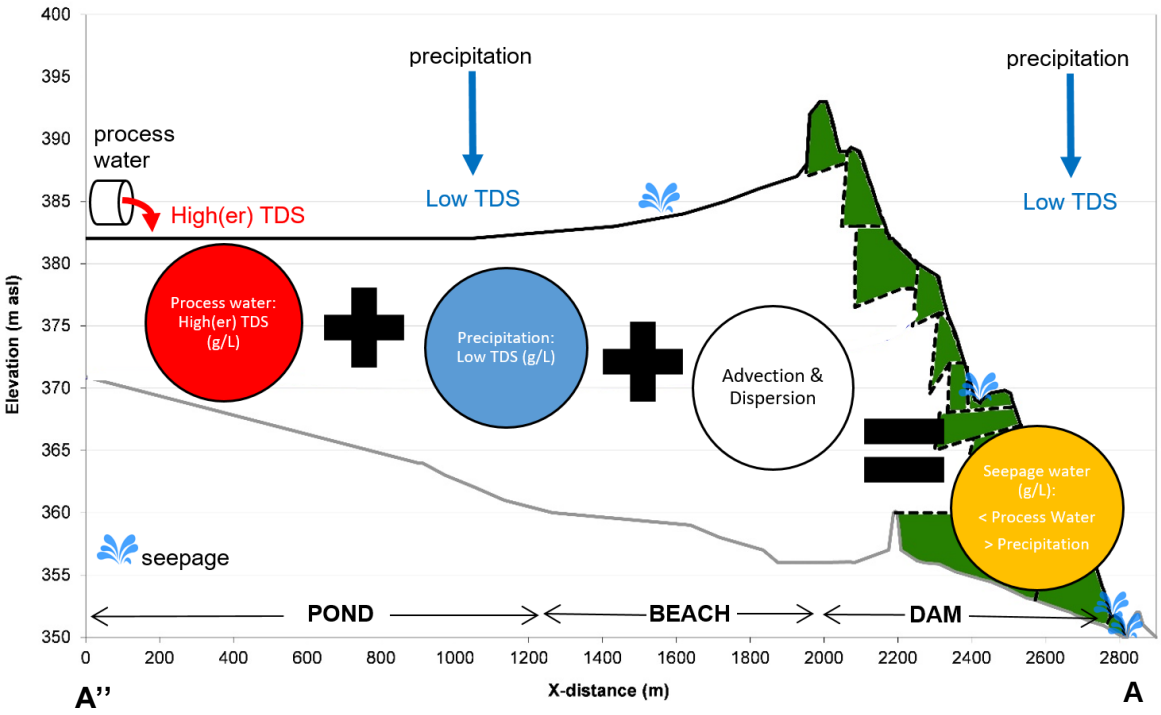

30x vertical exaggeration

Figure 8**.** Section A" to A conceptual TDS transport model (modified after Price, 2005). Process water is high in TDS concentrations (red) and precipitation is low in TDS concentration (blue). The two waters mix within the section which then discharges (seeps) along the dam face and the lower beach.

4. DEVELOPMENT OF THE NUMERICAL MODEL

Development of the model was performed in stages with the flow system developed and calibrated first, then the solute transport parameters added. The subsequent sections detail the software and methodologies used to develop the numerical model and are organized in the following order:

- Introduction to HYDRUS (2D/3D)
- Discretization of the hydrologic elements
- Model domain and material properties (geometry, mesh generation)
- Model parameters (soil hydraulic and solute transport models)
- Initial and boundary conditions for fluid flow and solute transport

4.1 Introduction to HYDRUS (2D/3D)

HYDRUS (2D/3D) is a software program capable of simulating water, solute and heat flow in variable saturated porous media, and was chosen for this project for its ability to represent the unsaturated zone. The program solves the Richards equation and the reader is directed to the the Technical and User Manuals for further details (Šimůnek et. al. 2011; Šimůnek et. al. 2011). Program validation information is available from the PC-Progress website (PC-Progress, 2016) and via numerous publications. HYDRUS was originally developed to simulate water and nutrient flow through agricultural soils but has expanded to include non-agricultural applications such as wetlands, dams, landfills, aquifer-river systems, aquifer pumping, stony soils, tunnel and highway design, and bacteria/virus transport.

As with all numerical models, the parameters and constraints must be prescribed for the system. For HYDRUS, this includes flow geometry, mesh generation, domain properties, initial conditions, and boundary conditions. A generic overview of each is provided in the following paragraphs starting with geometry. The flow and transport parameters must also be prescribed. Time units are offered in seconds, minutes, hours, days or years with the time steps managed and optimized by the program within the users designated ranges.

The geometry of a domain is defined as either a two-dimensional plane or three-dimensional space that is constructed with a series of points and lines. Surfaces are discretized by relating adjacent lines to form a closed loop. Surfaces usually represent units or zones of interest within the domain, and for this project they represented different hydrogeologic zones. Next the program requires the surfaces be divided into smaller, simpler triangles called finite elements, as the Finite Element Method (FEM) is employed to solve the numerical equations. The resulting mesh can be refined (smaller triangles) or stretched to suit the users needs. In general, refinement is warranted along flux boundaries and near the location of the water table.

The domain properties include materials and their distribution, anisotropy, observation nodes, and flowing particles. The saturated and unsaturated properties of the materials include hydraulic conductivities, porosity, residual saturation, alpha, and n. Observation nodes are nodes (points) within the domain that record pressure head, water content, temperature, and solute concentration over the simulated time frame. Flowing particles allow for the placement of a virtual “particle” anywhere within the domain that will move with the water flow and record its movement over the simulated time frame.

The initial conditions provide the starting point for the equations and need to be defined for pressure head and solute concentration. HYDRUS employs pressure head, as opposed to hydraulic head, whereby the water table is the zero plane with positive values below (the saturated zone) and negative values above (unsaturated zone). A positive pressure head value is equal to the height of the overlying water column (or depth if measured from the top of the water table) in a 1:1 relationship. The initial solute concentrations are entered in units of [mass]/m^3 and assigned to surfaces of the user choosing.

The program allows for nine flow boundary conditions which are defined and described in the following Table 7. For solute transport, there are four options (no flux, first-type (Dirichlet), third-type (Cauchy), and volatile-type (permitting gaseous diffusion)).

Table 7**.** HYDRUS available boundary conditions and definitions

Boundary Condition Type	Definition
No flux	No water/solute movement; impermeable boundary
Constant (pressure) head	A defined/fixed pressure head to represent in this model a surface body of water at a defined/fixed depth; e.g. a 1 m deep pond = +1.0 m pressure head value with equilibrium from the lowest located nodal point.
Constant flux	A consistent/fixed flux rate
Variable (pressure) head	A variable/changeable pressure head to represent in this model a surface body of water with a variable water depth; e.g. a ditch with a water depth of 0.55 m in summer but frozen in winter = pressure head value that is either +0.55 m or 0 m with equilibrium from the lowest located nodal point.
Variable flux	A variable/changeable flux rate
Free drainage	Gravity driven flow
Deep drainage	Vertical drainage across a lower boundary of a soil profile
Seepage face	Where water/solute in the saturated zone leaves the domain where the pressure head is equal to zero
Atmospheric boundary	The infiltration and actual evaporation rates are calculated by HYDRUS when given precipitation and potential evaporation rates, and the maximum and minimum soil surface pressure heads are assigned.

4.2 Discretization of the Hydrologic Elements

The water balance of the SWSS is relatively simple (process water and precipitation enter the system; water leaves the system via evaporation/evapotranspiration and seepage/discharge) (Fig. 6) and the flow conceptual model (Fig. 7) illustrated where the water enters and exits the A' to A cross-section and the general flow directions. To aid in model development, the specific elements and pathways of the hydrological cycle needed to be discretized (Fig. 9).

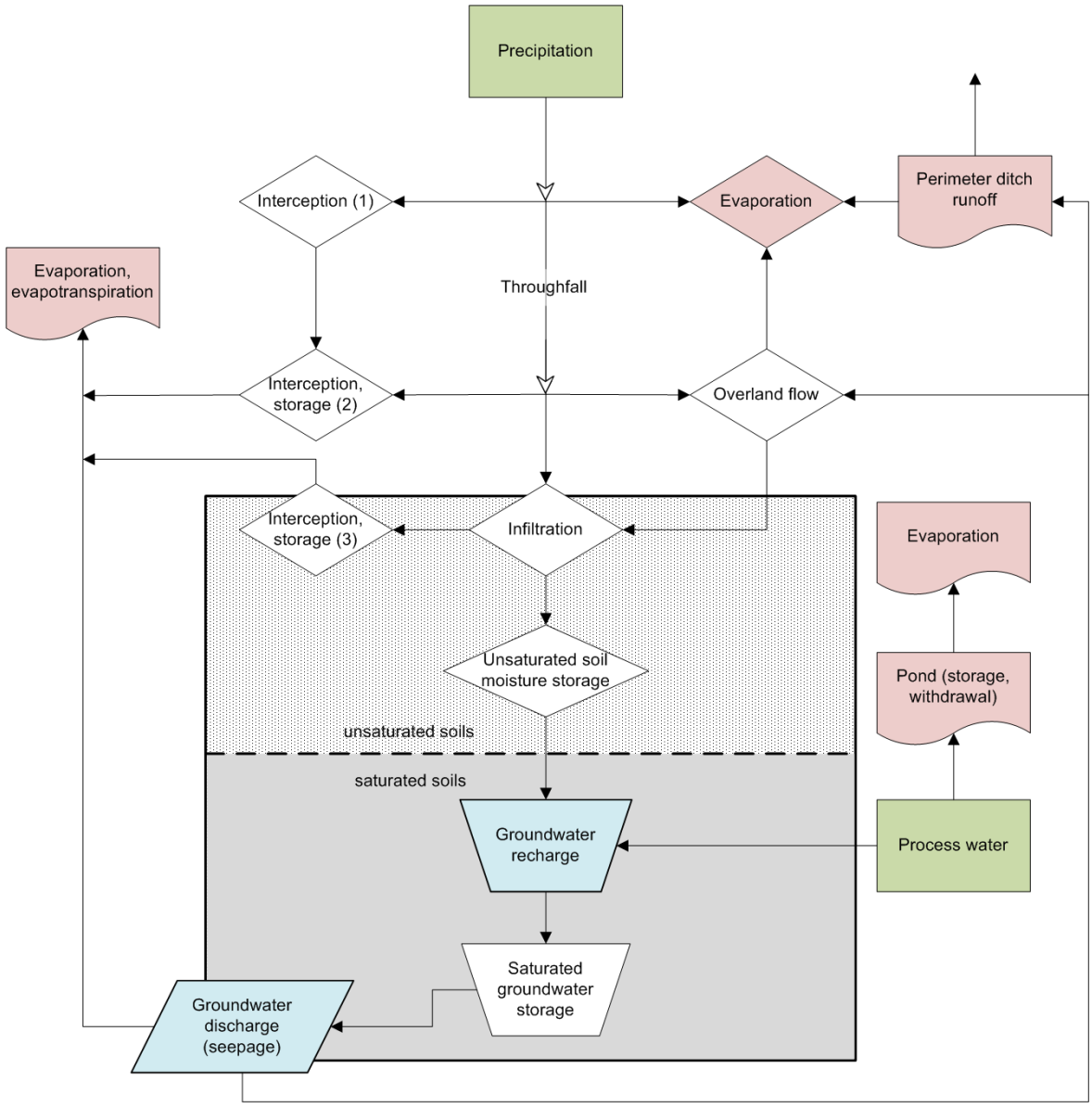

Figure 9. Hydrologic cycle in 2003 (inspired after Freeze and Cherry, 1979). Diamond shapes represent the "other demands" on precipitation which divert water away from groundwater recharge. Color fill code: greens are water sources (system gains); pinks are water sinks (system losses); and blues are the focus of this model. Interception (1) = canopy; Interception, storage (2) = leaf litter; Interception, storage (3) = roots and stems.

For the modelled cross-section, process water (high TSD concentrations) can either evaporate, remain in the pond (for storage or withdrawal), or recharge groundwater. There are many demands on precipitation (rain, snow) (low TDS concentrations) from both the atmosphere and vegetation. Precipitation can be intercepted and stored by vegetation either in the canopy, on the ground, or within shallow soils. Stored water will eventually be respired to the atmosphere. Some precipitation will also evaporate before reaching the ground. Based

on ground observations (C. Mendoza, pers. comm.), throughfall that becomes overland flow will, in most cases, infiltrate and not leave the system. There is also likely exfiltration of unknown rates (not illustrated on Fig 9).

After all the water demands of the other elements in the hydrologic cycle, the water remaining for recharging the groundwater can be minimal. This is important to note as precipitation is the only source of water available for dilution of the relatively higher TDS concentration process water.

4.3 Model Domain and Material Properties

The depositional history of the SWSS was reconstructed by Price (2005) using digital contour maps, detailed designs, and measured ground elevations. These hydrostratigraphic layers, cells, and topography formed the model domain surfaces (Fig. 10). The deeper layers are semi-compacted due to the weight of the overlying deposits. The mechanically compacted dam-side tailings (worked tailings) were separated from the beach and pond-side tailings (unworked tailings) to allow for discretization of different material properties due to differential placement methods. The model did not include any surfaces to simulate the cover on the lower dam.

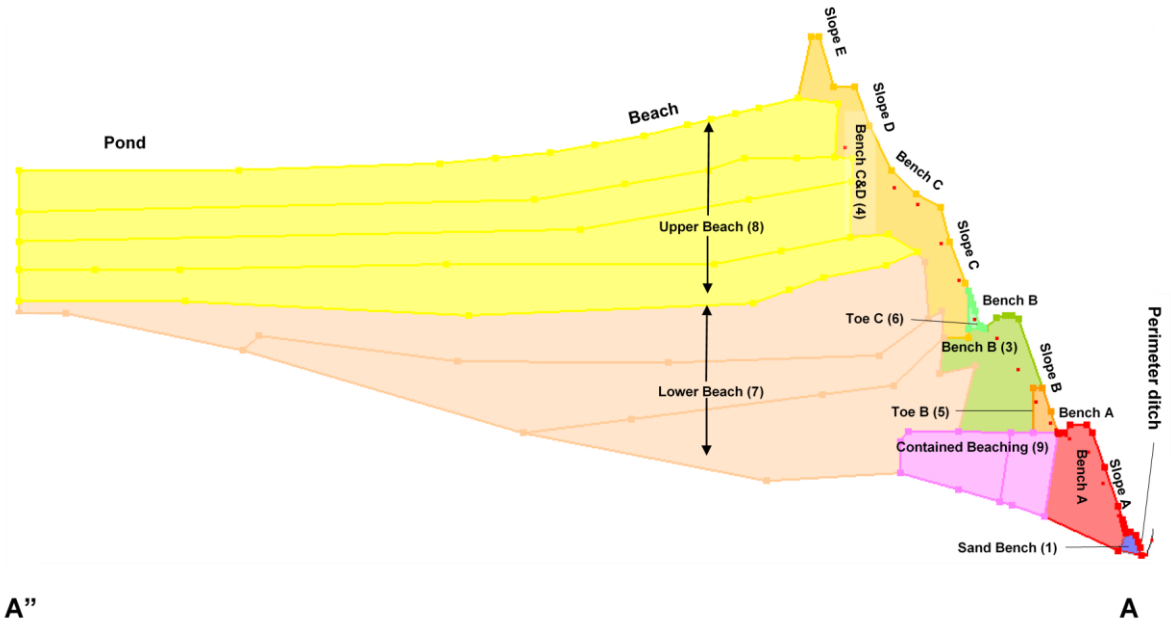

Figure 10. Model domain based on depositional history, physical geometry, and hydrostratigraphic zones.

The domain was constructed on the x-z planes with several modifications to simplify the geometry. Pinch outs and sharp angles were squared or softened to allow for mesh generation. The mesh was generated with a targeted finite element (FE) size of 30 m with a stretch[10] in the z-direction of 0.0333 making the finite elements smaller in that direction. As recommend for large transport domains (Šimůnek, undated), a smoothing factor[11] of 2.5 was applied to the mesh making it less smooth by decreasing the number of elements. Along the upper boundary, and within the area occupied by the water table, the mesh was refined to a

[10] the degree of mesh anisotropy (Šejna, 2017)
[11] the ratio of the maximum and minimum height of the finite element triangle: minimum of 1.1

FE size of 10 m horizontally to provide better resolution. The final mesh consisted of 6379 nodes, 1357 1D elements, and 12,178 2D elements and is illustrated on Fig. 11 along with the water flow boundary conditions. The modelled section represented an area of 58,492 m^2, and at calibrated initial conditions held 20,256 m^3/m of water.

4.3.1 Material Properties

Hydrus requires the following saturated and unsaturated material properties:

- hydraulic conductivity – horizontal and vertical
- residual soil water content (θ_r)
- saturated soil water content[12] (θ_s)
- alpha and n

Initially, the values from Price (2005) were used for the nine hydrostratigraphic zones. Using the tailings material properties data compiled from other sources (App. A), the properties of each zone were varied within a range, resulting in the values tabulated on Table 8. These values represent the calibrated system. The material properties were assumed to remain constant over the simulated time frames.

Table 8**.** Calibrated material properties[13]

Hydrostratigraphic Zone	K (m/d)	K_h/K_v	θ_r	θ_s	α (m^{-1})	n
(1) Sand Bench	1.270	20	0.15	0.40	1.24	1.7
(2) Bench A	0.500	20	0.2	0.35	1.24	1.7
(3) Bench B	0.183	16	0.15	0.35	1.24	1.7
(4) Bench's C & D	0.150	5	0.13	0.35	1.24	1.7
(5) Toe B	0.390	1	0.18	0.35	1.24	1.7
(6) Toe C	0.461	5	0.15	0.35	1.24	1.7
(7) Lower Beach	0.137	10	0.15	0.35	1.24	1.7
(8) Upper Beach	0.322	10	0.15	0.35	1.24	1.7
(9) Contained Beaching	0.536	16	0.15	0.35	1.24	1.7

4.4 Model Parameters

4.4.1 Soil Hydraulic Model

The default single porosity van Genuchten (1980) soil hydraulic model (without hysteresis) was selected and an air entry pressure of -2 cm was not chosen as, although the n value was low (1.7), the recommended threshold to enable the -2 cm air entry pressure is an n value of about 1.2 or less (for clay soils) (Jirka, 2015). The program defaulted to a specific storage (L^{-1}) value equal to zero for the fully saturated zone resulting in an solution that was always at

[12] Equivalent to total porosity (entire pore space) (Jirka, 2017).
[13] Discussed in detail later in thesis

instantaneous equilibrium (Jirka, 2004). This meant that a volume[14] of water released (or added) from (to) storage was instantaneously equal to a unit volume of the aquifer multiplied by a unit decrease (or increase) in head.

4.4.2 Solute Transport

The solute transport used the default Crank-Nicholson time weighting scheme and the Galerkin finite-element space weighting scheme. These are recommended by the program developers for solution precision (Šimůnek et al, 2017). The pulse duration was chosen as 1 day to represent the concentrations on January 1, 2003. The default Millington and Quirk tortuosity formulation was used. TDS was transported only by means of advection and dispersion and any potential interactions with residual bitumen, cations and ions were ignored. In addition, decay or degradation was not considered.

As TDS is a summation of the major ions, it was not possible to input "TDS" as a solute into the program, therefore sodium (Na^+) ion was used in its place. The following parameters were used to model solute transport:

- Soil bulk density 1,600,000 g/m^3
- Longitudinal dispersivity 10 m
- Transverse dispersivity 1 m
- Diffusion coefficient in water 5.1 x 10^{-5} m^2/d
- Diffusion coefficient in soil air 3.24 x 10^{-6} m^2/d

4.4.2.1 Diffusion Coefficients in water and soil air

As diffusion coefficients in water are weakly temperature dependant (Fetter, 1999; Robinson and Stokes, 1965) using the reference values (which are reported at 25°C) were not appropriate for the Northwestern Forest climate of the study area. The mean annual near surface soil temperature of the study area ranges between 0°C and 5°C (GSC, 2000; O'Kane, 2007) therefore model values were modified by dividing the value in half (Fetter, 1999) assuming that the near surface groundwater temperature is the same as the near surface soil temperature (Table 9). Groundwater temperature data was not available for the study wells.

HYDRUS also requires a gaseous diffusion coefficient for the solute. Only one reference for the diffusion coefficient in air for sodium was found in the literature although for a temperature of 23°C ± 2°C (Table 9). The diffusion coefficient in air was also assumed to be temperature dependant (although not explicitly stated in the references) and therefore was also divided in half to calculate a value for a temperature of 5°C.

[14] The word "volume" is used in this context as per the normal convention of imagining the aquifer and water as filling three-dimensional spaces, but as the model was constructed in two-dimensional space the water units are in lengths.

Table 9. Summary of sodium ion diffusion coefficients in water and air

Reference	Value at 25°C (m^2/d)	Value at 5°C (m^2/d)
Water		
Fetter, 1999	1.15×10^{-4}	5.75×10^{-5}
Rowe and Badv, 1996	8.99×10^{-5} *	4.5×10^{-5}
Air		
Rowe and Badv, 1996	6.48×10^{-6} *^	3.24×10^{-6}

* at 23°C ^ mean of range reported

The average value of the two water references at 5°C were used in the model (5.1×10^{-5} m^2/d).

4.5 Initial and Boundary Conditions – Fluid Flow

4.5.1 Initial Condition – Pressure Head

The initial pressure heads only served as temporary settings until the flow regime was calibrated and verified against field data (details in Chapter 6). The initial pressure head distribution was a linear distribution from the upper boundary to the lower boundary, but due to the configuration of the modelled section, was split into two. The pond and the beach were assigned a top pressure head of -7.6 m and a bottom pressure head of 30 m. The dam was assigned a top pressure head of -7.6 m and a bottom pressure head of zero metres with a -2.5 degree slope in the x-direction (parallel to the slope of the dam face). This roughly approximated the elevation of the water table for the entire section, but was insufficient to use for calibration as it did not represent the system. Therefore, the model was spun-up with several years of repeating water flux and head data applied to the boundaries until the simulated water elevations at the observation points harmonised with the measured groundwater elevation of the corresponding well. The water content of the vadose zone was also monitored for equilibrium. The final pressure head distribution at the end of the spin-up run was then imported into the new simulations as the initial pressure head distribution.

4.5.2 Water Flow Boundary Conditions

The modelled section had three boundaries: an upper boundary representing the ground surface; a lower boundary representing the base of the SWSS; and a western boundary at the limit of the research section (Table 10, Fig. 11). A no flow boundary was established along the western edge and along the original (now buried) ground surface. The SWSS sits on glacial till with a low horizontal hydraulic conductivity (10^{-2} to 10^{-4} m/d) based on slug tests and low vertical hydraulic conductivity (10^{-3} to 10^{-6} m/d) based on laboratory tests and was expected to contribute very little water to the system (see Appendix A). The western vertical edge of the modelled section represents the middle of the SWSS impoundment where groundwater movement is expected to be very slow or stagnant. The upper boundary represents the ground surface of the pond, the beach, and the dam and takes or gives water depending upon the location.

Table 10**.** Flux Boundary conditions

Boundary	Representative Feature	Condition
Upper	Pond, beach, dyke, dam face	Constant/variable flux, constant/variable head, seepage
Lower	Top of glacial Till	No flow
Western	Centre of pond	No flow

After some experimentation, it was decided not to use the atmospheric boundary condition as it did not allow for sufficient control over the timing and length of the spring melt, which had a crucial influence on the groundwater system. To simplify the model, only recharge (precipitation anticipated to reach the water table) was applied to the upper boundary. Specifically, the upper boundary consisted of three input fluxes, and three head conditions (Table 11, Fig. 11).

Table 11. Water flow boundary definitions – fluxes and heads

No.	Fluxes	Heads
1	Bare unworked tailings (beach), Unreclaimed worked tailings (Bench E through to Slope C)	Central pond
2	Reclaimed Benches (Benches B, A and Sand Bench)	Ditch at Toe C
3	Reclaimed Slopes (Slopes B and A)	Ditch at Toe B

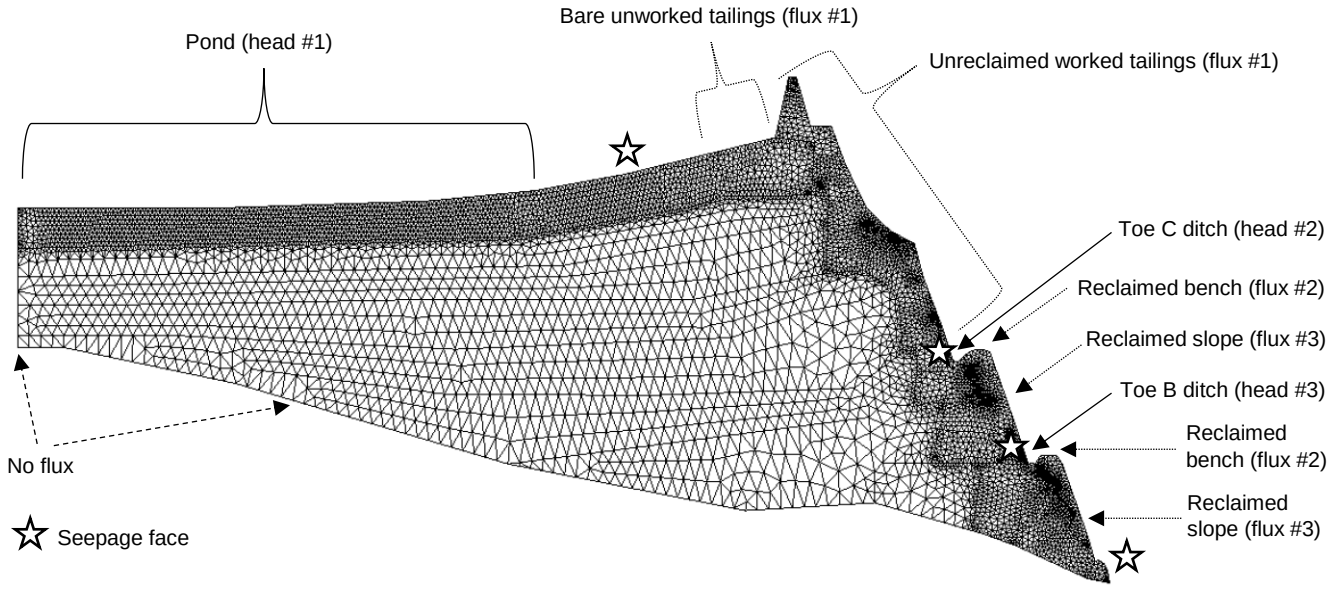

Figure 11. Water flow boundary conditions displayed on mesh section

There were no layers or zones to simulate a cover or vegetation. While HYDRUS has the capabilities to apply an atmospheric boundary condition with the inclusion of actual precipitation and potential evaporation lengths (these values were available in the data set), but after some experimentation it was decided not to use the atmospheric boundary condition as it did not allow for sufficient control over the timing and length of the spring melt, which had a crucial influence on the groundwater system.

4.6 Initial and Boundary Conditions - Solute Transport

4.6.1 Initial Concentrations – Solute Concentrations

Process water was entrained during deposition with the solids leading to the stratification within the groundwater. The TDS values reported in Liggett (2004) were used as initial concentrations (Table 12), which were calculated by the summation of the major ions Ca^{2+}, Na^{+}, Mg^{+}, NH_4^{-}, HCO_3^{-}, Cl^{-}, SO_4^{2-} from the supplied water chemistry data. The entrained process water was estimated to have a TDS value equal to the yearly average at time of deposition, as groundwater velocities beneath the pond and beach are very low (or stagnant). Any dilution[15] due to total precipitation (rainfall plus snowmelt) was minimal as the volume of process water generally exceeded precipitation by 1.4 to 21 times. The exception was in 2002, when total precipitation inputs were calculated to almost equal process water input. Retaining the yearly average concentration made the model more conservative. Liggett TDS values were rounded up to the nearest tenth to reflect less precision in the data.

The depositional layers for the years 2001, 2002, and 2003 were removed from the model for simplicity and incorporated into 2000 layer (Fig 12). Therefore, the TDS concentration (3241 ppm) reported in the uppermost layer was the average of 2000, 2001, and 2002. There were

[15] rainwater TDS = 20 ppm (Liggett, 2004)

no TDS values reported for 2003 in Liggett (2004). The small wedge of 1993 layer was incorporated into the 1994 layer to simplify the model.

Table 12. Annual deposits, measured and model TDS concentrations (Liggett, 2004)

	Units	2002	2001	2000	1999	1998	1997	1996	1995	1994	1993
Measured TDS	(g/m^3)	3300	3500	3000	3100	2900	2300	2300	2400	2200	1900
Model TDS	(g/m^3)		3300		3100	2900	2300	2300	2400	2200	

For the hydrostratigraphic units within the dam, data from the 2003 groundwater sampling events were used to determine an annual concentration for each cell (Table 13, Fig. 12). First, the geometric average of the TDS concentrations was calculated for each monitoring well and these results were averaged with the other monitoring wells screened within that cell. For the Sand Bench (1) there were no groundwater samples collected in 2003, therefore the TDS concentration from the adjacent Bench A (2) were used. Similarly, Toe C was assumed to have the same TDS as Benches C&D.

Table 13. Groundwater TDS concentration, measured and model

Hydrostratigraphic Zone	Geometric Mean TDS 2003* (g/m^3)	Model TDS (g/m^3)
(1) Sand Bench	2800	2800
(2) Bench A	2800	2800
(3) Bench B	2700	2700
(4) Bench's C & D	3300	3300
(5) Toe B	2900	2900
(6) Toe C	3300	3300
(7) Lower Beach	See Table 12 above	
(8) Upper Beach	See Table 12 above	
(9) Contained Beaching – east	2500	2500
(9) Contained Beaching – west	3000	3000

* Price, 2005

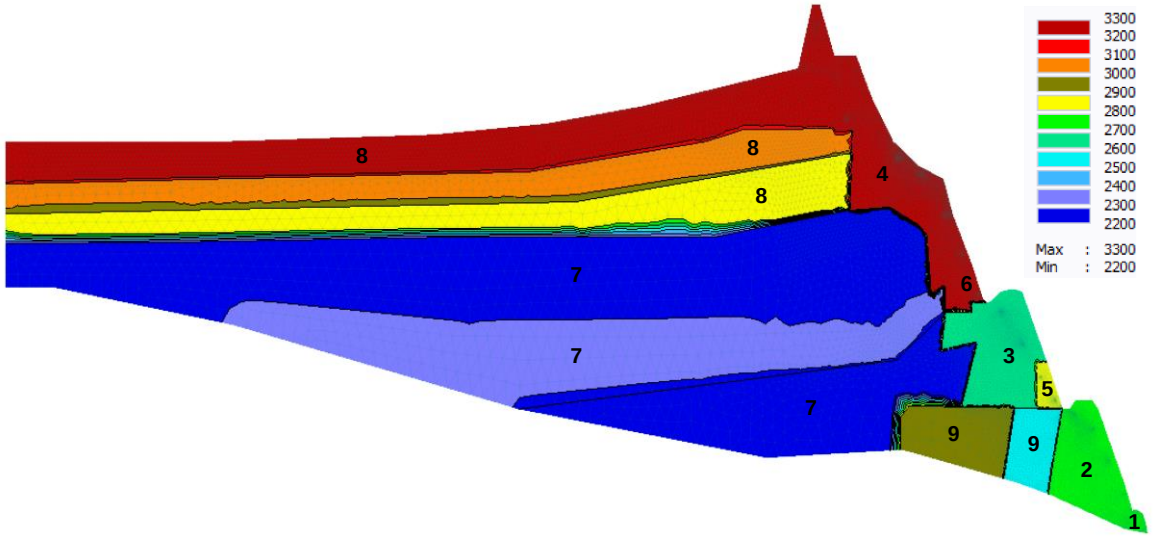

Figure 12. Initial TDS concentration distribution (g/m^3) labelled with hydrostratigraphic zone numbers.

4.6.2 Solute Boundary Conditions

HYDRUS offers the choice of fours types of solute transport across boundaries: no flux; first-type (Dirichlet); third-type (Cauchy); and volatile-type (permitting gaseous diffusion). The model boundaries were assigned as either no flux or third-type (Cauchy) (Table 14). The Cauchy type uses solute flux (as opposed to solute concentration) across the boundary and is recommended by the developers as it is "physically more realistic and preserves solute mass in the simulated system" (Šimůnek, 2011, p. 105). The input concentration along the upper boundary was assigned a concentration of 3300 g/m^3 at the pond and 0 g/m^3 for the remaining upper boundary.

Table 14**.** Solute boundary conditions

Boundary	Representative Feature	Transport Model
Upper	Pond, beach, dyke, dam face	3rd type (Cauchy) solute flux
Lower	Top of glacial Till	No flux
Western	Centre of pond	No flux

5. MODEL CALIBRATION

The model was calibrated through an iterative process of groundwater elevation curve matching, attaining equivalent measured discharge values, and successful model convergence. Although the following sections compartmentalize the calibration details, the process of determining the most representative boundary conditions was non-linear and run in parallel with characterization of oil sand tailings material properties. The calibration of the model is detailed in the following sections in the following order:

- Input fluxes and heads
- Output heads (groundwater elevations)
- Output fluxes (discharges)
- Quantitative evaluations
- Model sensitivity
- Mass balance error
- Solute output

Within the context of calibrating the model, a constant flux across the boundary was called a “steady-state” boundary condition and a variable flux was called a “transient” boundary condition.

5.1 Input Fluxes and Heads

First, model calibration started with the steady state boundary condition, then progressing onto the more complex transient boundary condition before returning to the steady state boundary for final refinement. While the transient boundary allowed for a nuanced calibration to seasonal variations, these details may become obscured and possibly irrelevant for future predictions, therefore both boundary representations were used for future simulations. The steady state boundary has the advantage of shorter calculation times. The final calibration step was to resolve any minor differences upon the addition of the solute.

As HYDRUS (2D/3D) only allows one boundary condition to be placed upon a node, the initial model ran with the entire dam face as a seepage boundary. After evaluation, almost all seepage faces were changed to fluxes except for those locations where the water table breached the top boundary (ground surface). This occurred at the toes of the slopes and at the perimeter ditch. This was consistent with field observations of ponded water at the toes of Slopes C, B, and A. A seepage face was also added to the lower beach for model convergence. Seepage discharge at Toe C was found to be very sensitive to the recharge rate applied to Bench C and Slope C; the higher the infiltration, the higher the discharge. Particle tracking indicated that it takes about 15 years for water to travel from Bench C to Toe C.

The central pond does not freeze over during the winter (C. Mendoza, pers. comm.) and therefore was retained as a constant head boundary, along with the zero-constant head at the ponds edge, for both the steady state and transient simulations (Table 15). The ditches at the toes of the slopes were assumed to be frozen between November and March, and therefore were assigned heads of zero during these months. For the remaining seven months, the ditches at the toe of Slope C and at the toe of Slope B were assigned depths of 5.5 cm and 5.0 cm, respectively. For the steady state boundary condition, the ditch depths required adjustment as it was found to affect the discharge rate at the adjacent seepage face; the higher

the head, the higher the discharge. This resulted in open water disappearing from the ditch at Toe C with a head of -1.0 cm and the water depth in the ditch at Toe B reduced from 5.5 cm to 1.0 cm. Note that these are small changes on a large model whose upper boundary is not a precise replication of the actual surface topography.

Table 15. Calibrated daily model boundary input values

Boundary Type and No.	Units	Steady State	Transient	
Flux				
No. 1 Bare unworked tailings	m/d	0.000508	0	(Nov – Mar)
No. 1 Unreclaimed worked tailings	m/d	0.000508	Table 16	(Apr)
No. 2 Reclaimed Benches	m/d	0.000247	Table 17	(May – Oct)
No. 3 Reclaimed Slopes	m/d	0.000194		
Head				
No. 1 Pond depth[ʁ]	m	1	1[ɣ]	(all year)
		0 (at ponds edge)	0 (at ponds edge)	
No. 2 Ditch depth at Toe C	m	-0.010	0	(Nov – Mar)
			0.055	(Apr – Oct)
No. 3 Ditch depth at Toe B	m	0.010	0	(Nov – Mar)
			0.050	(Apr – Oct)

[ʁ] Syncrude, 2010 [ɣ] C. Mendoza, pers. comm.

Transient boundaries simulating the vegetative cover were more difficult to calibrate than the bare tailings. The lower half of the dam was planted with grasses and trees (illustrated on App. H) which were designed to provide slope stability and restrict water infiltration. The uptake and/or interception by vegetation can be especially large during the spring and during periods of drought (Chaikowsky, 2003; Young-Robertson, 2016). As the reclaimed slopes are planted with deciduous and coniferous trees, these boundaries transmit less precipitation than the reclaimed benches which are planted with grasses and supported hardy herbaceous plants (i.e. weeds). The surficial topography was also considered to play a role in recharge rates in that there was less recharge on the reclaimed slopes and more recharge on the reclaimed benches, which was a concept employed by Price (2005) and so carried forward into this work.

Liggett (2003) reported that evapotranspiration dominates outputs with percentages of applied precipitation between 44 % to 108 % across the entire facility. The potential daily evapotranspiration (using the Penman-Monteith method) ranges from a low of 1 mm/d at the beginning of the growing season to a maximum of 6.9 mm/d in July (Chaikowsky, 2003) meaning that the volume of water available for recharge changes during the growing season. However, it was not possible to incorporate this into the model, as a fixed percentage of precipitation (recharge) was applied as flux to the boundary as opposed to the application of an atmospheric boundary with a root zone. Although this was possible with HYDRUS (2D/3D), it was too complex for the size of the modeled section. In addition, the growth of the trees over the modelled time spans (nine years for calibration, 200 years for future predictions) and their subsequent greater water demand, was also ignored.

Runoff was measured with runoff frames in 2002 (June, July, August, September) at 15 locations on the neighbouring Cell 32 on reclaimed Slopes A and B, and on Benches A and B (Chanasky, 2002). The geometric mean of the total annual runoff measurements was 34 mm, which accounted for 8 % of the total annual precipitation (422 mm) (Environment Canada). Runoff during spring melt accounted for more than 96 % of the total at 11 of the 15 stations.

At two stations on Bench A, it accounted for a slightly lower percentage (78 % and 87 %) of the total precipitation. Only one station reported an almost equal volume of spring melt runoff to rain runoff (5 % more spring melt) and was located on Slope B. These data indicated that spring melt was the major contributor to runoff. This likely holds true, and even more so for the non-reclaimed and beach areas which have no vegetation to slow runoff. However, these data were ignored as most water from the spring melt does not appear to leave the facility by overland flow (C. Mendoza, pers. comm.) and is either lost to evaporation or infiltration (and subsequent evapotranspiration) leading to minimal amounts available for recharge.

The average of the March measured snow water equivalent (SWE)[16] was divided evenly over either the first or last 10 days of April (whichever was the best match to the measured data) and used to simulate recharge from the spring melt. To determine the appropriate rate of SWE to assign as recharge, 90 % of the total was used as a starting point, then either increased or decreased through an iterative process of curve matching and model convergence (Table 16, Charts 4, 5, and 6, Appendix E). In general, those years with large snowfall required a decrease in the melt rate for model convergence. SWE ranged from a high of 100 % to a low of 30 %. The geometric average recharge rate from snow melt equivalent for the years 2003 to 2009 was 51 % for the reclaimed slopes, 66 % for reclaimed benches and 68 % for bare unworked tailings and unreclaimed worked tailings. Although research has shown that infiltration can occur while soils are frozen (in the absence of concrete frost) (Redding, 2009), for simplicity this was not considered during the simulations.

Table 16. Calibrated transient boundary recharge rates in for SWE (April).

Year	Measured SWE	Calibrated SWE Recharge Rates					
		No. 1		No. 2		No. 3	
	m	%	m	%	m	%	m
2003	0.142	45	0.064	45	0.064	35	0.050
2004	0.0614	60	0.037	60	0.037	60	0.037
2005	0.0911	90	0.082	100	0.091	90	0.082
2006	0.0545	80	0.044	90	0.049	90	0.049
2007	0.1286	70	0.090	60	0.077	40	0.051
2008	0.1373	70	0.096	50	0.069	30	0.041
2009	0.0971	70	0.068	60	0.058	45	0.044
Geomean	0.096	68	0.065	64	0.063	51	0.049

A similar iterative process was used for rainfall but initially starting with rates used by Price[17] (2005) and modified until calibration was achieved. To avoid issues with model convergence due to large inputs of rain over short periods of time (e.g., heavy rainfall events), the monthly total for that month was evenly divided over the days[18] of that month. This was not an averaging, but a redistribution of the rain to ensure the capture of all potential recharge. If water flux at a boundary exceeds the infiltration capacity of the soil, HYDRUS treats the excess as runoff that leaves the system, which was determined during the discretization of the hydrologic elements (section 4.2) to be low or zero. When snow melt was applied in the first 10 days of April, the remaining 20 days were applied with rain. The final calibrated recharge

[16] SWE = 0.01* density of snow pack (kg m^{-3}) * depth of snow pack (cm)
[17] 0.158 m/y recharge on bare unworked tailings and unreclaimed worked tailings, 0.086 m/y recharge on reclaimed benches, 0.032 m/y recharge on reclaimed slopes
[18] Model input was daily

rates were 44 % for the bare unworked tailings and unreclaimed worked tailings, 10 % for reclaimed benches, and 8 % for the reclaimed slopes (Table 17).

Table 17. Calibrated transient boundary recharge rates for rain (May to October).

Year	Measured Rain	Calibrated Rain Recharge Rates					
		No. 1		No. 2		No. 3	
	m	%	m	%	m	%	m
2003	0.3696	44	0.163	10	0.037	8	0.030
2004	0.2049	44	0.090	10	0.020	8	0.016
2005	0.3223	44	0.142	10	0.032	8	0.026
2006	0.3185	44	0.140	10	0.032	8	0.025
2007	0.2224	44	0.098	10	0.022	8	0.018
2008	0.3069	44	0.135	10	0.031	8	0.025
2009	0.2144	44	0.094	10	0.021	8	0.017
Geomean	0.273	44	0.120	10	0.027	8	0.022

The water flux rates were calculated for daily inputs (Chart 3) and copied into HYDRUS from a MS Excel worksheet.

Chart 3. HYDRUS daily water input fluxes for Boundary No. 1 (blue), Boundary No. 2 (orange), and Boundary No. 3 (green). Negative values represent inputs into the model domain.

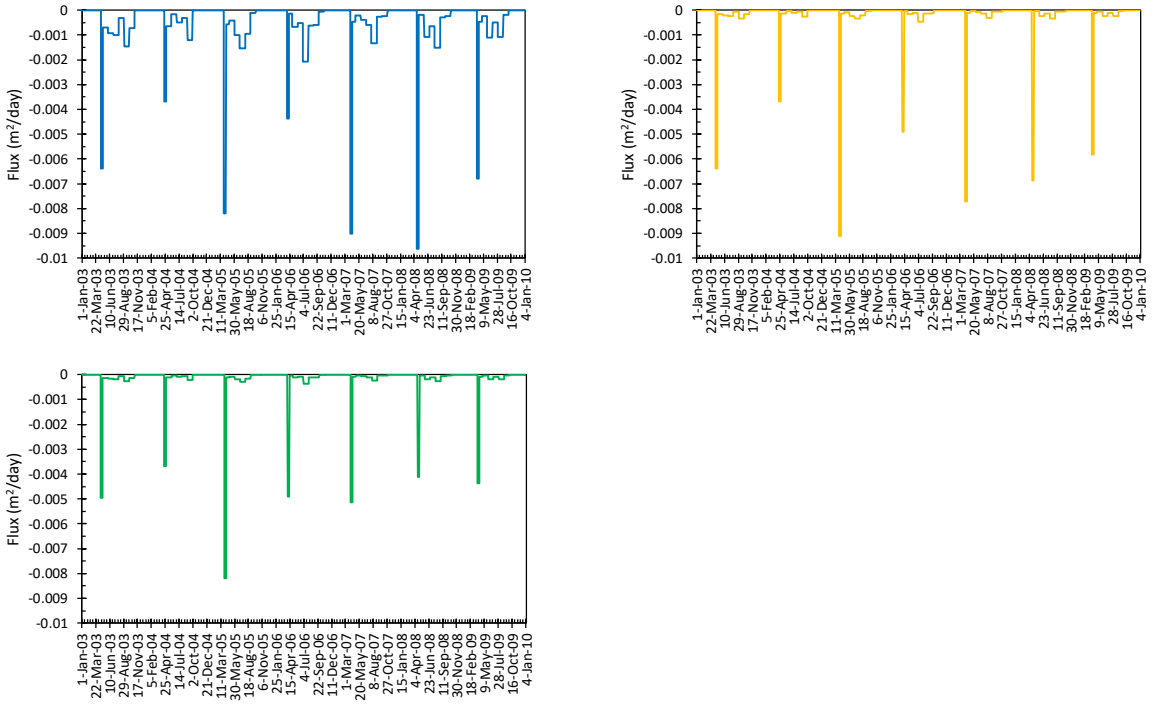

These calibrated recharge rates (Tables 16 and 17) meant that between 32 - 49 % (0.047 – 0.031 m) of the annual snow melt, and 56 - 92 % (0.153 - 0.251 m) of annual rainfall was lost to evaporation or evapotranspiration (assuming runoff was negligible). These rates were in line with those in the reference literature. The data presented in Tables 16 and 17 were charted per boundary along with the annual measured total precipitation (total snow plus total rain) (Charts 4, 5, and 6). From the charts, it is easy to observe the calibrated rate of recharge from SWE (blue, orange, or green fill) and rain (grey fill) for year, along with the calculated geomeans over the seven-year calibration period for SWE (blue, orange, or green line), rain

(grey line), and SWE+rain (black line). As the steady state boundary flux represents the annual water flux, evenly distributed over the days of the year, it's value (red dashed line) was also charted.

Chart 4. Boundary No. 1 (beach and unreclaimed worked tailings) calibrated annual recharge rates for transient and steady state conditions.

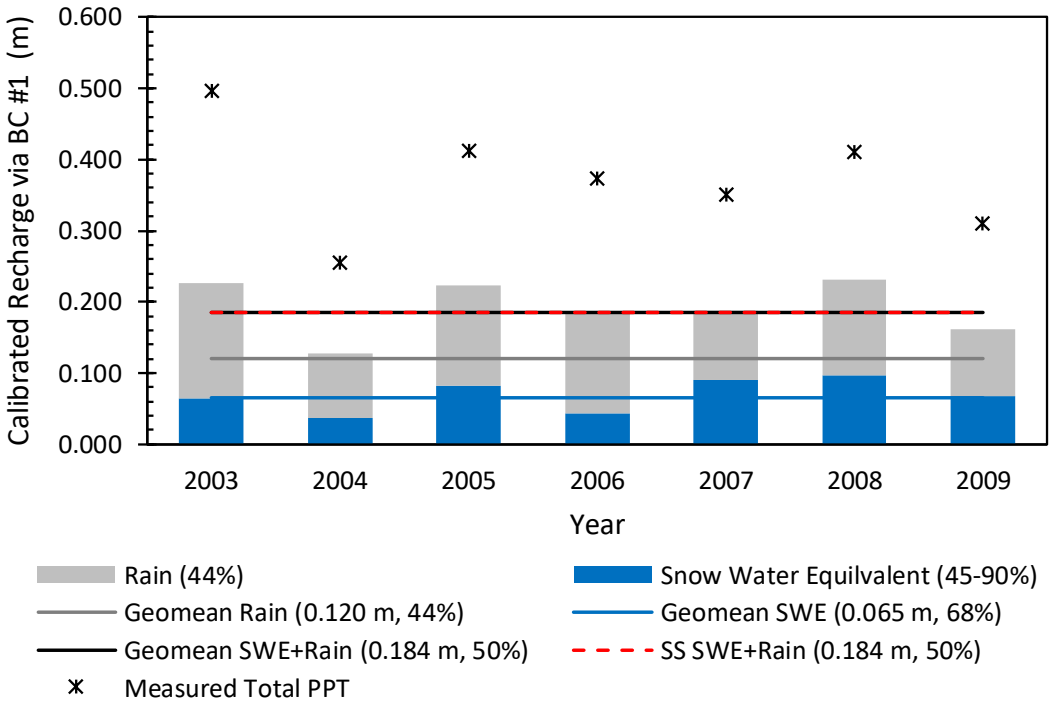

Chart 5. Boundary No. 2 (reclaimed benches) calibrated recharge rates for transient and steady state conditions.

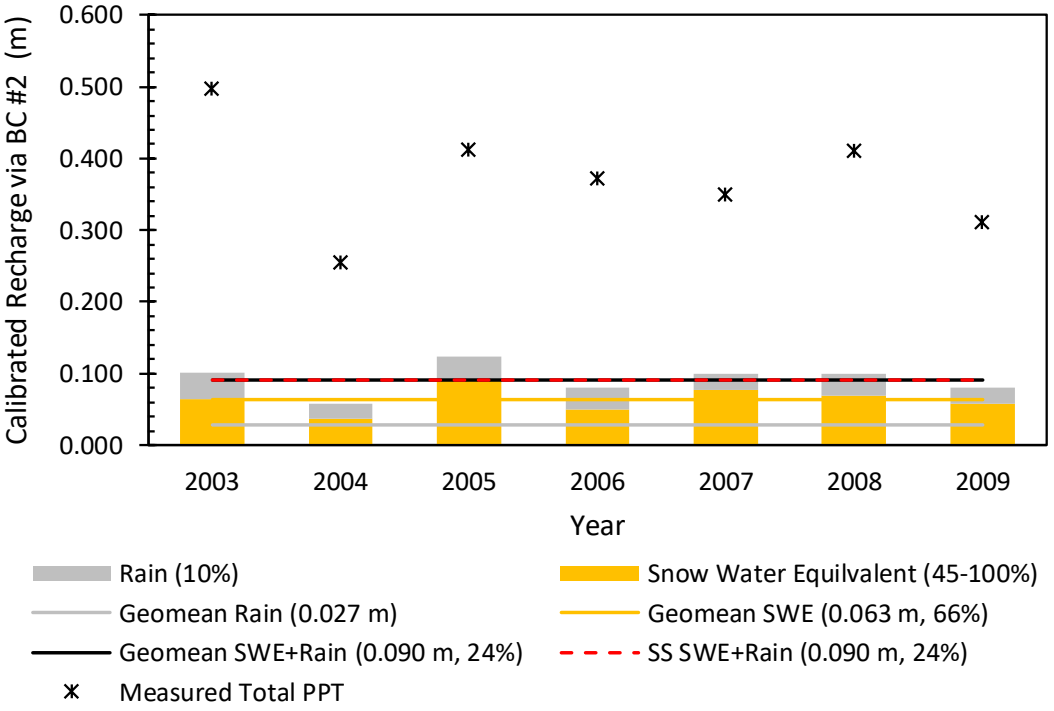

Chart 6. Boundary No. 3 (reclaimed slopes) calibrated recharge rates for transient and steady state conditions.

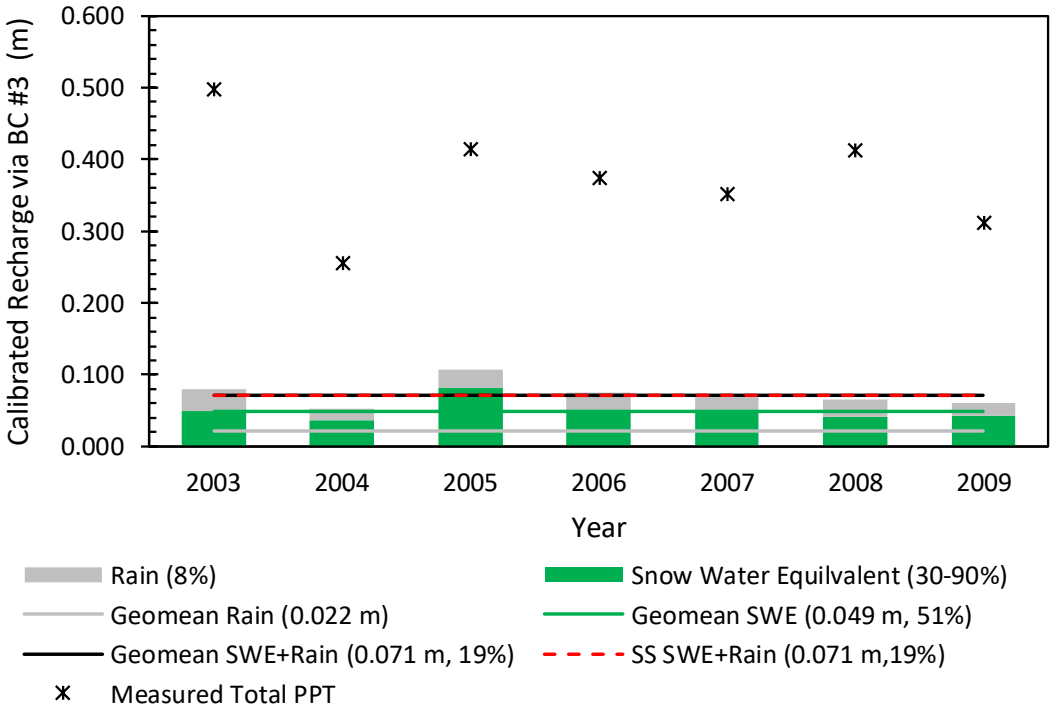

The following two tables (Tables 18 and 19) and three flow charts (Figs. 13, 14, and 15) illustrate how 370 mm of precipitation was portioned into recharge for the three boundaries. It was interesting to note that all three boundaries had similar lengths of recharge from snow melt of 65 mm, 63 mm, and 49 mm for Boundaries 1, 2, and 3, respectively. This meant that the vegetative cover was not a factor in how much snow melt reached the water table. However, vegetative and atmospheric demands ranged between 90 % to 92 % for rain. As laid out in the previous Fig. 9, other demands on precipitation include: evaporation; evapotranspiration; canopy interception; litter interception (near ground plants and leaf litter); exfiltration; and root uptake.

Table 18. Comparison of the boundary flux rates.

Boundary No.	Transient Boundary			Steady State Boundary
	Calibrated Recharge Rates Geomeans			Calibrated Recharge Rates
	SWE m/y	Rain m/y	SWE+Rain m/y	SWE+Rain m/y
1	0.065	0.120	0.185	0.185
2	0.063	0.027	0.090	0.090
3	0.049	0.022	0.071	0.071

Table 19. Comparison of the boundary flux percentages

Boundary No.	Transient Boundary			Steady State Boundary
	Calibrated Recharge Rates Geomeans			Calibrated Recharge Rates
	SWE %*	Rain %*	SWE+Rain %*	SWE+Rain %*
1	68	44	50	50
2	66	10	24	24
3	51	8	19	19

* Geomeans' annual precipitation (GAP) 2003-2009 was 0.273 m (rain) + 0.096 m (snow melt) = 0.370 m

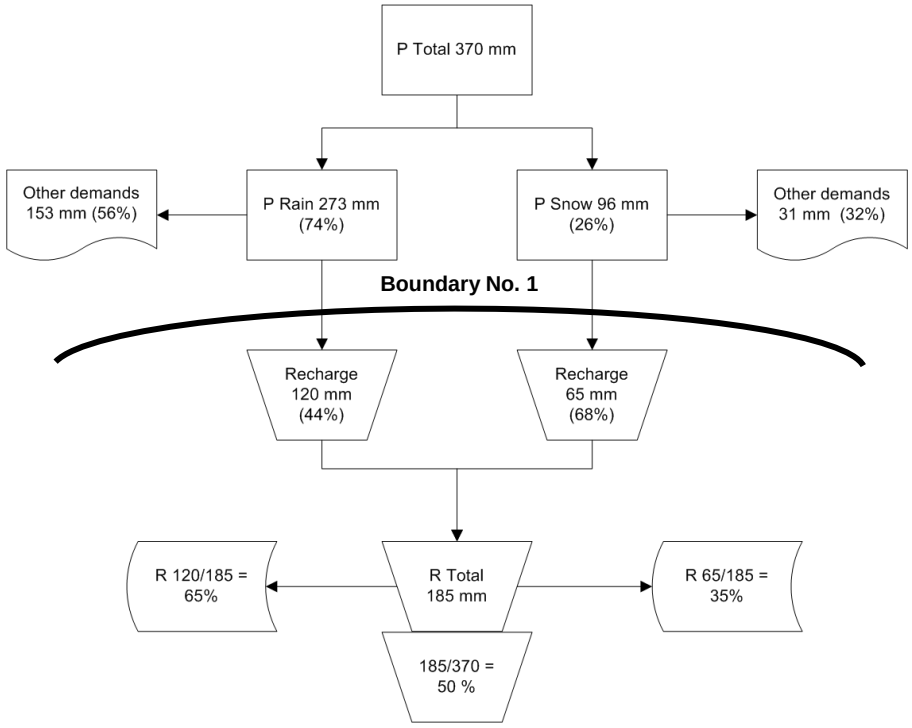

Figure 13. Boundary No. 1 division of annual Precipitation (P) into groundwater Recharge (R) (non-reclaimed and beach)

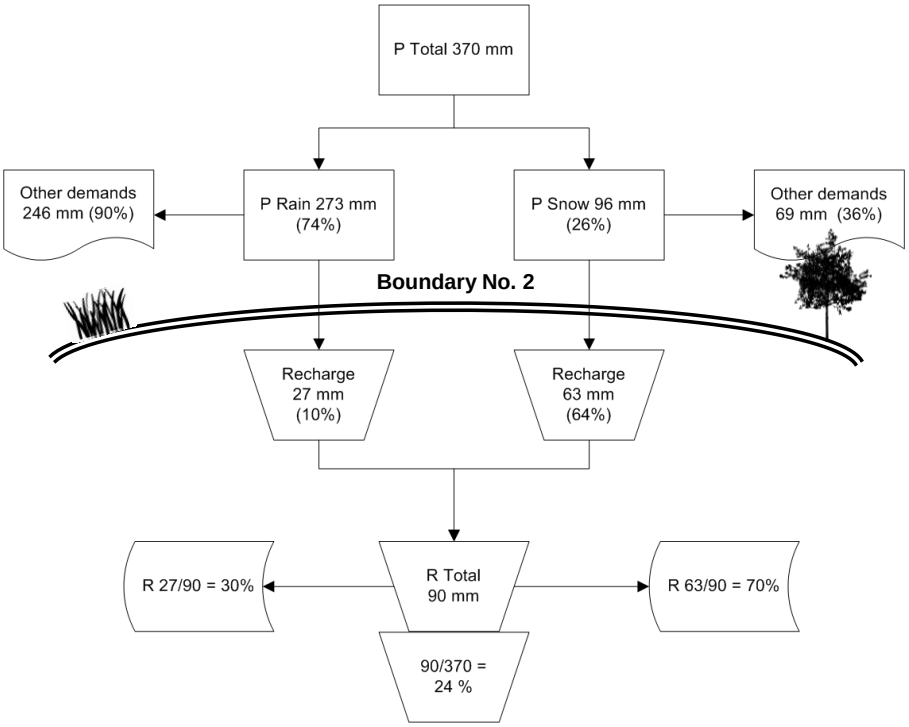

Figure 14. Boundary No. 2 division of annual Precipitation (P) into groundwater Recharge (R) (reclaimed benches)

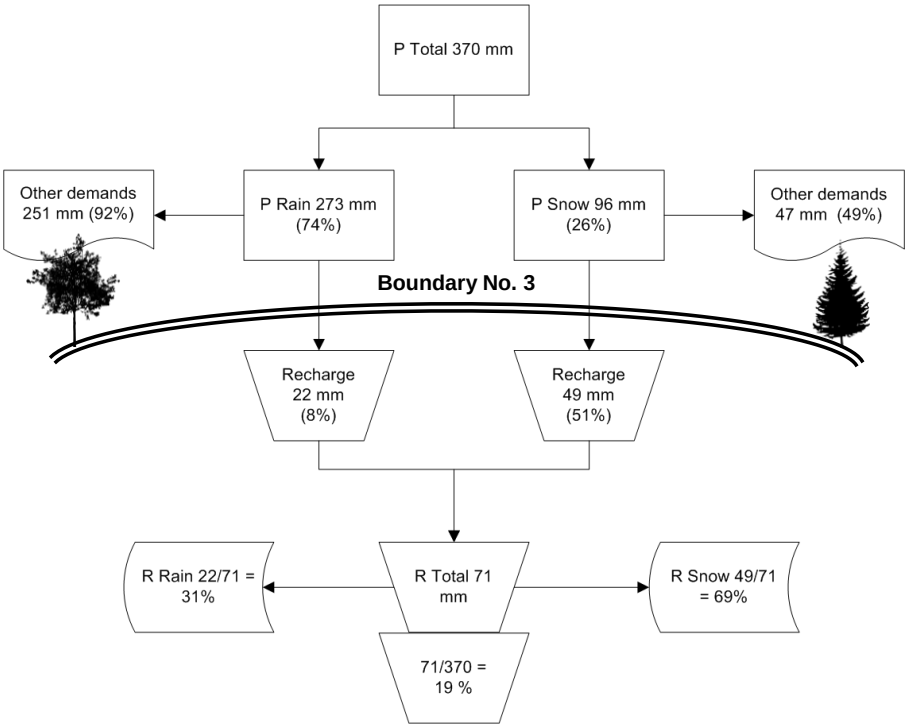

Figure 15. Boundary No. 3 division of annual Precipitation (P) into groundwater Recharge (R) (reclaimed slopes)

5.2 Output Heads (groundwater elevations)

The simulated groundwater elevations were calibrated against the measured values at 14 monitoring wells, specifically installed by Price (2005) to monitor the water table elevation (water-table wells). Fourteen observation nodes were placed into the simulation mesh at the elevation of the groundwater on August 28, 2003 and used as the reference elevation for that well. The groundwater elevations on this date were close-to or identical to the mid-screen elevation. Initially, the simulated pressure head data were overlain onto the measured groundwater elevation data to compare and calibrate the shape of the curve. Next, the pressure heads were converted into elevations and plotted again against the elevation data to calibrate the vertical position of the water table (Chart 7). Two locations (GW02-2.5wt and GW13-2.5wt) are illustrated here within the text while the remaining 12 charts are attached in Appendix E.

Chart 7. Transient calibration curves for GW02-2.5wt and GW13-2.5wt. Measured groundwater elevations and simulated pressure head vs. time. Average Depth to Water (ADTW) 2003 – 2009.

GW02-2.5wt, Slope A, ADTW 1.768 m

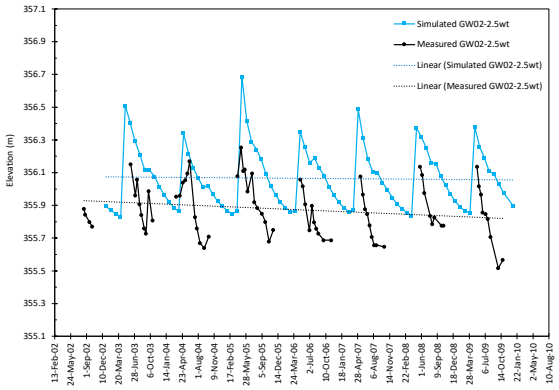

GW13-2.5wt, Bench C, ADTW 1.007 m

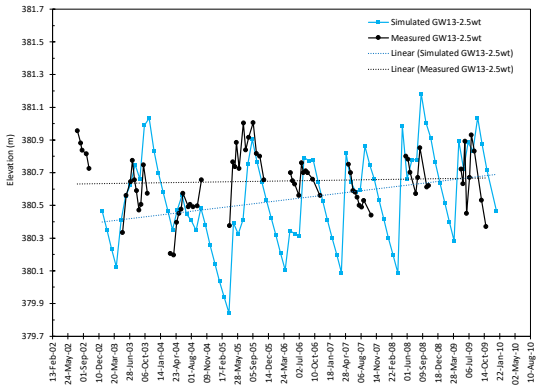

The process of calibration was scrutinized and balanced at all 14 locations, so that one location was not better calibrated at the expense of another. This holistic approach led to a satisfactory result except for GW15-6.8wt, located near the top of the dam on Bench D, which defied all efforts. It is possible that this location was not calibratable to due to the impact of adjacent earth works, therefore it was excluded from the quantitative calibration which is detailed in the following section 4.5.5. One other location, GW7-5wt, located on Bench B was also difficult to calibrate due to a rising trend in the measured groundwater elevation which could not be simulated without compromising the calibration of the adjacent wells. The resulting slope (2×10^{-5} m/d) of the simulated water table was an order of magnitude less than the measured slope (1×10^{-4} m/d) meaning that an acting force (such as a preferential pathway) was not captured by the model. This force could also be responsible for the much earlier arrival of the spring peak which was delayed in the simulation by two to four months, depending upon the year. However, despite these disparities, the simulated response was considered to satisfactorily model the measured response as the range and amplitude of elevations were similar.

For the remaining 12 wells, comparing the trends of the groundwater elevations over the calibration period between the measured and the simulated data indicated that three were matching, four were mismatched, and six varied by an order of magnitude (in the same

direction) (Table E3). However, given that the maximum slope equated to a change of 0.1 mm over seven years, which is much smaller than the margin of the field measurement error, the impact on long term future predictive simulations will be minimal. Similarly, the mismatched slopes were on the order of 10^{-5} and 10^{-6} and calculated to difference of less than 1 mm over 200 years, therefore were considered to be satisfactorily calibrated to the measured data.

5.3 Output Fluxes (seepage)

The simulated discharge rates were measured using mesh-lines, a feature of the program enabling a cross-section to be placed upon a series of adjacent boundary nodes to calculate water flow[19] and solute flux and provides node details about pressure head, water content, velocity, and concentration. The program back calculated flux at each print time for each node along a mesh-line once the pressure head had been fixed, and then reports the sum of flux of all these nodes. Mesh-lines did not share any nodes as this would double-count the flux. The mesh-lines overlapped with the seepage boundaries to capture the flux leaving the system but only included seepage nodes (as opposed to seepage boundaries which extended out to the next node) meaning that the mesh-line length was always shorter than the seepage boundary length. Finding the most appropriate length of seepage boundary such that the maximum wetted length during spring melt was captured was a detailed and iterative process. While the final seepage face lengths were greater than the maximum wetted lengths, meaning that some recharge flux was excluded, the final calibration was considered satisfactory in terms of the project scale and goals.

The calibrated seepage discharge rates for the steady state boundary condition were 0.0805 m^2/d at Toe C, 0.0798 m^2/d at Toe B, 0.0164 m^2/d at Toe A, and 0.0558 m^2/d at the perimeter ditch (Table 20). The calibrated seepage discharge rates for the transient boundary condition were almost identical with 0.0809 m^2/d at Toe C, 0.0814 m^2/d at Toe B, 0.0168 m^2/d at Toe A, and 0.0558 m^2/d at the perimeter ditch.

Table 20. Calibrated seepage discharge rates for transient and steady state boundary conditions.

Location	Transient Boundary	Steady State Boundary
	m^2/y	m^2/y
Toe C	29.5	29.4
Toe B	29.7	29.1
Toe A	6.2	6.0
Perimeter Ditch	20.4	20.4

The simulated discharge at the toe of the dam (along the surface of Zone 1, Sand Bench) was measured along a 26 m long mesh-line (Table 21, Fig 16). Along the basal 1.8 m portion of this mesh-line (the lowest portion of the dam), where the water table was within 12 cm of the

[19] Reported as m^2/d: mesh-line flux = length of the mesh line (m) * q (m/d)

boundary, the discharge rate was 0.030 m^2/d (10.8 m^2/y) which accounted for roughly half of the seepage along this mesh-line.

For comparison, the average seepage flow rate (May to June 2003) measured by Liggett (2004) along a 2.5 m tall seepage face at the perimeter ditch of Cell 31 was 0.069 $m^3m^{-1}d^{-1}$. A 15 % lower value of 0.059 $m^3m^{-1}d^{-1}$ was recalculated by Liggett using the July 2001 measurements of McKenna (2002); however, McKenna stated that discharge measurements likely varied by 25 % (possibly up to 50 %) indicating that discharge rates are subject to natural and/or anthropogenic induced variation. Therefore, the simulated values were considered reasonable even though they were lower than the measured values.

It was not possible to calibrate the discharge rates at the other three seepage faces as there eres no field data to compare against. While the values of 0.081 m^2/d at Toe C and Toe B seemed reasonable, the value at Toe A of 0.017 m^2/d seemed low and not consistent with field observations (C. Mendoza, pers. comm.). The total simulated steady state seepage discharge along the entire dam face was 0.23 m^2/d (85 m^2/y).

Table 21. Lengths of seepage boundaries, mesh-lines, and zero-heads.

Location	Seepage boundary length	Mesh-line Length	Transient		Steady State
			Maximum* zero-head length	Minimum zero-head length	Constant zero-head length
	m	m	m	m	m
Toe C	28.2	24.3	24.3	13.0	14.8
Toe B	20.7	17.2	12.5	6.0	7.9
Toe A	19.4	16.1	16.1	7.5	12.8
Perimeter Ditch	37.3ᵝ	26.1	1.5	1.5	1.5

* during spring melt ᵝ the entire upper boundary of the Sand Bench (Zone 1)

Most groundwater discharge occurred within the basal half or third of the slopes, except for the perimeter ditch which had a short and consistent 1.5 m long zero[20] pressure head at the toe of the dam (Table 21). During spring melt the wetted length briefly increased to its maximum length and then slowly shortened as the water table declined until the spring melt returned the following year (Figs. 16 and 17). The difference between the maximum and the minimum zero-head length was 11.3 m at Toe C, 6.5 m at Toe B, and 8.6 m at Toe A. The wetted length with the constant flux boundary condition was consistent over time, and fell between the maximum and minimum zero-head lengths of the variable flux boundary condition. The previous work by Price (2005) estimated wetted slope lengths of 14 m for Slope C, 10 m for Slope B, and 46 m for Slope A (assumed to also include the perimeter ditch) but suggested that these were likely to be overestimated by the SEEP/W (Geo-slope International Limited, 2002) model. Except for Slope A, these previous SEEP/W lengths were roughly the same as those predicted by HYDRUS (2D/3D).

[20] Zero-head is defined for this purpose as water within 10 cm of the boundary.

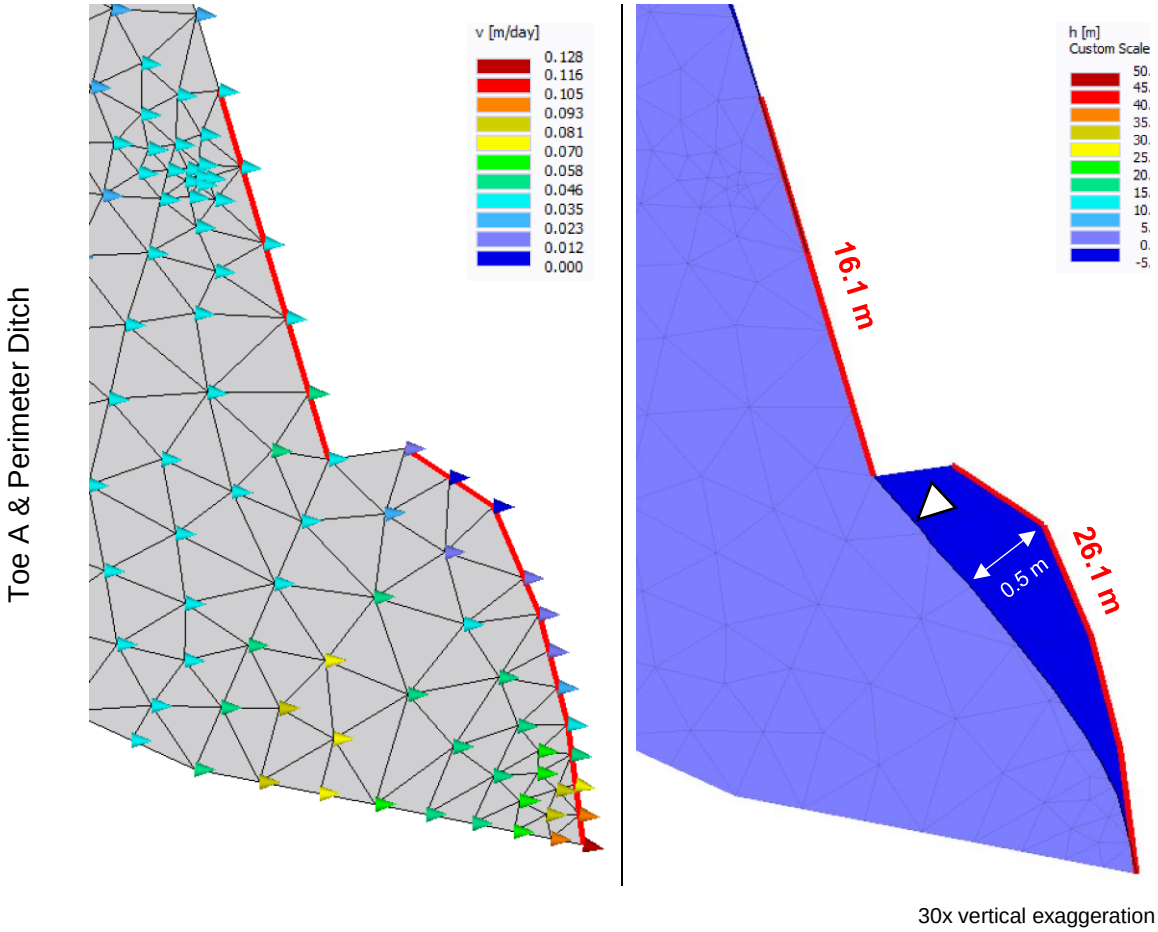

Figure 16. Maximum velocity vectors and pressure head at Toe A and Perimeter Ditch seepage faces. Mesh-lines are denoted as red lines and top of the water table with white triangle.

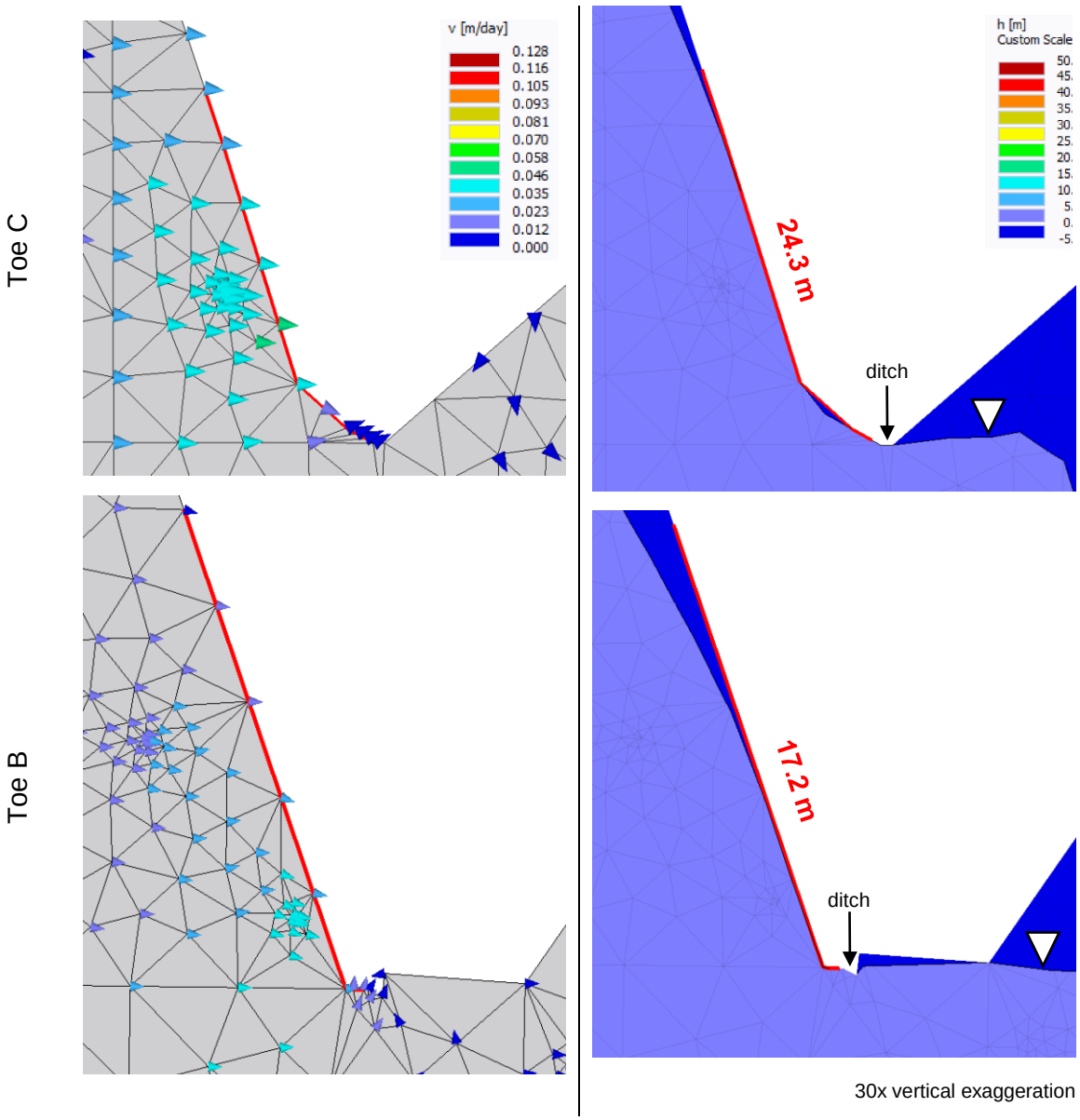

Figure 17. Maximum velocity vectors and pressure head at Toe C and B seepage faces. Mesh-lines are denoted as red lines and top of the water table with white triangle.

The spring snow melt had a noticeable impact on the discharge rates at Toes C, B, and A but minimal impact on the perimeter ditch (Chart 8). The groundwater discharge at Toes B and A had slight downward slopes (10^{-7}) which tracked with the rate of input precipitation flux which was also declining (-8.0×10^{-8}), although the slope of the perimeter ditch curve had an increasing trend (2.0×10^{-8}) indicating that it was buffered from precipitation trends. Winter conditions could not be completely simulated[21], therefore the simulated discharge rates are orders of magnitude greater than reality during the winter months.

There was also groundwater discharge along the lower half of the beach, which was simulated with a seepage boundary, but not used for calibration as the discharge would flow into the

[21] Although possible via a reduction to the hydraulic conductivity which can be accomplished via changes to the software code.

pond or evaporate. The model with the transient boundary condition simulated a geometric average annual discharge rate of 3.2 m^2 along this 463 m long seepage face.

Chart 8. Daily and averaged (2003-2009) simulated groundwater discharge rates with a transient boundary condition. Slopes: Toe C 2E-06; Toe B -2E-07; Toe A -5E-07; PD 2E-08.

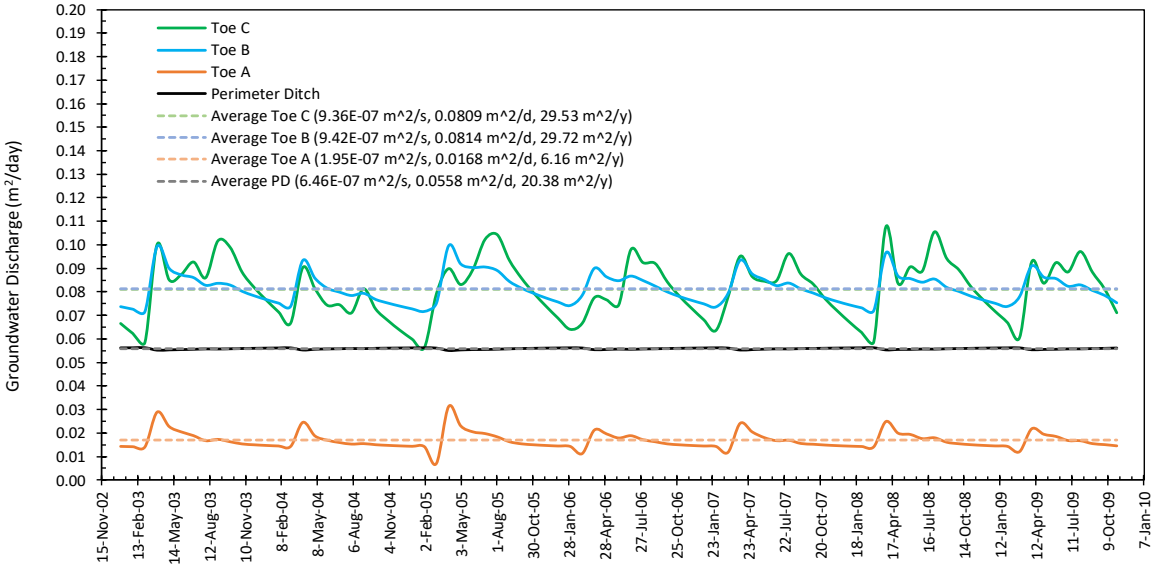

5.4 Quantitative Evaluation of Calibrations

Along with the qualitative curve matching discussed above, a quantitative evaluation of the simulated groundwater elevations was undertaken by the three measures recommended by Anderson and Woessner (1991): mean error; mean absolute error; and root mean squared error (Table 22). Of these three measures of error, the RMS error is considered the best (if the errors are normally distributed). Only 13 water-table wells were used for the transient evaluation as GW15-6.8wt was removed as it was could not be calibrated to (as previously discussed).

The simulated groundwater elevations were in good agreement with the measured groundwater elevations (Charts 9 and 11). RMS errors of 0.231 m (steady state) and 0.180 m (transient) were considered acceptable given the range of elevation observed across the study section (approx. 32 m). The ratio of the RMS error to the total head loss over the dam was 0.006, a small number indicating that the error was only a small part of the overall model response (Anderson and Woessner, 1991). The averaged groundwater elevations spanning the calibration period (2003-2009) were used instead of specific date comparison as it was quicker and easier.

Table 22. Quantitative evaluation of averaged (2003-2009) groundwater elevations results for all wells for steady state and transient boundary conditions

Measure	Units	Steady State	Transient
No. of Wells	-	14	13
Coefficient of determination (R^2)	m	0.999	0.998
Mean Error (ME)	m	0.202	0.138
Mean Absolute Error (MAE)	m	0.403	0.349
Root Mean Squared (RMS) error	m	0.231	0.180

In general, the simulation under estimated the groundwater elevation for those wells located on benches (black bars, Charts 10 and 12), and over estimated those located on slopes (white bars, Charts 10 and 12). The exception was GW10-2.5wt, which was located half-way up Slope C and had a lower simulated elevation than it's measured value (approx. 0.40 m). Efforts were made to add more recharge to Boundary No. 1 (which included Bench C) to try and overcome the underestimation at GW11 and GW12 but this led to model convergence issues and the water table breaching the surface at the toe of Slope D. The final differences were considered acceptable.

The height of the simulated water table was generally affected by three key elements: the rate of recharge to the boundary above; the base flow; and the hydraulic conductivity. More recharge raised the water table, and inversely a reduction lowered the water table but only to the certain minimum elevation whereby the base flow would take over. A reduction of the hydraulic conductivity raised the water table as migration was restricted, and inversely an increase in hydraulic conductivity lowered the water table.

Chart 9. Average measured groundwater elevation vs. average simulated steady state groundwater elevations. Listed left to right in descending elevation from top of the dam.

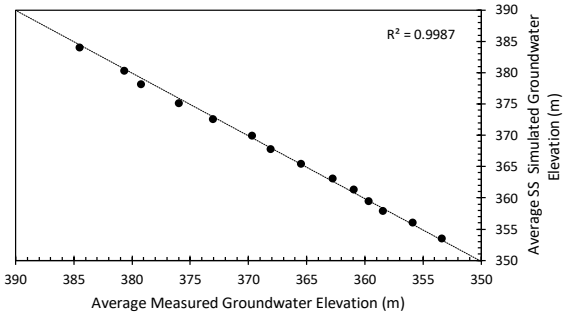

Chart 10. Difference between averaged simulated steady state and measured groundwater elevations. Bench locations (black) and slope locations (white). Listed left to right in descending elevation from top of the dam.

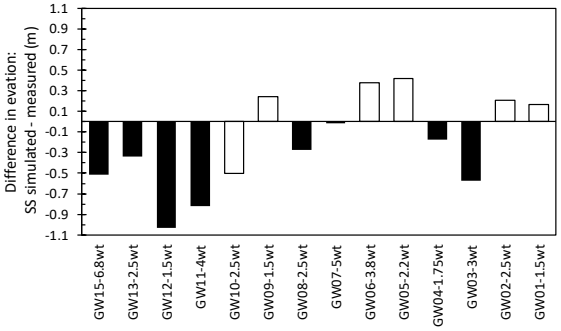

Chart 11. Average measured groundwater elevation vs. average simulated transient groundwater elevations. Listed left to right in descending elevation from top of the dam.

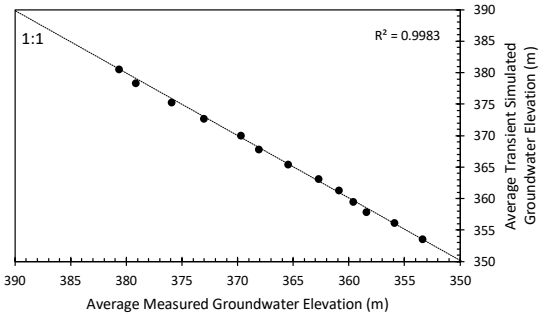

Chart 12**.** Difference between average simulated transient and average measured groundwater elevations.Bench locations in black fill and slope locations in white fill. Listed left to right in descending elevation from top of the dam.

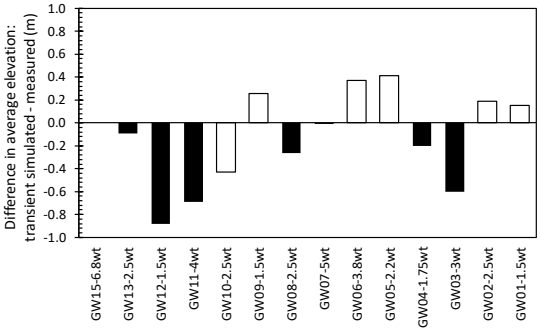

5.5 Sensitivity Analyses

Sensitivity analyses were conducted on the material properties using the steady state boundary condition to quantify the fractional change in the elevation of the water table and the seepage flux rates at Toe C, B, A and the perimeter ditch. The change in the values was varied based on the calibration experience and the reference values and are listed in Table D1 of Appendix D. The simulations were allowed to come to steady state and often run for 5000 days to achieve this. A parameter was sensitive if the value changed by ± 25%.

For changes to the elevation of the water table, the percentage change of the geometric mean of the 14 wells/observations points was calculated (Tables 23 and 24) and determined to be insensitive to all changes. The percentage change at each individual well/observation point was also calculated and the maximum change was 0.5 % (1.9 m rise) at GW13-2.5wt for a 50 % decrease in K_h in Zone 9 (Contained Beaching). Neighbouring GW12-1.5wt had a 0.4 % (1.6 m rise) change, and the other wells/observations points on Bench D, Bench C, and Slope C had more change (for both ways of variance) than the majority, which were less than 0.05 %. The reduction in K_h in Zone 7 (Lower Beach) also had a similar, but attenuated, effect. An increase in the K_h for both these zones had the opposite, but again attenuated, effect. It was notable how changes to the zones located at the base of the section could raise the water table by almost two metres near the crest of the dam. In other words, the rate of basal groundwater flow impacted the elevation of the water table.

The seepage rates at the perimeter ditch, Toe A, and Toe C were most sensitive to changes in horizontal hydraulic conductivity in Zones adjacent to these seepage faces. Additionally, changes to K_h propagated changes to the seepage rates upwards (towards the top of the dam) rather than downwards into the adjacent Zone leading to a redistribution of the discharge. For example, an increase in K_h in Zone 1 (Sand Bench) resulted in an increased seepage discharge across the perimeter ditch (+105 %) and a decrease seepage discharge across the above Toe A (-99 %) by roughly equal percentages; the perimeter ditch stole water from Toe A. However, a decrease in Zone 1 K_h resulted in an unequal distribution with a percentage change of +164 % at Toe A for a -52 % change at the perimeter ditch. Of all the seepage faces, Toe A was the most sensitive with a +325 % change when the K_h of Zone 2 was

increased by 50%. The inverse variance did not have as large of an effect with only a -99 % change. Toe A either steals or gives water to Toe B, the seepage face above, but not to the perimeter ditch below.

Changes in Zone 9 (Contained Beaching) not only influenced seepage discharge at the adjacent Toe B, but also influencing seepage discharge at Toe C.

In general, the seepage faces were insensitive to changes in residual saturation, porosity, alpha, and n except for n at Toe A which had a 33 % decrease in seepage flux for a 125 % increase in the value of n, and a 31 % increase for a 25 % increase in the value of n. N is a fitting parameter of the van Genuchten equation and is a measure of the pore size distribution. It increases with increasing grain size (sand 2.68, silt 1.37, clay 1.09 (Rosetta Lite, 2003)) and in this case it appeared to restrict seepage as it increased in value (became more clay like) which is somewhat counter-intuitive. Toe B seepage face mimicked Toe A, but the perimeter ditch did not and either discharged more water (with an increase in n) or less water (with a decrease in n). Toe A also showed some minor sensitivity to an increase in alpha.

Table 23. Results of sensitivity analyses (percentage change[22] from calibrated steady state values). Value's in bold are >25 % change.

Parameter	Change	Water table	Perimeter ditch	Toe A	Toe B	Toe C
K_h Sand Bench (1)	↑	0	**104.8**	**-98.8**	-1.6	0.1
K_h Sand Bench (1)	↓	0	**-52.7**	**164.7**	0.9	0
K_h Bench A (2)	↑	0	-4.0	**325.3**	**-69.1**	-4.1
K_h Bench A (2)	↓	0	1.9	**-99.6**	**50.4**	2.5
K_h Bench B (3)	↑	0	-0.1	4.2	15.3	5.7
K_h Bench B (3)	↓	0	0.1	-2.1	-7.7	-8.6
K_h Bench C&D (4)	↑	-0.1	0	-0.1	-0.3	1.8
K_h Bench C&D (4)	↓	0	0	0	0.1	-0.8
K_h Toe B (5)	↑	0	0.1	-2.5	11.8	-3.3
K_h Toe B (5)	↓	0	0	1.2	-5.7	2.0
K_h Toe C (6)	↑	0	0	-0.7	-2.1	**48.0**
K_h Toe C (6)	↓	0	0	0.4	1.8	-17.3
K_h Lower Beach (7)	↑	0	0	0.4	1.5	12.2
K_h Lower Beach (7)	↓	0	0	-0.4	-1.4	-8.1
K_h Upper Beach (8)	↑	0	0	0.1	0.5	2.1
K_h Upper Beach (8)	↓	0	0	-0.3	-0.4	-1.7
K_h Contained Beaching (9)	↑	0.1	-0.2	7.0	**114.6**	**65.6**
K_h Contained Beaching (9)	↓	0.1	0.2	-6.9	**-57.4**	**26.5**
K_h/K_v (global)	↑	0	4.3	**76.2**	-7.9	-9.9
K_h/K_v (global)	↓	0	-11.7	**-47.3**	18.6	**-236.6**
Residual Saturation (global)	↑	0	0	0	0	0
Residual Saturation (global)	↓	0	0	0	0	0
Porosity (global)	↑	0	0	0	0	0
Porosity (global)	↓	0	0	0	0	0
Alpha (m^{-1}) (global)	↑	0	-8.6	20.1	4.2	-1.1
Alpha (m^{-1}) (global)	↓	0	1.0	-1.7	-0.6	-0.1
n (global)	↑	0.1	14.9	**-32.7**	-8.3	-1.9
n (global)	↓	0	-8.6	**30.6**	4.8	-1.9

↑ increase in value ↓ decrease in value

Table 24. Summary sensitivity analyses at seepage locations

Seepage flow location	Most sensitive to changes in:
Perimeter Ditch	Increase & decrease in K_h at Sand Bench (1)
Toe A	Increase & decrease in K_h at Sand Bench (1) Increase & decrease in K_h at Bench A (2) Increase & decrease in K_h/K_v (global) Increase & decrease in n (global)
Toe B	Increase & decrease in K_h at Bench A (2)

[22] $[(X_2 - X_1) / |X_1|] * 100$ = percent change from X_1 to X_2

	Increase & decrease in K_h at Contained Beaching (9)
Toe C	Increase in K_h at Toe C (6)
	Increase & decrease in K_h at Contained Beaching (9)
	Decrease in K_h/K_v (global)

During the calibration process using the transient boundary condition, changes to the material properties resulted in subtle but important changes to the groundwater elevation curves at each of the 14 wells/observations points. Changes to the hydraulic conductivities (K_h and K_v) shifted the water table upwards or downwards with almost no change to the shape of the curve. Specifically:

- An increase in K_h = decline in the water table; and vice versa
- An increase in anisotropy ratio (decrease in K_v) = decline in the water table; and vice versa

The shapes of the groundwater elevation curves were somewhat affected by changes to the residual saturation, porosity, alpha, and n values. Specifically:

- An increase in residual saturation = minor to moderate increase in curve amplitude; and vice versa
- An increase in porosity = minor decrease in curve amplitude; and vice versa
- An increase in alpha = moderate to major decrease in curve amplitude; and vice versa
- An increase in n = moderate decrease in curve amplitude; and vice versa

5.6 Mass Balance Error

HYDRUS calculates the absolute and relative mass balances for water for each region at each of the chosen print times (the time at which data are displayed and outputted). The entire modelled section was designated as one region with 83 print times. The relative water balance error ranged from 0.014 % to 0.022 % across the 2555 day run time, indicating that the inflow water rates were equal to the outflow water rates meaning the system was balanced.

5.7 Solute Output

To test the model's ability to predict the TDS concentration, simulated data (using a transient boundary flow condition) were compared against measured groundwater data at one shallow location (GW02) located near the base of the dam (Chart 13). As laboratory TDS concentration data were not available for the observation point of GW02-2.5wt, the data from closest well GW02-03 were used instead. The vertical distance between these two wells was approximately 0.5 m and therefore considered to analogous. The simulated and the measured data were in reasonably good agreement although the measured TDS concentration was declining at a faster rate[23] than the simulated TDS concentration. It was not expected that the simulated values would exactly match the measured values as groundwater samples are subject to natural variation in concentrations and the goal of the model was to simulate the entire modelled section, not a specific locale, therefore precisely matching the data were not

[23] Mann Kendall trend evaluation, decreasing, S value of -20

essential. However, this test lent confidence that the model could reasonably predict future TDS concentrations.

Chart 13. Simulated and measured TDS concentrations vs. time at GW02-2.5wt and GW02-3. (transient flow boundary condition).

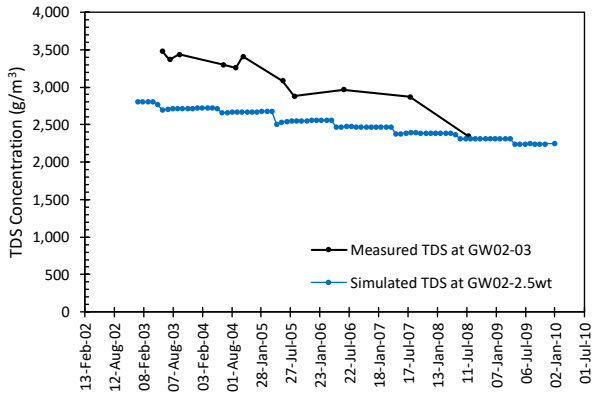

6. FUTURE FLOW AND TRANSPORT SCENARIOS

Three future scenarios were simulated to evaluate the change in groundwater elevation, TDS distributions, and salt flushing times:

- Future I: 200 years of flow and solute transport with 2003 configuration (partial cover applied to lower dam section)
- Future II: 200 years of flow and solute transport with three different covers (applied to entire boundary length) and hummocky terrain:
    - 50 mm/y of recharge
    - 24 mm/y of recharge
    - 5 mm/y of recharge
- Future III: 200 years of flow and solute transport with 50 mm/y recharge rate (cover) and flat terrain

For simplicity, one year was assumed to have 365 days leading to the exclusion of 47 leap days over the course of the 200 years run time. This did not impact the results as the difference in groundwater elevation and solute concentration are gross yearly estimates and not predictive of a specific future day.

The upper boundary received different timings of recharge depending on whether a constant or variable flux was applied. The boundary under steady state conditions received a constant daily flux every day of the year (365 days), whereas under transient conditions the boundary received one of three daily fluxes: no flux over winter; spring melt flux over the first 10 days in April; and rain flux between mid-April and the end of October. This worked out to 151 days of no flux (November 1 to March 31), 10 days of spring melt flux (April 1 to 10), and 204 days of rain flux (April 11 to October 31).

The solute boundary conditions varied based upon the prescribed future surface cover. The upper boundary flux was assigned a constant concentration of 3300 g/m^3 at the pond and 0 g/m^3 for the remaining boundary along the dam surface for the Future I scenario (description in following section). All other scenarios used a boundary flux concentration of 0 g/m^3 including at the constant and variable heads of the two ditches. These two ditches collected both seepage and precipitation water and although they reported TDS concentrations of around 3000 g/m^3 (May 2003, staff gauge wells) it was assumed that dilution from precipitation would be available.

To test for differences between the specification of a constant or a variable boundary condition, both cases were applied to the future simulations I and II.

6.1 Future I: Partial cover, as-is scenario

6.1.1 Methods

This future scenario used the 2003 configuration with a cover applied to the lower dam face, no cover on the upper dam and beach, and a central pond (Fig. 11). The recharge was applied to the boundaries in daily time steps for a total of 73,00 days of flux. The variable flux lengths were calculated by taking the calibrated geomean 2003-2009 recharge snow melt equivalents for each boundary (No. 1 0.065 m, No. 2 0.063 m, No. 3 0.049 m) and dividing it evenly over the 10 days of the spring melt (Table 25). The same was done for rainfall recharge (No. 1

0.120 m, No. 2 0.027 m, No. 3 0.022 m) and evenly distributed over 204 days. There was no recharge flux applied during the winter months. The three constant heads assigned during the calibration process were retained with year-round ponding depths of 0.055 m and 0.05 m (ditch at Toe C and ditch at Toe B, respectively) for the steady state boundary condition, and seasonally assigned these depths between April 1 and October 31 for the transient boundary condition. Between November 1 and March 31, the heads were zero. The pond was consistently 1 m deep for both boundary conditions. This simulation represented an unlikely future scenario, but was useful for setting a benchmark of a "do-nothing" reclamation plan. It was also a scenario reported by Price (2005) ("current steady state flow system") and therefore provides a comparison point between the two studies.

Table 25. Future I simulated daily recharge rates for steady state and transient boundary conditions for partial cover.

Boundary No.	Transient Boundary			Steady State Boundary
	SWE	Rain	Winter	SWE+Rain
	m/d	m/d	m/d	m/d
1	0.00651	5.89×10^{-4}	0	5.18×10^{-4}
2	0.00629	1.34×10^{-4}	0	3.52×10^{-4}
3	0.00490	1.07×10^{-4}	0	1.38×10^{-4}

6.1.2 Results

Particle tracking was used to determine groundwater travel times from various points along the section (Fig. 18). Particles originating near the top of the dam (five metres beneath the top of the dam) had predicted travel times to the perimeter ditch on the order of five to seven decades. The particle travelling along the groundwater divide did not reach the perimeter ditch after 200 years, but forecasting its future path placed it there in around 225 to 250 years' time. This value is similar to that predicted by McKenna (2001) (250 years). The shortest travel times were along the dam face with travel times around one decade for particles originating from around two metre's depths. Particle tracking also indicated that recharge applied on Bench C and Slope C discharged at Toe C, recharge applied on Bench B discharged at Toe B, and recharge applied to Bench A discharged at Toe A. To the west of the groundwater divide, the particles nicely illustrated the stagnation and very slow travel times of the groundwater there.

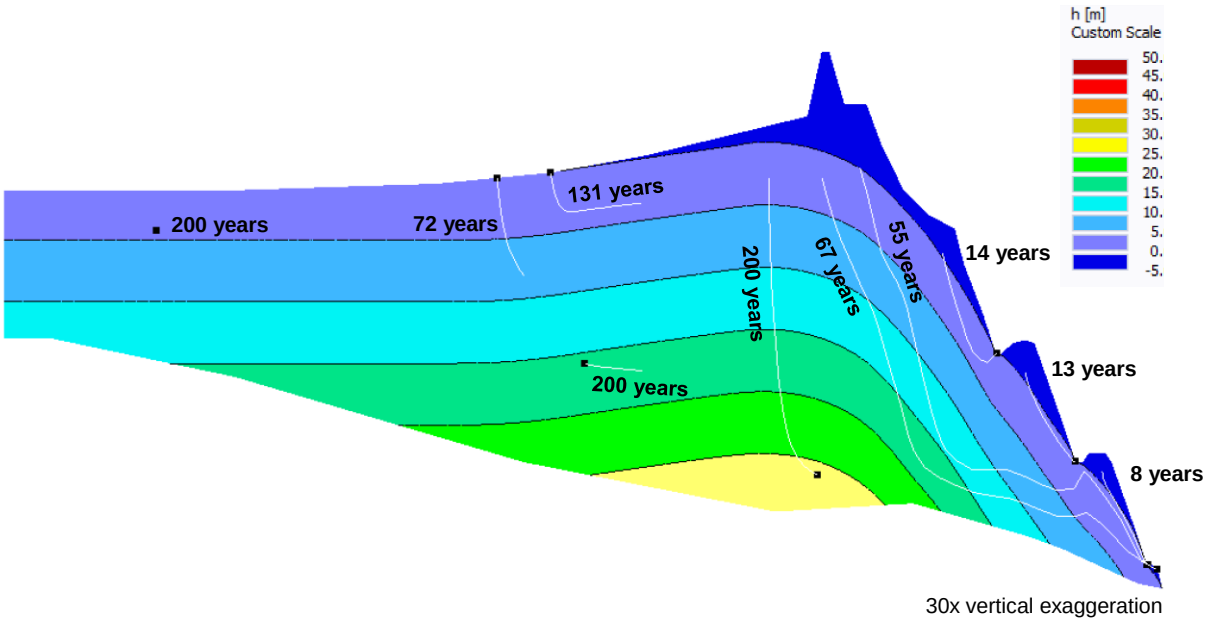

Figure 18. Future I: Particle tracking after 200 years using the steady state boundary condition (trajectories in white, particles black square)

Particle tracking using the transient boundary condition demonstrated similar travel times as the steady state boundary condition, except for the particle travelling along the groundwater divide which turned slightly westward (instead of eastwards) near the base of the dam. Also, the “55 year” particle deviates more upwards towards the Toe B ditch, coming within 0.70 m laterally and vertically to it. By comparison, the particle under steady state BCs came within 18 m laterally and 1.7 m vertically. The flow paths within Bench A illustrated the upward deviation in the migration pathways towards the Toe B ditch before continuing onwards to the perimeter ditch. This upward pull was observed during the model calibration process and resulted in the highest horizontal hydraulic conductivities and anisotropies being applied to the two lower most zones (Sand Bench (1), Bench A (2)) in order to “push” the groundwater laterally and mitigate this mounding.

The simulated velocity vectors indicated that overall groundwater is either flowing laterally westwards or eastwards except for at, below, and adjacent to the ditches at Toes C and B where flow is upwards. The elevation of the water table did not changed over the course of this simulation.

The two boundary conditions produced similar TDS concentration and mass flux results at the observation points and the seepage faces (Charts 14 to 19). The cumulative TDS mass flux after 200 years was about 2800 kg at the Perimeter Ditch, 4600 kg at the toe of Slope A, 4600 kg at the toe of Slope B, and 3700 kg at the toe of Slope C, for a total flux of about 15 megagrams (Mg) (aka tonnes). The total groundwater discharge over this same period was around 16 km^3/km. The lower down the dam, the better the agreement between the steady state and transient boundary conditions mass flux value, although the differences at Toe C and B were insignificantly minor (Charts 14 and 15).

Chart 14. Future I cumulative TDS mass flux at Toes C and B

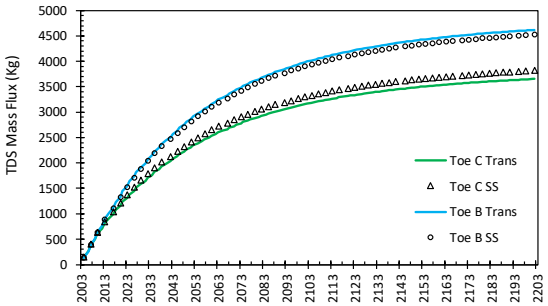

Chart 15. Future I cumulative TDS mass flux at Toe A and PD

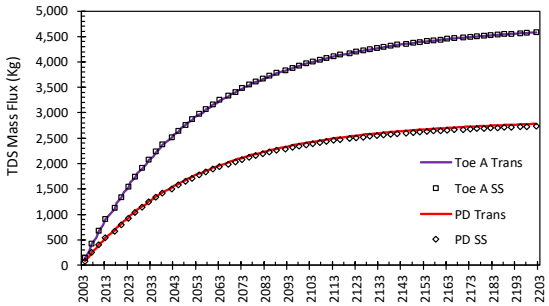

The TDS concentration declined steadily at all four seepage boundaries such that the discharge concentrations were around 400 g/m^2 at 100 years run time (2103) and less than 100 g/m^2 at 200 years run time (Chart 16). The exception was the concentration at Toe A which, due to the reduced water flux (previously illustrated on Chart 8), always reported an excessively elevated TDS concentration[24]. The concentration at a closest observations points of GW01-1.5wt (Chart 19) and GW27 (located on the boundary at the base of Toe A) were in-line with those at the perimeter ditch, therefore the data for mesh-line A were excluded for being erroneous.

Chart 16. Future I TDS concentration at Toes C, B and PD for steady state and transient BCs

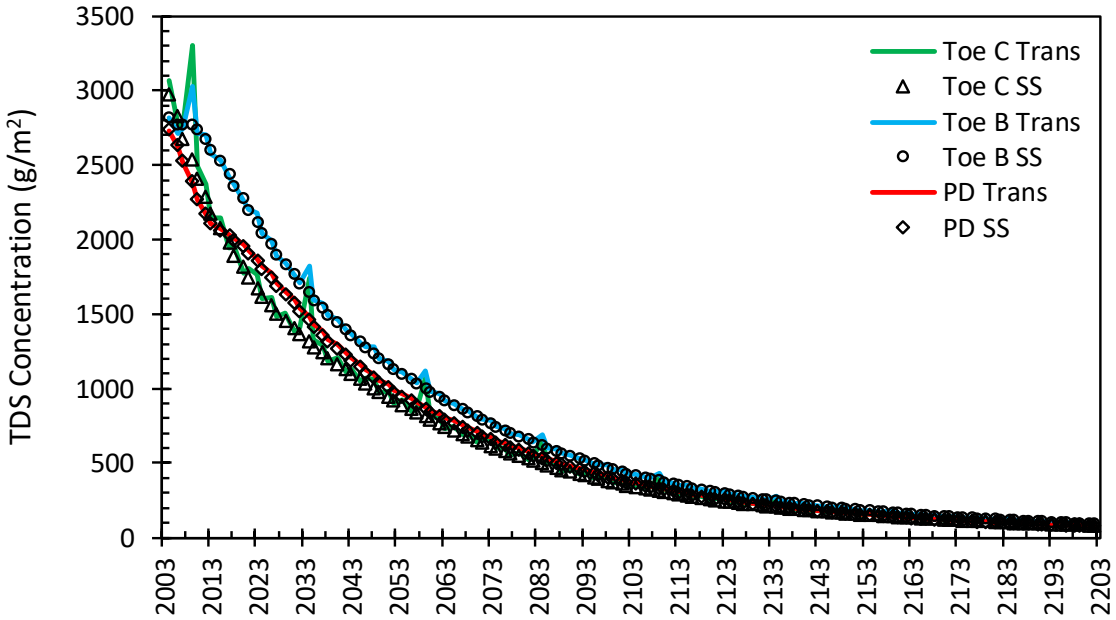

The TDS concentration curves at the observation points indicated that the TDS concentration decreased rapidly within the first 30 years before tailing off (Charts 17 to 19). This was especially pronounced at those locations on the upper half of the dam where more dilution was possible. The curves best fit (0.99 coefficient of determination (R^2)) a power function with

[24] HYDRUS (2D/3D) (Šejna et al, 2017) reports water and mass flux along mesh-lines, not concentration. Concentration was calculated manually by dividing the mass flux by the water flux at each print time.

exponents around -3.5. The steady state and transient boundary conditions produced similar results as illustrated by the overlaid datasets for observation points for wells GW1-1.5wt, GW9-1.5wt, and GW12-1.5wt (Chart 19).

Chart 17. Future I TDS concentration at observations points with steady state BC

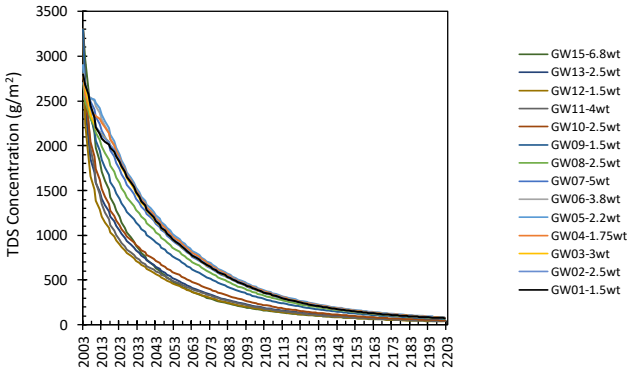

Chart 18. Future I TDS concentration at observation points with transient BC

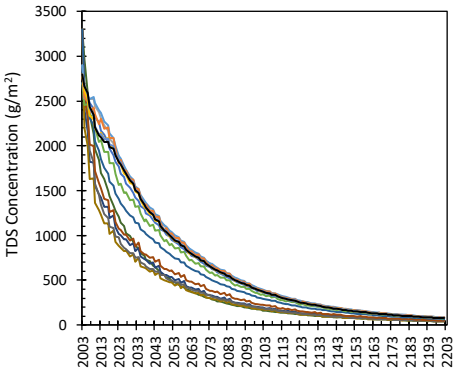

Chart 19. Future I TDS concentration at GW12-1.5wt, GW9-1.5wt, and GW1-1.5wt with steady state and transient BCs. Time interval of 570 days for the transient data; 1140 days for steady state data. Locations of wells illustrated on Fig. 5 and App H.

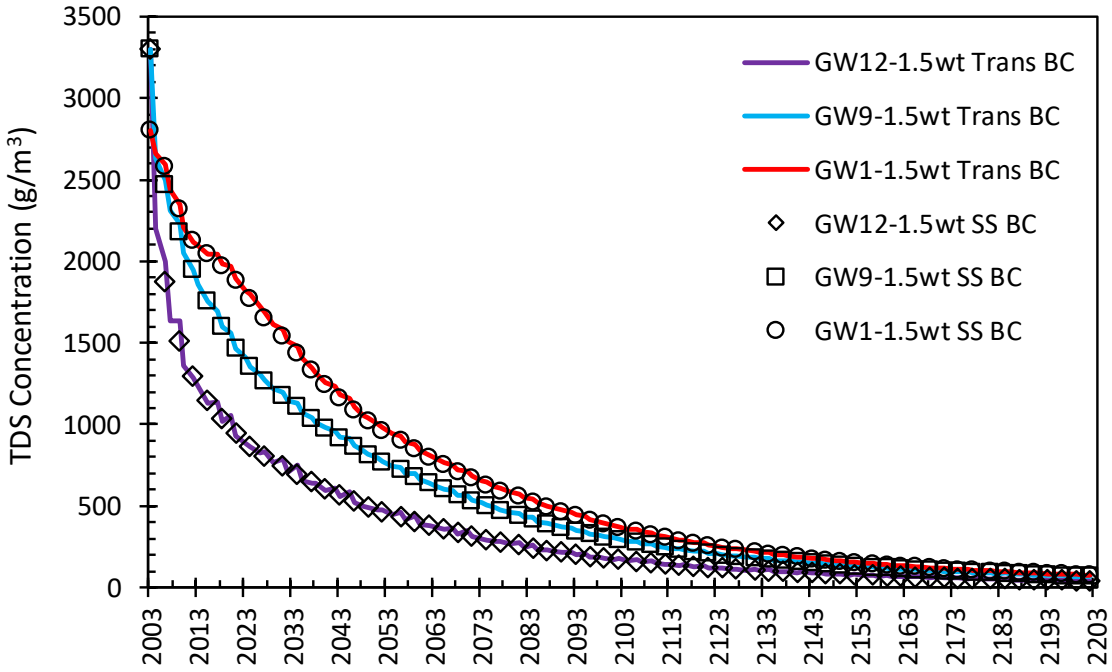

The model predicted that in 200 years' time, the entire dam and half of the beach will be flushed by fresh recharge water to a concentration of less than 300 g/m^2 (Fig. 19). The pond area remains almost unchanged throughout the entire simulation, as was expected as a constant TDS concentration of 3300 g/m^3 was applied to that boundary. The TDS distribution was almost identical for both boundary conditions, except for some minor differences in the concentrations upwelling to the ditch at Toe C and along Slope A. These differences reflect the slightly faster dilution occurring along the dam face between Bench B and the Perimeter

Ditch due to the constant application of recharge with the steady state condition versus the intermittent application with the transient conditions.

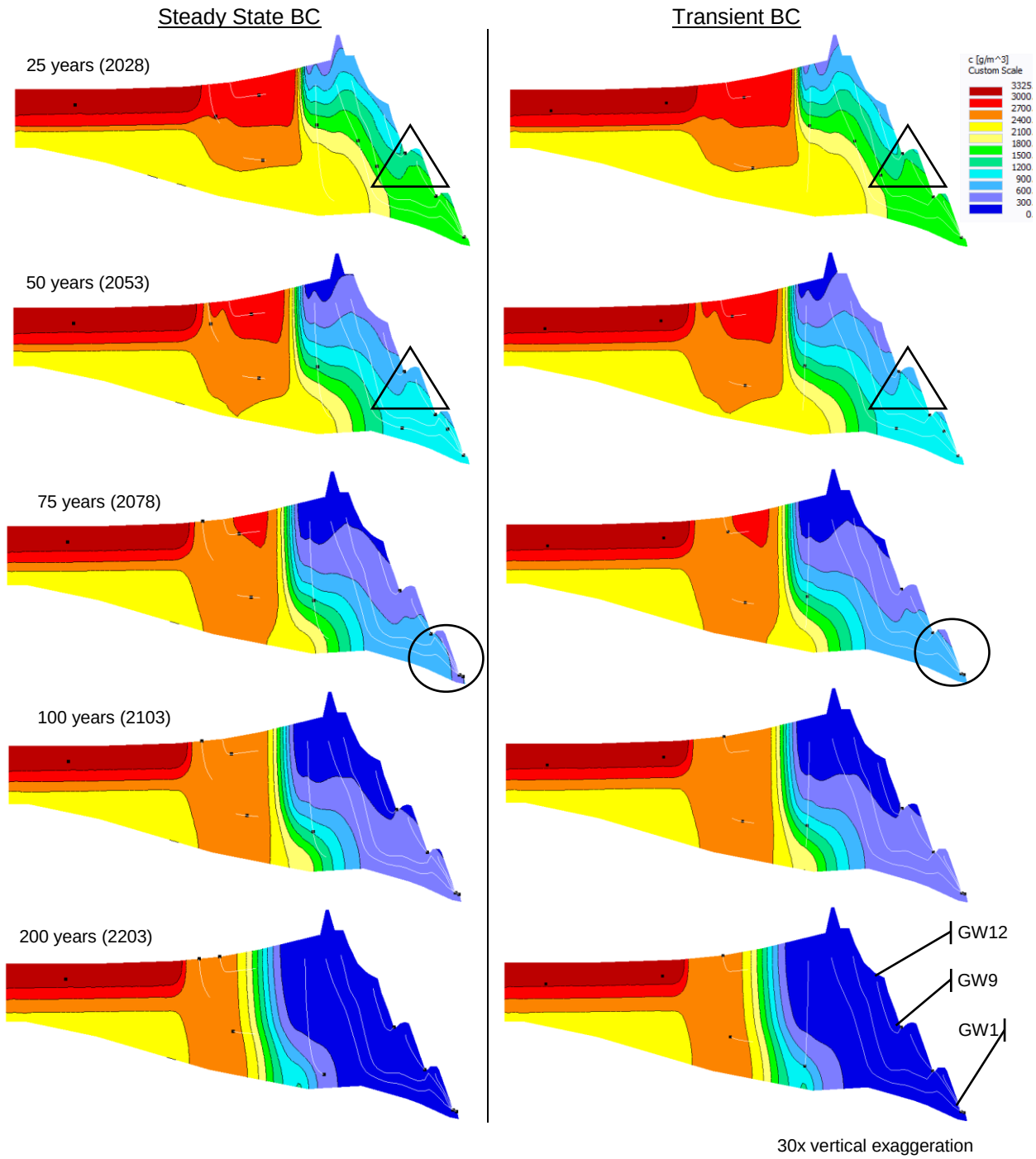

Figure 19. Future I: TDS distribution predictions (g/m^3) for both boundary conditions at 25 years, 50 years, 75 years, 100 years, and 200 years (g/m^3). Particle trajectories (white) and particles (black). Areas of difference denoted with black triangles(Bench B) and circles (Bench A).

Based on the highest velocity in the simulation the maximum Peclet number was 4.99, which was a reasonable value. The HYDRUS developers recommend a Peclet number less than 5 to avoid oscillatory behavior. The Courant number was constrained between 0.2 and 1 which

was also considered to be reasonable as it indicated that fluid particles were moving from one cell to the next within one time step.

6.2 Future II: Full hummocky cover, three scenarios

6.2.1 Methods

The impact of three different rates (covers) were evaluated over a period of 200 years: 50 mm/y; 24 mm/y; and 5 mm/y. These aquifer recharge rates were previously simulated by Price (2005) who's rational was derived from infiltration data in Skopek's (1996) study of local reclaimed mine areas. Skopek proposed infiltration rates ranging between 50 to 100 mm/y, but with the data favoring the low end of the scale, a threshold of 50 mm/y was set as the largest simulated recharge rate. The two lower rates were chosen to simulate more restrictive covers at 5.5 % of the averaged annual precipitation (AAP)[25] (24 mm/y) and 1 % of AAP (5 mm/y). The recharge was applied daily and assumed to be evenly distributed both spatially and temporally[26] over the boundary representing an ideal condition.

To calculate how much of the 50 mm, 24 mm, and 5 mm recharge to apply during the 10 days of spring melt and how much during the remaining 204 days, the calibration worksheets were consulted and determined that aquifer recharge below the covered benches and slopes (boundaries No. 2 and No. 3) was composed of 70 % snow melt and 30 % of the rain fall. These percentages were used to portion the recharge into a variable boundary condition that was applied daily to the entire upper boundary, except for seepage faces (Chart 20, Table 26).

The daily flux rate for the steady state condition was simply the annual recharge (50 mm, 24 mm, or 5 mm) divided by the number of annual days (365).

- 50 mm/y
  - SWE 70 % x 50 = 35 mm
  - Rain fall 30 % x 50 = 15 mm
- 24 mm/y
  - SWE 70 % x 24 = 16.8 mm
  - Rain fall 30 % x 24 = 7.2 mm
- 5 mm/y
  - SWE 70 % x 24 = 3.5 mm
  - Rain fall 30 % x 24 = 1.5 mm

Chart 20. Future II recharge split into SWE and rain fall

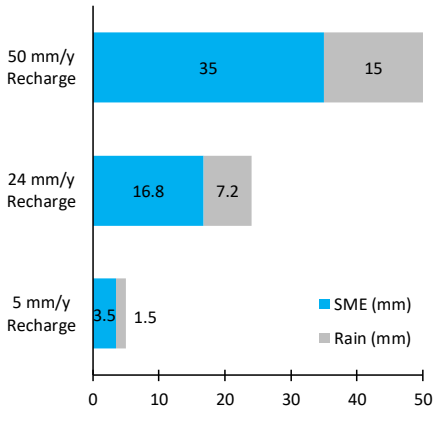

[25] Environment Canada averaged annual precipitation 1971-2000 was 456 mm (Price, 2005)
[26] Spring melt distributed over the first 10 days of April; rain distributed evenly over half-April to end October.

Table 26. Future II simulated daily recharge rates for steady state and transient boundary conditions for three covers.

Future Recharge Scenario	Transient Boundary			Steady State Boundary
	SWE	Rain	Winter	SWE+Rain
mm/y	m/d	m/d	m/d	m/d
50	0.0035	7.4×10^{-5}	0	1.4×10^{-4}
24	0.0017	3.5×10^{-5}	0	6.6×10^{-5}
5	3.5×10^{-4}	7.4×10^{-6}	0	1.4×10^{-5}

The water filled ditches at the toes of Slopes C and B were retained, and either assigned constant heads of -0.010 m (ditch at Toe C) or 0.01 m (ditch at Toe B), or variable heads of the 0.055 m and 0.05 m between April 1 and October 31. To simulate winter conditions, the head of the ditches was set to zero between November 1 and March 31.

A few changes were made to the geometry of the calibrated model to better reflect Future II configurations (Fig. 20). The central pond was removed by elevating the ground surface by one metre (383 m geodetic) and low profile hills[27] (simulating hummocks) were added. The western vertical boundary was changed from no flux to free drainage to allow groundwater to leave the section from this side, simulating groundwater migration towards a future central drainage ditch. Although a free drainage boundary condition is intended only for a lower boundary, as by definition it simulates downward/gravitation flow, it produced better results than a seepage boundary (which led to a drastic decline in the water table or model non-convergence). The water and solute flow across this western vertical boundary was not included in the results as the central drainage ditch will not interact with the cover in the modelled section. These changes resulted in a 5 % increase in the number of nodes (6689), a 10 % increase in the number of 1D elements (1486), and a 5% increase in the number of 2D elements (12,789).

[27] Dimensions x = 400 m, z = 2 m

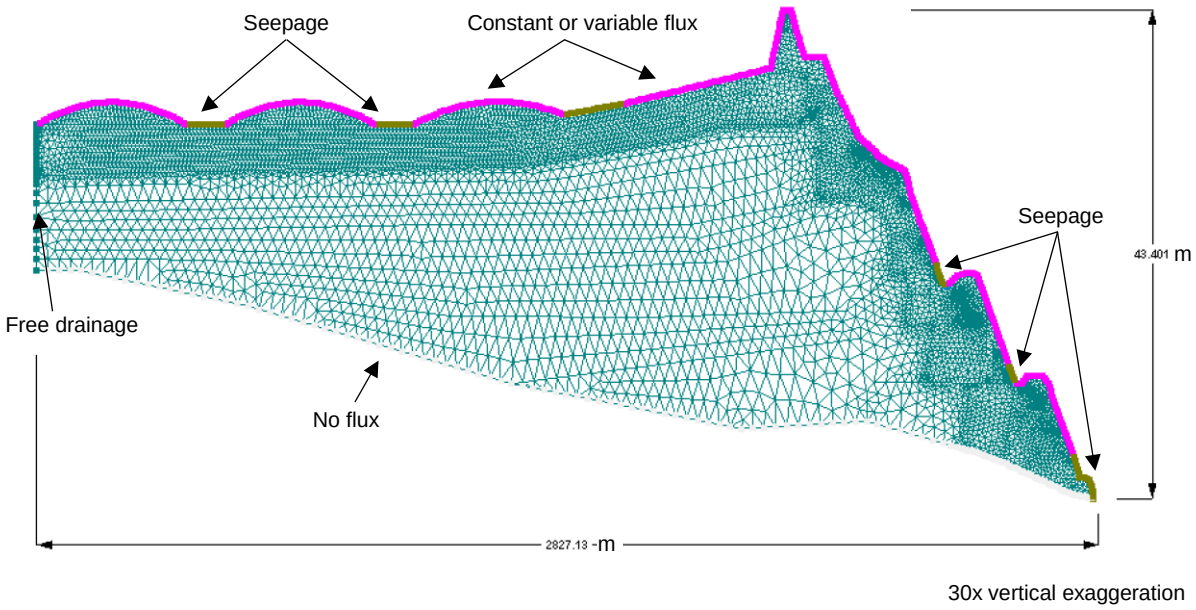

Figure 20. Future II geometry, mesh, and boundary conditions

6.2.2 Results

The model simulated the three different covers scenarios with the hummocky terrain. As with the Future I, the choice of a constant or a variable boundary condition had minimal impact on the results; The TDS distributions were similar (Fig. 21) and the concentrations at the observation points correlated well (Chart 21). Minor differences in the TDS distribution were observed along the tops of the hummocks where the model predicted more dilution along the tops of the hummocks with the steady state BC, and more dilution along the lower dam face with the transient BC. Although, dilution was observed along the lower dam face for both boundary conditions, the transient BC illustrated it better. When studied at a reduced vertical scale (closer to natural), the dilution force of the Toe C ditch, Bench B, and Bench A was observed in the concentration gradients (Fig. 22).

The hummocks created distinct patterns in the TDS distribution (Fig. 21, 24 and 26). Dilution occurred along the tops without causing the groundwater to mound and breach the boundary. The seepage faces between the hummocks were areas of higher TDS concentration as groundwater migrated towards and discharged there. The model predicted shallow pools to form here, which would gradually decline in TDS concentration over time. Initially the elevated TDS concentration may prohibit re-vegetative efforts, however additional dilution maybe available than simulated as fresh water runoff would collect in these swales. Infiltration would also occur, but this is beyond the current capabilities of the program.

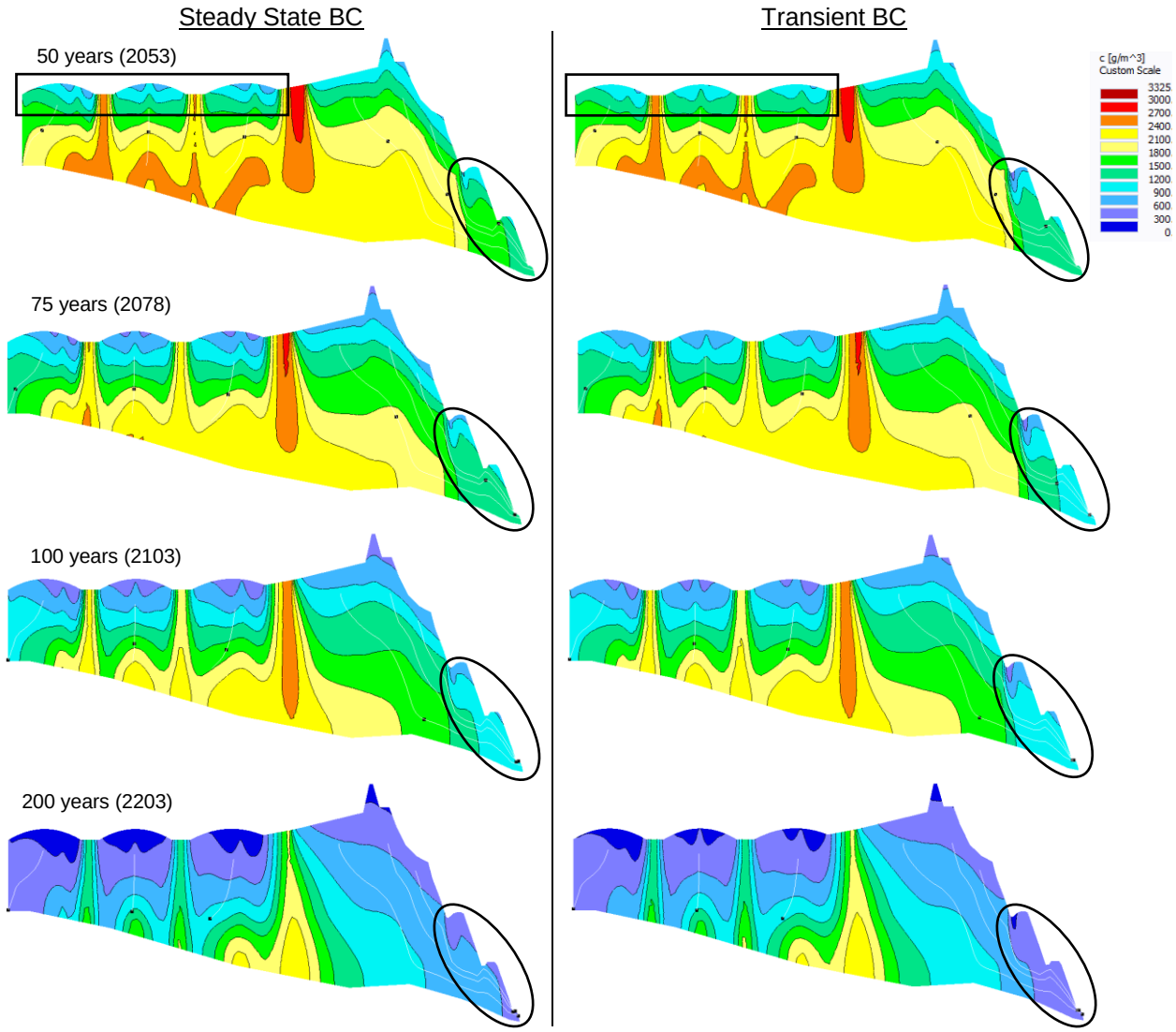

Figure 21. Future II: TDS distribution predictions (g/m^3) both boundary conditions at 25 years, 50 years, 75 years, 100 years, and 200 years with a 50 mm/y recharge rate (cover). Particle trajectories (white) and particles (black). Areas of difference denoted with black rectangles and ovals.

Chart 21. Future II TDS concentrations at GW12-1.5wt, GW9-1.5wt, and GW1-1.5wt with both steady state and transient BCs and a 5 mm/y recharge rate (cover).

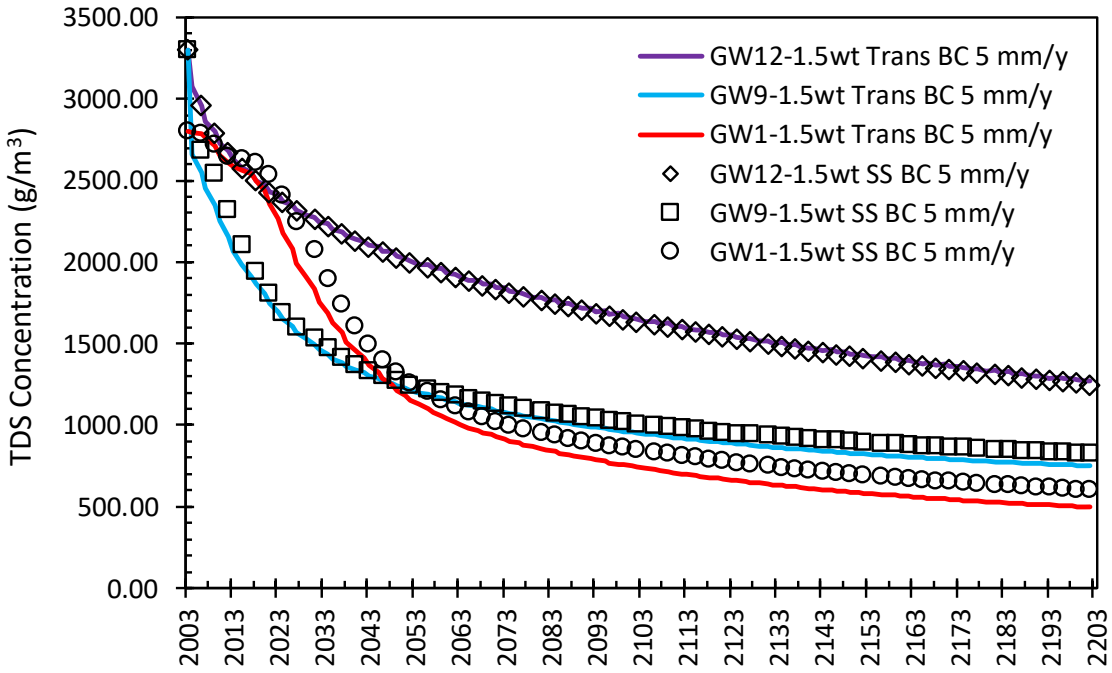

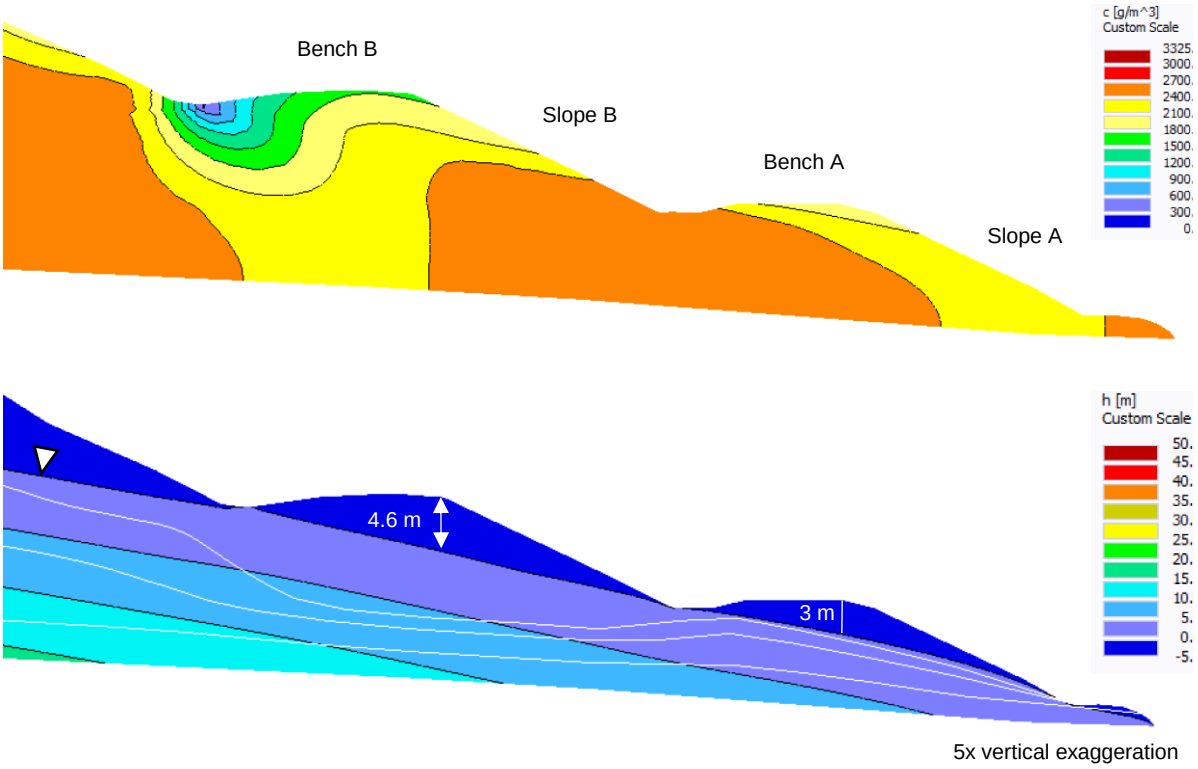

Figure 22. Future II: Bench B to Perimeter Ditch TDS distribution prediction (g/m^3) and pressure heads (m) , transient BC at 7.5 years (2011) with a 50 mm/y recharge rate (cover). Five times vertical exaggeration to demonstrate the effect of dam topography on solute dilution.

As both boundary conditions produced similar results, only the transient one will be presented here for clarity. Steady state data tables are appended in App. F.

For all three covers, the cumulative TDS mass flux resulted in between 4 to 5 Mg of TDS being discharged at the perimeter ditch over 200 years (Chart 22, Table 27). This is around half that predicted in Future I. The rate of increase was generally linear at all the dam seepage faces (data not presented) except at Toe C, which went dry under the 24 mm and 5 mm rates (covers) due to a declining water table. The largest mass flux was predicted at Toe A. The total TDS mass flux ranged between 13 and 19 Mg which was similar to the 15 Mg predicted for Future I. This meant that although the mass flux at the perimeter ditch was half, the overall mass flux from the dam was roughly the same, via a re-distribution to Toes A and B.

Chart 22. Future II cumulative TDS mass flux's at the perimeter ditch, transient BC

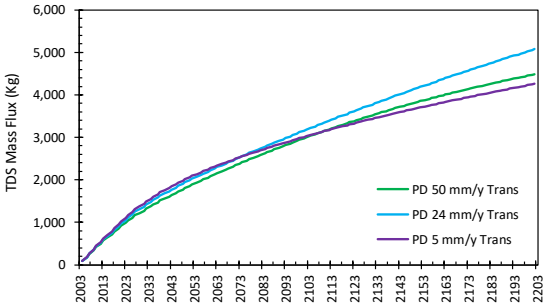

Chart 23. Future II TDS concentrations at the perimeter ditch, transient BC

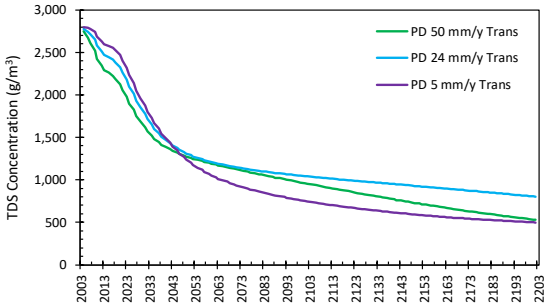

Table 27. Future II Summary: Cumulative TDS mass flux after 200 years, transient BC

Future Recharge Scenario	Perimeter Ditch	Toe A	Toe B	Toe C	Total
mm/y	kg	kg	kg	kg	kg
50	4486	6896	6046	2383ɣ	19,811
24	5078	7138	5204	522*	17.942
5	4261	5541	3124	408**	13,334

ɣ Intermittently dry * Dry after 28 years ** Dry after 14 years

The TDS concentration at the perimeter ditch (Chart 23) and at GW1-1.5wt (Chart 26) had similar concentration curves with a rapid decrease in the first 30 years then slowing with a long tail. This was simulated for all three covers. The decline in the water table (Fig. 23 and 25) slowed the dilution rates in those soils left stranded above it. This combined with the more restrictive covers led to much slower dilution rate which was best observed in the linear curves of the observation points of the upper dam (Charts 24 and 25). This led to a larger spread in the observation point concentrations at the end of the simulations. With a 50 mm/y rate (cover), the difference between the highest and lowest concentrations was around 200 g/m^3, whereas the difference was around 1675 g/m^3 for the 5 mm/y rate (cover).

Chart 24. Future II TDS concentrations at observation points with 24 mm/y rate(cover), transient BC

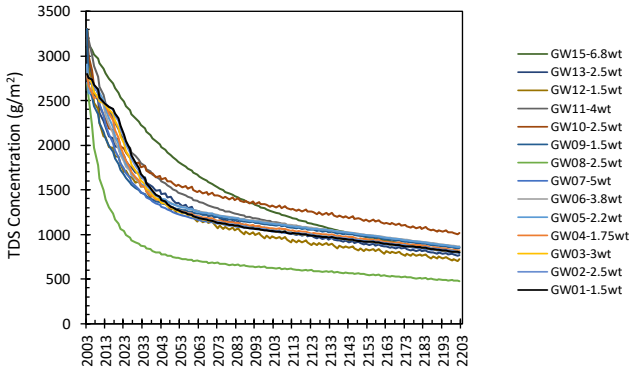

Chart 25. Future II TDS concentrations at observation points with 5 mm/y rate(cover), transient BC

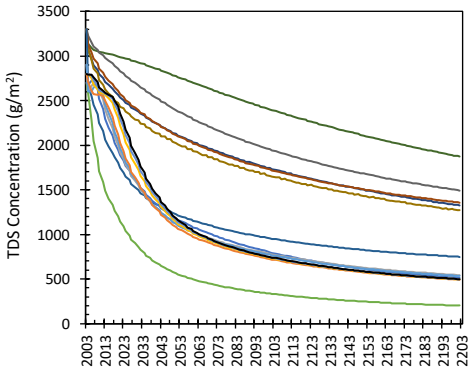

Chart 26. Future II TDS concentration at GW12-1.5wt and GW1-1.5wt, three covers, transient BC.

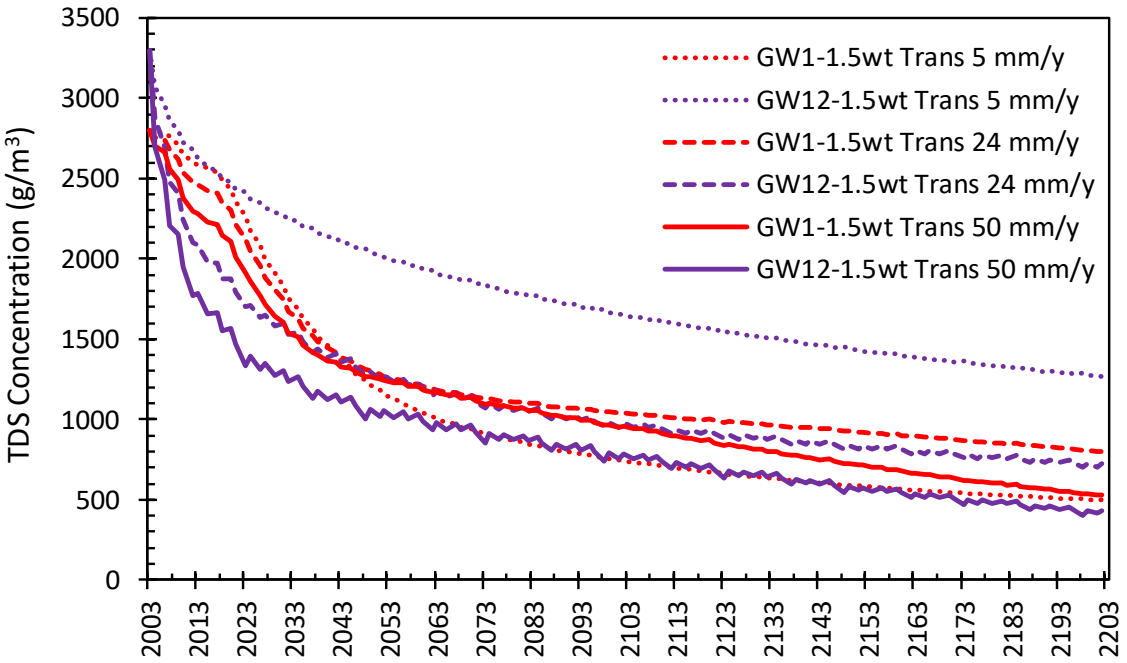

The pressure heads and TDS distribution for all three covers at 25 years (2028) and 75 years (2078) are illustrated on the following Figs. 23 through 26. Reduced recharge rates led to a slower rate of dilution, which was anticipated. Only the lower beach (Bench B, eastern half of Contained Beaching, Bench A, and Sand Bench zones) was relatively unaffected by reduced recharge rates whereas the upper dam, beach, and “pond” areas had significant differences. The impact of the ditch at Toe C was large and was an important source of dilution. However, a word of caution, the simulated ditch water was assigned a boundary concentration of 0 g/m^3 when in fact the ditch collected seepage water from Toe C and previously reported TDS

concentrations around 3100 mg/L[28]. Therefore, this dilution effect may be magnified in the numerical simulations.

For the entire model section, the mean TDS concentration was about 2.5 times lower (927 g/m^3) with the 50 mm/y cover than with the 5 mm/y cover (2160 g/m^3) after 200 years. This represents a 65 % decrease versus a 19 % decrease from the initial mean concentration of 2680 g/m^3.

All three covers led to a decline in the water table until it reached equilibrium. This time was approximately 7 years for the 50 mm/y cover, 8 years for the 24 mm/y cover, and 27 years for the 5 mm/y cover.

The groundwater velocity at the perimeter ditch was consistently around 0.113 m/d (41 m/y) for all three covers. This was slightly slower than the maximum simulated during the calibration process of 0.128 m/y (47 m/y). However, most of the dam, and all the beach and pond areas had velocities less than 0.011 m/d (4 m/y). This is the same seepage velocity used by McKenna (2001) to model salt flushing times. The lower dam (Sand Bench, Bench A, and Contained Beaching zones) had velocities greater than 0.045 m/d (16 m/y).

[28] May 2003

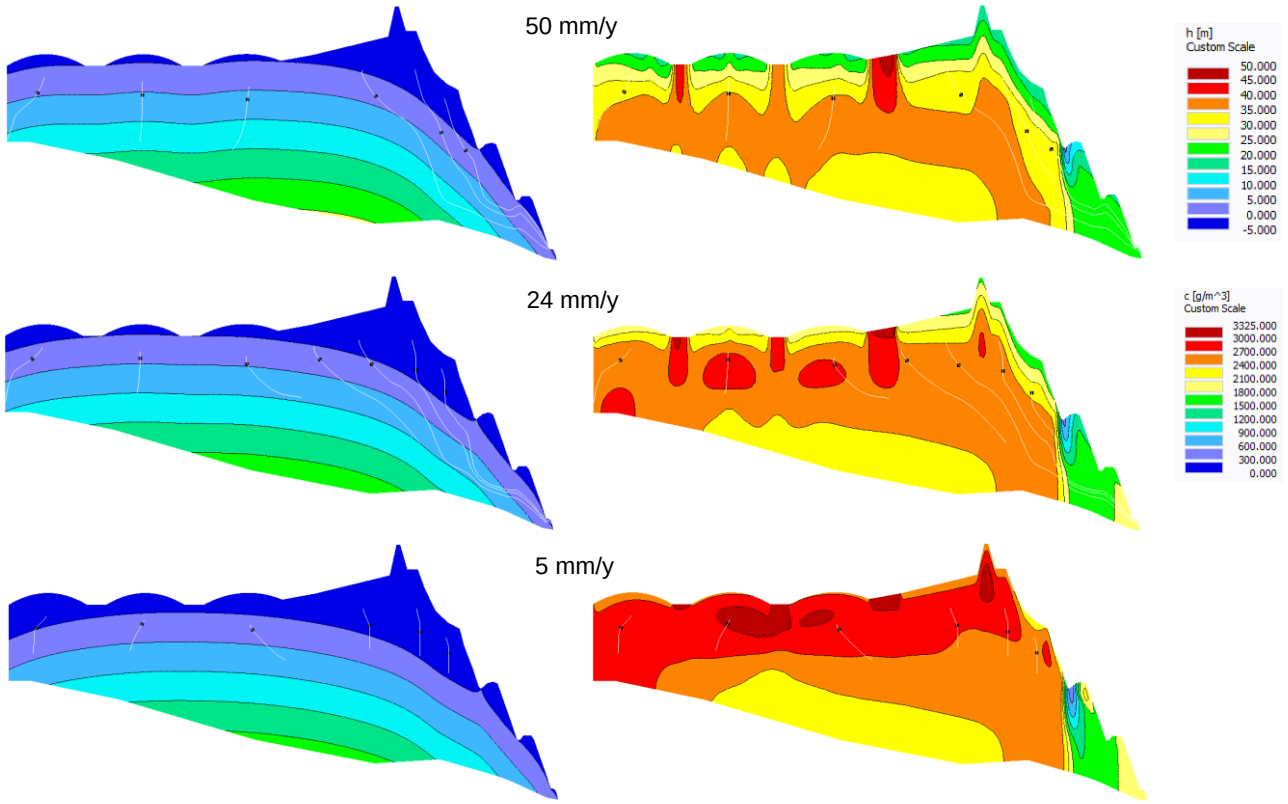

Figure 23. Future II: Pressure heads (m) at 25 years (2028) for all three covers with transient BC. Particle trajectories (white lines) and particles (black dots).

Figure 24. Future II: TDS distribution (g/m^3) at 25 years (2028) for all three covers with transient BC.

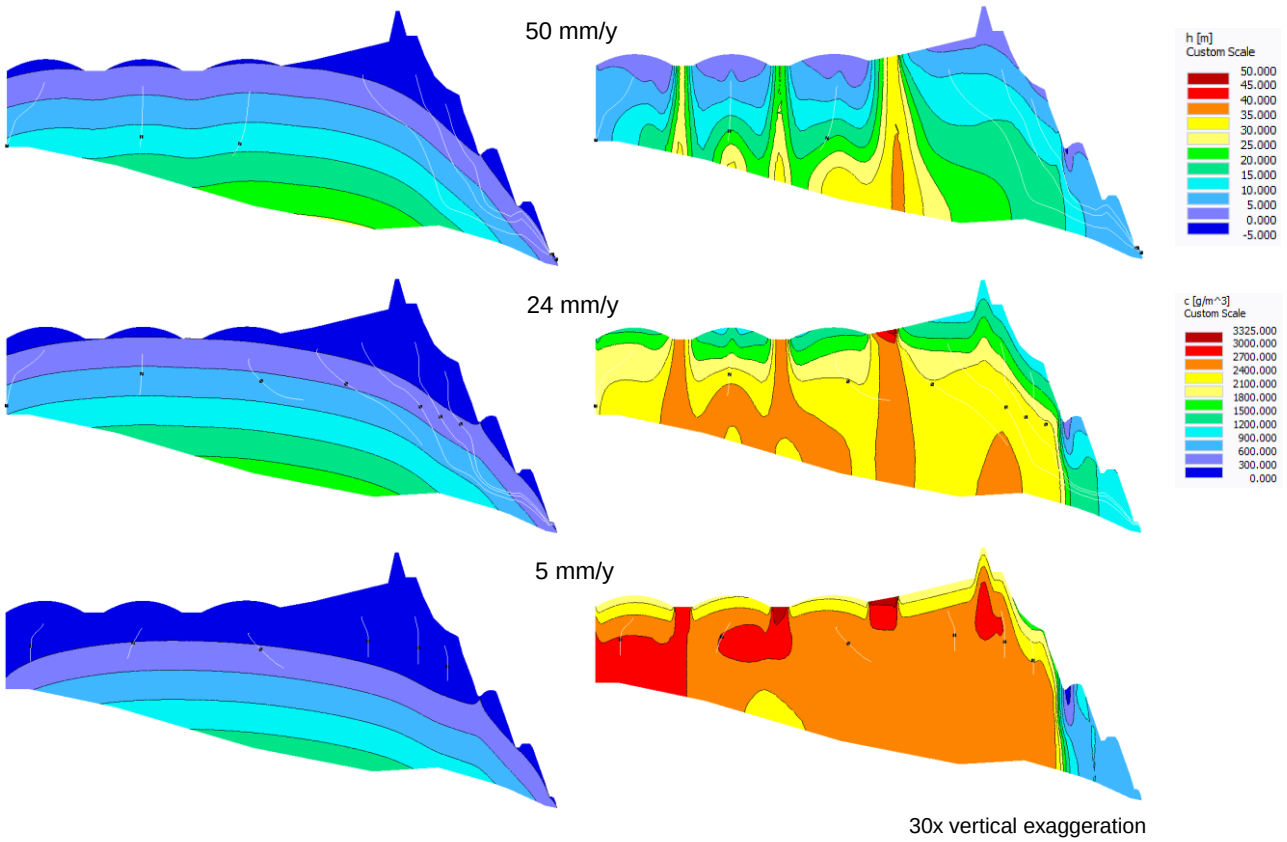

Figure 25. Future II: Pressure heads (m) at 75 years (2078) for all three covers with transient BC. Particle trajectories (white lines) and particles (black dots).

Figure 26. Future II: TDS distribution (g/m^3) at 75 years (2078) for all three covers with transient BC.

6.3 Future III: Full flat cover, 50 mm/y

6.3.1 Methods

As an future alternative to the hummocky terrain, the elevation of the “pond” area was raised three metres (386 m geodetic) and a 50 mm/y recharge rate (cover) was applied under steady state conditions (Fig. 27). For model convergence, the uppermost portion of the western vertical boundary was designated a seepage boundary.

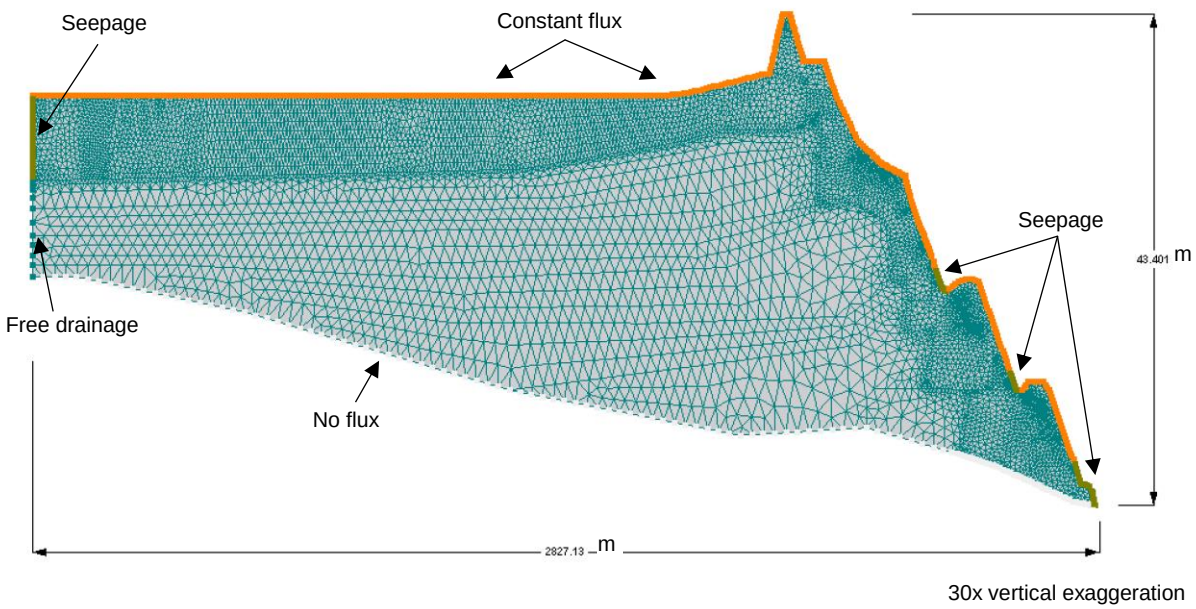

Figure 27. Future III geometry, mesh, and boundary conditions

6.3.2 Results

The application of a flat cover had interesting results. The groundwater mounded appreciably, breaching the boundary, and the divide shifted westwards (Fig. 28). The TDS distribution was altered; Less dilution occurred along the boundary surface, but the > 1200 g/m^3 plume was smaller at the end of the simulation (Fig. 29). The TDS concentrations at GW1-1.5wt were similar in value and decline as with Future II with values of 1902 g/m^3, 1545 g/m^3, 1168 g/m^3, and 684 g/m^3 at 25, 50, 100, and 200 years' time, respectively. The cumulative TDS mass flux at the perimeter ditch was 5280 kg, with a dam total of about 24,265 kg. This is greater than that predicted with the hummocky terrain.

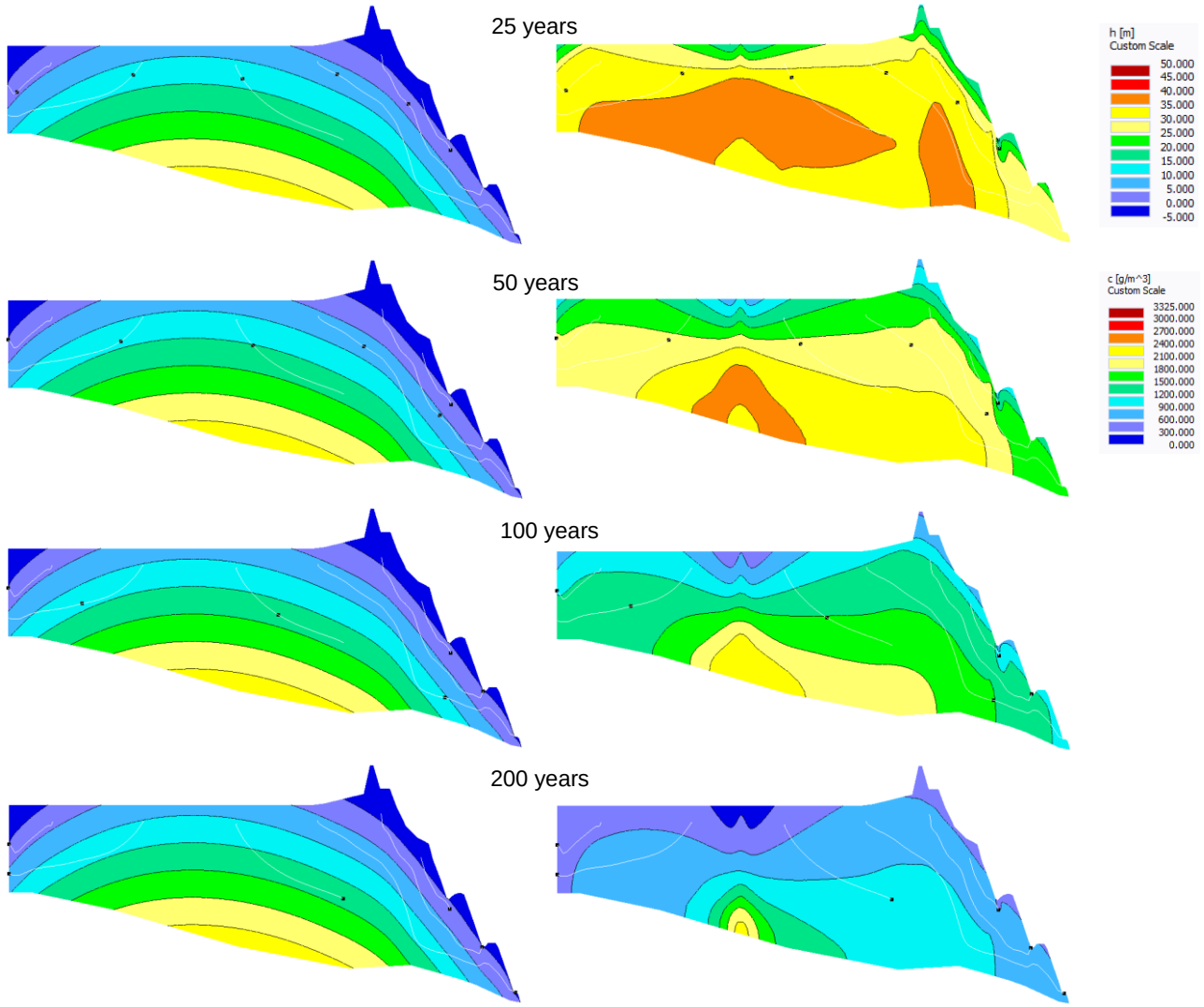

Figure 28. Future III: Pressure heads (m). at 25 years (2028), 50 years (2053), 100 years (2103), and 200 years. Particle trajectories (white lines) and particles (black dots).

Figure 29. Future III: TDS distribution (g/m^3) at 25 years (2028), 50 years (2053), 100 years (2103), and 200 years.

7. DISCUSSION

General

The groundwater flow and solute transport model of the SWSS was successful and an improvement on the previous models by McKenna (2002) and Price (2005). These improvements were accomplished by calibrating the model against seven years of data that had been acquired during the intervening years.

The model accurately predicted the position of the four seepage faces along the dam and the groundwater divide. Particle tracking indicated decadal long flow times or less within the Benches (from Bench to nearest seepage face) and demi-centennial to centennial long flow times from the top of the dam to the lower seepage faces. This nested system with both local (Bench scale) and intermediate (dam/dyke scale) flow was reported by Price (2005) and was confirmed with this model.

Calibration of the model to a variable boundary condition was vital to understanding not only of material properties, but the timing and length of spring melt. As dilution is important to the successful reclamation of the SWSS, the contribution of the spring melt should not be underestimated. Due to the limited amount of rain recharge transmitted through the cover, the reclamation measures should endeavor to capture as much as possible and mitigate factors that interfere with it's infiltration.

The measured groundwater elevations at GW15-6.8wt had an erratic pattern, which was most likely due to activities on the beach and pond and specifically due to earthen works on the ring dyke in 2005. Therefore, calibration of the model at this point was not possible so was ignored during the calibration process, however the location still provided a valuable observation point.

Water balance

The conceptual water balance diagram (Fig. 6) was updated from Liggett (2004) to reflect transient conditions; specifically, runoff no longer leaves the system and instead infiltrates into the soil, where a portion will reach the water table. This is particularly relevant to the melting of the snow pack, when large volumes of water are available for runoff, infiltration, and recharge over a short period.

This conceptual diagram was further updated to reflect the enhanced understanding of flow system (Fig. 30). Evaporation and evapotranspiration demands have been quantified with 32 % to 49 % of snow and 56 % to 92 % of rain being lost to the atmosphere. The reclaimed slopes lost the most and the non-reclaimed areas lost the least which is logical as vegetation reduces infiltration and recharge rates. Rain had the biggest impact on recharge at non-reclaimed boundary with around 65 % contributing, and the lowest impact on the covered boundaries of around 30 %. The water from snow melt had to opposite affect with about 70 % contributing to recharge on the covered boundaries and 35 % on the non-reclaimed boundary. As the recharge rates on the covered boundaries from rain are very low (10 % and 8 %) the water from snow melt is an important annual contributor.

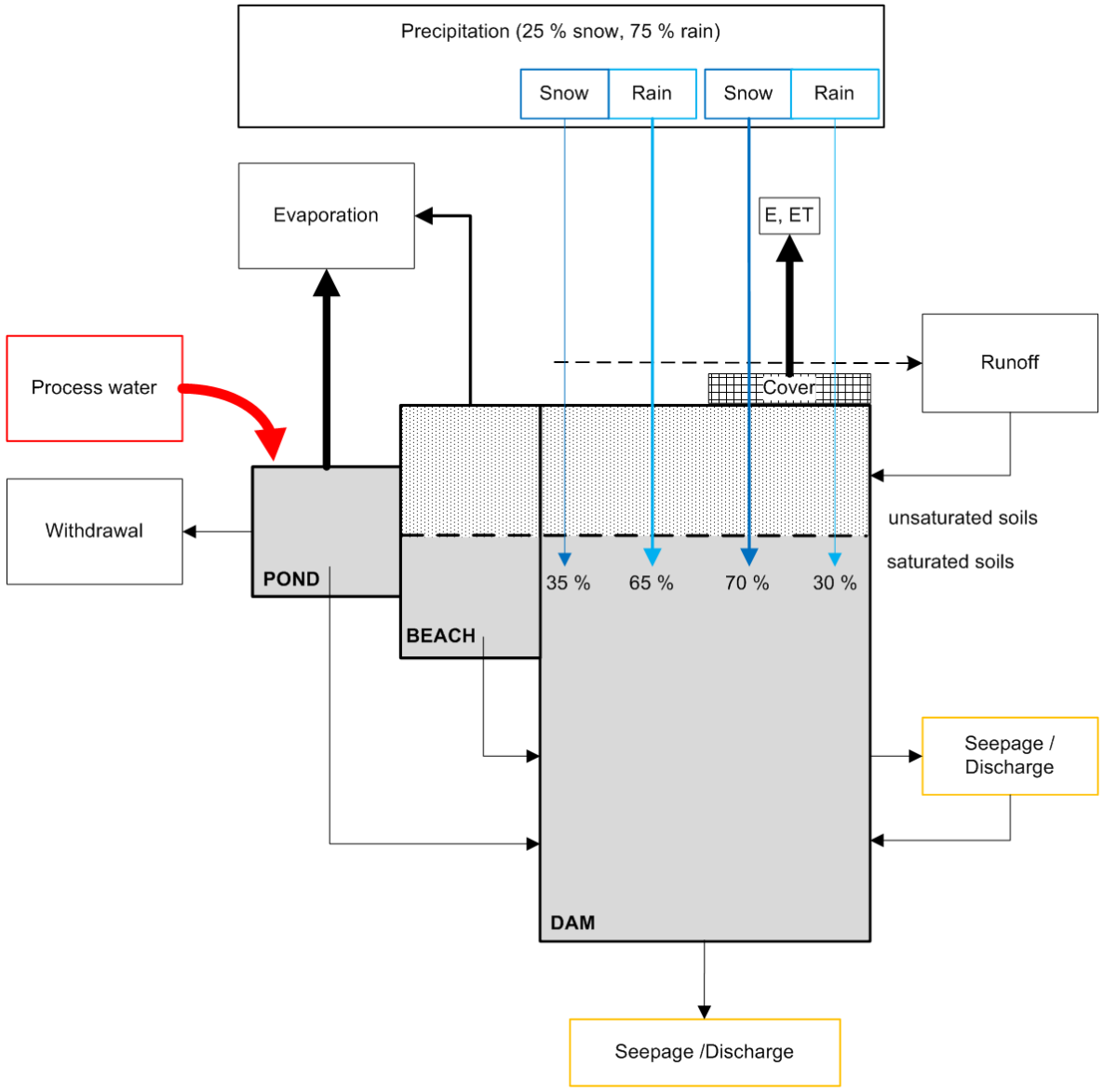

Figure 30. Revised conceptual water balance diagram for 2003 condition. Box size representative of volume outflow. Arrow thickness representative of rate of water movement (thicker = more; thinner = less). Percentages of snow and rain infiltrating into the saturated zone of the dam and the beach (not illustrated) through the covered and bare tailings ground surfaces. Box color code: red = High TDS concentrations; blue = low TDS concentrations; and orange = moderate TDS concentrations.

Material properties

In comparison to the previous work by Price (2005), the calibrated material properties were different but not radically (Table 28). The horizontal hydraulic conductivities were within the range of Price's slug tests values and those of the various other references. The porosity was the lower but still within an acceptable range. The residual saturation ranged between 0.13 and 0.2 which was double Price's value of 0.07, however an evaluation of the Soil Water Characteristics Charts (SWCCs) from the various references revealed curves without distinct inflection points and therefore difficult to determine precise residual saturation values. The curves for tailings sand start to break between 0.05 and 0.15 then gradually decline with

increasing suction. So, although the residual saturation in zone 2 could be unrealistically high, the other 8 zones were not. This studies' unsaturated parameters (alpha and n) were lower than Price's values but were in keeping with the reference values for sand tailings.

Table 28. Comparison of the material properties, Price (2005) and this study

Price (2005)						Zone	This study					
K_h	K_h/K_v	θ_r	θ_s	α	n		K_h	K_h/K_v	θ_r	θ_s	α	n
m/d	-	-	-	m^{-1}	-		m/d	-	-	-	m^{-1}	-
0.605	10	0.07	0.4	5.11	3.51	1	1.270	20	0.15	0.40	1.24	1.7
0.259	10	0.07	0.4	5.11	3.51	2	0.500	20	0.20	0.35	1.24	1.7
0.181	20	0.07	0.4	5.11	3.51	3	0.183	16	0.15	0.35	1.24	1.7
0.216	5	0.07	0.4	5.11	3.51	4	0.150	5	0.13	0.35	1.24	1.7
0.648	1	0.07	0.4	5.11	3.51	5	0.390	1	0.18	0.35	1.24	1.7
0.562	1	0.07	0.4	5.11	3.51	6	0.461	5	0.15	0.35	1.24	1.7
0.138	20	0.07	0.4	5.11	3.51	7	0.137	10	0.15	0.35	1.24	1.7
0.406	20	0.07	0.4	5.11	3.51	8	0.322	10	0.15	0.35	1.24	1.7
0.285	10	0.07	0.4	5.11	3.51	9	0.536	16	0.15	0.35	1.24	1.7

*1993 and 1994 layers only θ_s - porosity

New insights were gained into understanding how changes to material properties impacted the elevation of the water table over time. Its vertical position was modified by changes to the hydraulic conductivities (K_h and K_v), and the amplitude of its curve was modified by changes to the residual saturation, porosity, alpha, and n.

Recharge

Annual recharge rates used for this study's boundary conditions were greater than those used by Price (2005) (Table 29); about 4 cm more was applied to the reclaimed benches; 2 cm more was applied to the reclaimed slopes; and 3 cm more was applied to the non-reclaimed areas and the beach. In terms of percentages[29], the values were comparable to slightly higher.

Table 29. Comparison of calibrated recharge rates and percentages between Price (2005) and this study, steady state BCs. The Price percentages were recalculated using the GAP to enable comparison.

[29] of the Geometric Average Precipitation (GAP) for 2003 to 2009

	Price (2005)				This study			
	Benches A & B	Slopes A & B	Benches & Slopes C, D, & E	Beach	Benches A & B	Slopes A & B	Benches & Slopes C, D, & E	Beach
m/y	0.086	0.032	0.158	0.158	0.128	0.050	0.189	0.189
%*	23	9	43	43	24	19	50	50

* percentage of GAP = 0.371 m/y

Future I

The "do-nothing" scenario of Future I is unrealistic and did not represent any reclamation plan, however it did provide insight into the travel times under steady state boundary conditions and provided a base of comparison to the other future flow and transport simulations. The results of Future I were generally inline with those reported by Price (2005), although the TDS concentrations in shallow piezometers at the toes of Slopes B and A were twice that of this study, mostly likely due to the increased recharge (and hence dilution) on this studies reclaimed benches and slopes. The TDS concentrations were similar for Toe C.

Future II

The hummocky cover scenarios resulted in three distinct future predictions. The more restrictive the recharge, the more slowly the TDS concentrations attenuated such that after 200 years with a 5 mm/y cover, approximately 30 % of the section had a TDS concentration greater than 2400 g/m^3. This represents a significant mass of TDS that would remain within the facility long past living memory. Compared to the 50 mm/y cover which had no areas greater than this value. An extended run of the 5 mm/y cover revealed that it would take more than 800 years for the facility to reach a TDS distribution like the 50 mm/y cover at 200 years. It was predicted to take around 650 years for the entire facility to reach concentrations less than 600 g/m^3 with the 50 mm/y cover.

The hummocky design worked well within the model and the addition of inter-hummock seepage faces prevented groundwater mounding. However, the model results were not fully representative of an actual future condition as these seepage faces would be a sort of wetlands, requiring a dual-boundary condition instead of the single output flux it was assigned.

Future III

The flat cover scenario (Future III) simulated groundwater mounding and breaching of the upper boundary creating a pond, which is not conducive to the planned remedial measures. An active pumping plan or a much more restrictive cover would be needed to keep the groundwater from surfacing.

Comments

In general, the steady state BC had the advantage of quicker calculation times with simpler boundary inputs over the transient BC, and would have been exclusively suitable for the Future II simulations. The transient BC would be suitable for studying the local impacts of recharge on a smaller scale (dimension and time wise).

Most the time required to build the model was occupied by the calibration process, specifically the refinement of the material properties and recharge rates for both boundary conditions. Some time was also spent trouble shooting technical issues (such as non-convergence) that were slow to be resolved for various reasons. The program could do a better job of informing and explaining the reasons for non-convergence.

The toes of the slopes acted as both discharge and recharge points depending upon the time of year, however as HYDRUS (2D/3D) cannot simulate dual boundary conditions, a comprise was made in the water table calibration for those monitoring well locations. The model poorly simulated the range of groundwater elevations near the toes of the slopes, adjacent to seepage faces, as illustrated on the charts of GW01-1.5wt, GW05-2.2wt and GW09-1.5wt (App. E). The simulated groundwater elevations declined slower than the actual groundwater elevations and were only moderately sensitive to changes in material properties. The spring freshet was simulated reasonably well at these locations but at lower amplitudes.

The strength of HYDRUS (2D/3D) is its capability to simulate water and solute movement from the surface or near surface environment, downwards through the unsaturated zone, to the water table. This focus on the unsaturated zone and its relationship to the water table, plus the ability to simulate weather and the influence of plants growing on the boundary (which was not done for this study) is an asset and presents future expansion opportunities for this project. The model failed to simulate winter conditions, as the program cannot model sub-zero soil temperatures (in the standard configuration). The simulated curves show the water table continuing to decline between the months of November to March, when in fact the soil, and the water it contains, is frozen to a depth of approximately one to two metres (frost line) halting most flow and movement within this zone.

8. CONCLUSIONS

A flow and transport model was built to simulate a cross-section through the SWSS facility, which is a large oil sands tailings dam and impoundment located on the Mildred Lake oil sands lease in northern Alberta, Canada. HYDRUS (2D/3D) was suitable program to use for this purpose, if somewhat novel in dimensions and attributes. The model was representative of the conditions to which it was calibrated against and should reasonably predict future groundwater flow and TDS transport.

The material characteristics of oil sands tailings were further refined by calibrating the model against a variable (transient) boundary flux which included both snow melt and rainfall on flat and sloped surfaces, for bare and covered tailings. The boundary geometry and flux conditions of the model could be easily modified to simulate different cover (recharge) and topographical scenarios.

Under the as-is scenario (Future I) the TDS concentration of the dam will be greater than 1000 mg/L until around 2075, but because of the presence of the pond, two-thirds of the model section does not attenuate. Future simulations with remedial covers and landscaping (Futures II and III) had more holistic TDS attenuation distributions with dilution proportional to the amount of recharge. However, even the most restrictive recharge rates produced TDS concentrations of less than 1000 mg/L at the perimeter ditch after about 60 years due to the local flow system on Benches B and A and the influence of the Toe C ditch.

Unlike a tailings facility at a hard-rock mine, which might employ a low permeability cover to prevent acid rock drainage (NRC, 2004), the cover for the SWSS needs to be leaky to speed up dilution and reclamation.

Future study

The dilution potential of the ditch at Toe C should be investigated further to determine its magnitude. This can be accomplished by the calibration of the model to the measured TDS concentrations in the ditch and in groundwater (wells GW1 to GW8). To aid this calibration it is also recommended to perform new field seepage analyses at the seepages faces (Toes C, B and A) and re-do the field seepage analyses at the perimeter ditch. This seepage water should be analyzed for the TDS concentration. Yearly TDS analyses of the ditch and seepage water would also be helpful.

It would be beneficial to investigate how more rain could be captured as recharge beneath a cover. The impact of not only of trees but their growth over time (increasing water demand) should be considered.

The option of a cover of variable recharge along the boundaries is another possible future avenue to explore. Perhaps more recharge is warranted along the boundary of the former pond than along the dam face. Additional insight into recharge rates could be gained by studying smaller sections of the upper boundary whereby the various zones (roots, covers, tailings sand) could be employed to fine tune the vegetative demand. A transient boundary condition is best suited for this simulation and should include winter conditions, and the associated reduction in temperature, hydraulic conductivity, and vegetative demands.

The Future II and Future III results could be exploited to estimate the water and solute flux to the future central drainage ditch by using the data generated across the western vertical boundary. This could aid in future remedial designs and highlight potential impacts that may require mitigation.

9. REFERENCES

Alberta Parks and Environment (AEP). 2016. Alberta Tier 1 Soil and Groundwater Remediation Guidelines. Land Policy Branch, Policy, and Planning Division. 197 p.

Alberta Environment and Parks. 2017. Lower Athabasca Region: Tailings Management Framework for the Mineable Athabasca Oil Sands. Edmonton, Alberta.

Alberta Government. Oil Sands Reclamation Fact Sheet [website]. https://open.alberta.ca/publications/oil-sands-facts-and-stats. Accessed August 14, 2017.

Alberta Energy. Oil Sands Glossary. Edmonton, Alberta. [website]. http://www.energy.alberta.ca/OilSands/1708.asp#M. Accessed November 9, 2016.

Alberta Environment and Parks. With data from Environment Canada, Alberta Environment, and U.S. National Climate Data Center. Climate in Alberta. [online]. 1971-2000. Edmonton, Alberta. http://albertawater.com/virtualwaterflows/climate-in-alberta. Accessed May 13, 2016.

Alberta Agriculture and Forestry. Freezing Date Possibilities. Edmonton, Alberta. [website]. http://www1.agric.gov.ab.ca/$department/deptdocs.nsf/all/agdex10. Accessed May 14, 2016.

Anderson, M.P., Woessner, W.W. 1991. Applied Groundwater Modeling – Simulation of Flow and Advective Transport. Academic Press, USA.

Barson, D., Barlett, R., Hein, F., Fowler, M., Grasby, S., Reidiger, C., Underschultz, J. 2000. Hydrogeology of Heavy Oil and Tar Sand Deposits: Water Flow and Supply, Migration and Degradation, Field Trip Notes (Geological Survey of Canada), Open File Report 3946.

Beier, N., Sego, D. 2008. The Oil Sands Research Facility. Geotechnical News. June, pg 72-77.

Brandt, J.P., Flannigan. M.D., Maynard, D.G., Thompson, I.D., Volney, W.J.A. 2013. An introduction to Canada's boreal zone: ecosystem processes, health, sustainability, and environmental issues. Environ. Rev. 21: 207-226. December 6, 2013.

Burgers, T.D. 2005. Reclamation of an Oil Sands Tailings Storage Facility; Vegetation and Soil Interactions. M.Sc. Thesis. University of Alberta, Edmonton, Alberta.

Canadian Association of Petroleum Producers (CAPP). Basic Statistics [website]. http://www.capp.ca/publications-and-statistics/statistics/basic-statistics#h2TOC_1. Accessed July 27, 2017.

Canadian Association of Petroleum Producers (CAPP), Crude Oil Forecast, Markets & Transportation. June 2015.

Carey, S.K. 2008. Growing season energy and water exchange for an oil sands overburden reclamation soil cover, Fort McMurray, Alberta, Canada. Hydro. Process. 22: 2847-2857.

Carrera-Hernandez, J.J., Mendoza, C.A., Devito, K.J., Petrone, R.M., Smerdon, B.D. 2011. Effect of aspen harvesting on groundwater recharge and water table dynamics in a subhumid climate. Water Resources Research, Vol 47, W05542.

Carrera-Hernandez, J.J., Mendoza, C.A., Devito, K.J., Petrone, R.M., Smerdon, B.D. 2012. Reclamation for aspen revegetation in the Athabasca oil sands: Understanding soil water dynamics through unsaturated flow modelling. Can. J. Soil Sci. 92: 103-116.

Chaikowsky, C.L. 2003. Soil moisture regime and salinity on a tailings sand storage facility. M.Sc. Thesis. Department of Renewable Resources, University of Alberta, Edmonton, Alberta. Spring 2003. 135 p

Chalaturnyk, R.J., Scott, J.D., and Özum̈, B. 2002, Management of oil sand tailings: Petroleum Science and Technology, 20 (9 and 10): 1025–1046.

Chanasky, D. 2002. Cell 32 summary of runoff data spring/summer/fall 2002. Unpublished data.

Devito, K., Mendoza, C., Qualizza, C. 2012. Conceptualizing water movement in the Boreal Plains. Implications for watershed reconstruction. Synthesis report prepared for the Canadian Oil Sands Network for Research and Development, Environmental and Reclamation Research Group.

Energy Resources Conservation Board (ECRB). 2010. Energy Resources Conservation Board (ECRB) News Release: ECRB conditionally approves suncor plan to reduce fluid tailings [online] http://www.aer.ca/documents/news-releases/NR2010-13.pdf. Accessed August15, 2017.

Environment and Climate Change Canada. Historical Climate Data, Government of Canada, Ottawa, Ontario. [online]. http://climate.weather.gc.ca/. Accessed March 8, 2016.

Esford, B. 2003. Hydraulic conductivity data from slug test of piezometers into glacial till at the Southwest Sands Storage Facility. Syncrude Canada Ltd.

Fetter, C.W. 1999. Contaminant Hydrogeology, Second Edition. Prentice Hall Inc., Upper Saddle River, New Jersey, 598 p.

Freeze, R.A., Cherry, J.A. 1979. Groundwater. Prentice Hall Inc., Englewood Cliffs, New Jersey, 604 p.

Fung, M.Y.P. and T.M. Macyk. 2000. Reclamation of oil sands mining areas. In: Reclamation of drastically disturbed lands. Agronomy Monograph no. 41: 755-774.

Geo-slope International Limited. 1998. SEEP/W Software Package for finite element seepage analysis.

Geo-slope International Limited. 2002. SEEP/W Software Package for finite element seepage analysis.

Geo-slope International Limited. 2017. SEEP/W Software Package for finite element seepage analysis, Available online at: http://www.geoslope.com/products/seepw.asp.

Geological Survey of Canada (GSC). 2000. Ground temperature database for northern Canada. Open file report 3954. Smith, S., Burgess, M.

Google Earth Pro V 7.3.0.3830. September 1, 2009. Regional Municipality of Wood Buffalo, Alberta, Canada. 12 V 453563.16m E 6314202.93 m N, Eye alt 8.35 km. DigitalGlobe 20016. Application.

Hein, F.J., Cotterill, D.K. and Berhane, H. 2000. An atlas of lithofacies of the McMurray Formation, Athabasca Oil Sands deposit, northeastern Alberta: surface and subsurface; Alberta Energy and Utilities Board, EUB/AGS Earth Sciences Report 2000-07, 217 p.

Hunter, G. 2001. Investigation of Groundwater flow within an Oil Sand Tailings Impoundment and Environmental Implications. Masters Thesis, University of Waterloo, Waterloo. 361 p.

HYDRUS 2D/3D [software]. V 2.05.0.250. Prague, Czech Republic. PC-Progress Ltd., 2017.

Jirka. 2004. What does hydrus do about specific storage. PC-Progress Discussion Forums [Online posting]. Accessed July 27, 2017. http://www.pc-progress.com/forum/viewtopic.php?f=4&t=311&p=5861&hilit=Specific+storage#p5861.

Jirka. 2015. Lack of convergence with small parameter n. PC-Progress Discussion Forums [Online posting]. Accessed May 11, 2017. http://www.pc-progress.com/forum/viewtopic.php?f=3&t=2630&p=9399&hilit=air+entry#p9399.

Jirka. 2017. Van Genuchten: effective/total porosity & Se. PC-Progress Discussion Forums [Online posting]. Accessed July 27, 2017. http://www.pc-progress.com/forum/viewtopic.php?f=3&t=3118&sid=3d3f0f38e07ae07088fe97c68474bfb5.

Kasperski, K.L., Mikula, R.J. 2011. Waste Streams of Mined Oil Sands: Characteristics and Remediation. Elements, Vol. 7, 387-392.

Klohn Leonoff Ltd. 1991. Southwest Sands Disposal Site – Detailed Design, Summary Report. PB 5063 0401. Prepared for Syncrude Canada Ltd. February 1991. 71 p.

Liggett, J. 2004. Water and Salt Budgets for a Sand Tailings Dam. Bachelors Thesis, University of Alberta, Edmonton. 53 p.

McKenna, G.T. 2001. Southwest Sands Storage Facility, Suggested remedial /redesign measures and planning changes 2001.SLRTAP Presentation. Department of Civil and Environmental Engineering, University of Alberta, Edmonton, Alberta.

McKenna, G.T. 2002. Sustainable mine reclamation and landscape engineering. Doctoral Dissertation, University of Alberta, Edmonton. 661 p.

Mendoza, C. A. 2016. Personal communication.

Naeth, M.A., Chanasyk, D.S., Burgers, T.D. 2010. Vegetation and soil water interactions on a tailings sand storage facility in the athabasca oil sands region Alberta Canada. Physics and Chemistry of the Earth 36: 19-30.

Natural Resources Canada (NRC). 2004. Design, construction and performance monitoring of cover systems for waste rock and tailings. MEND 2.21.4, Vol. 1, Summary.

O'Kane Consultants Inc. 2007. Syncrude Canada Ltd. Instrumented Watershed Monitoring Program at the Southwest Sands Storage Facility, Monitoring Data Summary Report for the Period January 2006 to December 2006. Report No. 690/01-07.

O'Kane Consultants Inc. 2008. Syncrude Canada Ltd. Instrumented Watershed Monitoring Program at the Southwest Sands Storage Facility, Monitoring Data Summary Report for the Period January 2007 to December 2007. Report No. 690/01-13.

O'Kane Consultants Inc. 2009. Syncrude Canada Ltd. Instrumented Watershed Monitoring Program at the Southwest Sands Storage Facility, Monitoring Data Summary Report for the Period January 2008 to December 2008. Report No. 690/01-19.

O'Kane Consultants Inc. 2013. Syncrude Canada Ltd. Instrumented Watershed Monitoring Program at the Southwest Sands Storage Facility, Monitoring Data Summary Report for the Period January 2009 to December 2009. Report No. 690/01-26.

PC-Progress. 2016. http://www.pc-progress.com/en/Default.aspx. Accessed June 11, 2016.

Price, A.C.R. 2005. Evaluation of groundwater flow and salt transport within an undrained tailings sand dam. Masters Thesis, University of Alberta, Edmonton. 129 p.

Redding, T.E. 2009. Hydrology of forested hillslopes on the Boreal Plain, Alberta, Canada. Doctoral Dissertation, University of Alberta, Edmonton. 201 p.

Rowe, R.K., Badv, K. 1996. Advective-Diffusive contaminant migration in unsaturated sand and gravel. Journal of Geotechnical Engineering. Vol. 122, No 12. December 1996.

Seki, K. 2007. SWRC fit – a nonlinear fitting program with a water retention curve for soils having unimodal and bimodal pore structure. Hydrol. Earth Syst. Sci. Discuss., 4: 407-437. [website]. Accessed on May 11, 2017. http://seki.webmasters.gr.jp/swrc/.

Šejna, M., Šimůnek, J. 2017. Graphical User Interface for the HYDRUS Software Package Simulating Water, Heat, and Solute Movement in Two- and Three-Dimensional Variably-Saturated Media, Version 2.05.0250, PC Progress, Prague, Czech Republic. Available online at: https://www.pc-progress.com/en/Default.aspx.

Šejna, M., Šimůnek, J., van Genuchten, M. Th. 2011. The HYDRUS Software Package for Simulating the Two- and Three-Dimensional Movement of Water, Heat, and Multiple Solutes in Variably-Saturated Media, User Manual, Version 2.0, PC Progress, Prague, Czech Republic, 280 pp.

Šimůnek, J., van Genuchten, M. Th., Šejna, M., 2011. The HYDRUS Software Package for Simulating the Two- and Three-Dimensional Movement of Water, Heat, and Multiple Solutes in Variably-Saturated Media, Technical Manual, Version 2.0, PC Progress, Prague, Czech Republic, 258 pp.

Shelby, D., Creaser, R.A. 2005. Direct Radiometric Dating of Hydrocarbon Deposits Using Rhenium-Osmiun Isotopes. Science Vol. 308 (5726), 1293-1295.

Šimůnek, J. undated. Notes on Spatial and Temporal Discretization (when working with Hydrus).

Skopek, P. 1996. Modelling of Long Term Seepage Regime of the SWSS. Project No. EG08082. AGRA Earth and Environmental Ltd., December 1996. 18 pp.

Syncrude Canada Ltd. 2001. 2001 Closure and Reclamation Plan, Syncrude Mildred Lake Operation. Prepared by Syncrude Closure and Reclamation Team. Syncrude Canada Ltd. 336 p.

Syncrude Canada Ltd. Various dates. Internal communications.

Syncrude Canada Ltd. 2008. Application for Approval of the Southwest Sand Storage Conversion Project. Vol. 1 to 4. Submitted to Energy Resources Conservation Board and Alberta Environment. CE03786. November, 2008.

Syncrude Canada Ltd. 2010. Directive 074, Baseline Survey for Fluid Deposits, Syncrude Mildred Lake and Aurora North, Baseline (2010). Submitted to Energy Resources Conservation Board. September 30, 2010.

Syncrude Canada Ltd. 2011. 2011 Annual Industrial Wastewater and Runoff Report. Mildred Lake and Aurora North Plants. Submitted to Alberta Environment and Water. March 30, 2012.

Syncrude Canada Ltd. 2012. 2012 Annual Industrial Wastewater and Runoff Report. Mildred Lake and Aurora North Plants. Submitted to Alberta Environment and Water. March 28, 2013.

Syncrude Canada Ltd. 2013. 2013 Annual Industrial Wastewater and Runoff Report. Mildred Lake and Aurora North Plants. Submitted to Alberta Environment and Water. March 31, 2014.

Syncrude Canada Ltd. 2001, 2006, 2010. Weather station photographs. Syncrude Watershed Research Database.

Syncrude Canada Ltd. 2017. Water efficiency, water use intensity. [website]. Accessed August 21, 2017. http://www.syncrude.ca/environment/water/water-efficiency/

United States Department of Agriculture. 1999. UNSODA database, maintained by U.S. Salinity Laboratory.

United States Geological Survey (USGS). 1987. Techniques for Water-Resource Investigations of the United States Geological Survey, Chapter B5, Definition of Boundary and Initial Conditions in the Analyses of Saturated Ground-water Flow Systems – An Introduction. Book 3 Application of Hydraulics. Franke, O.L., Reilly, T.E., and Bennett, G.D..

Webster, K.L., Beall, F.D., Creed, I.F., Kreutzweiser, D.P. 2015. Impact and prognosis of natural resource development on water and wetlands in Canada's boreal zones. Environ. Rev. 23: 78-131. February 17, 2015.

Young-Robertson, J.M., Bolton, W.R., Bhatt, U.S., Cristóbal, J., Thoman, R. 2016. Deciduous trees are a large and overlooked sink for snowmelt water in the boreal forest. Sci. Rep. 6, 29504.

APPENDIX A – REFERENCE PARAMETERS

A1. Hydraulic Conductivity – horizontal

Slug testing was conducted by Price (2005) at 45 monitoring wells screened within the tailings sands in order to calculate hydraulic conductivity using a computer program and Horselvs' method. Nine of the tests were excluded due to uncertain data quality (Table A1); the remaining 36 results were used to calculate the geometric mean for each hydrostratigraphic zone (Table A2) excluding the highest and the lowest measurements. For zone 1 (Sand Bench), the hydraulic conductivity was determined using the measured seepage discharge (from seepage meters) divided by the gradient (Liggett 2004). These hydraulic conductivies are within the range of those previously measured (Table A3).

Table A1. Hydraulic conductivity testing results (Price, 2005)

ID	K (m/d) Horslev Kh/Kz=1	ID	K (m/d) Horslev Kh/Kz=1	ID	K (m/d) Horslev Kh/Kz=1	ID	K (m/d) Horslev Kh/Kz=1
GW1-3	0.197	GW6-6	0.309	GW9-8	0.093	GW12-4	0.306
GW2-3	0.118	GW7-7	0.319	GW10-3	0.187	GW12-6	0.378
GW3-4	0.134	GW7-8	0.157	GW10-5	0.183	GW13-2	0.259
GW3-6	0.050	GW7-15	0.378	GW10-7	0.136	GW13-6	0.770
GW3-8	0.343	GW8-3	0.217	GW11-6	0.637	GW13-9	0.086
GW4-4	0.410	GW8-7	0.123	GW11-7	0.178	GW15-7	0.168
GW4-6	0.363	GW9-2	0.461	GW11-15	0.218	GW15-15	0.530
GW5-8	0.510	GW9-4	0.239	GW11-23	0.174	GW15-24	0.093
GW6-5	0.492	GW9-6	0.235	GW12-2	1.045	GW15-33	0.321

Table A2. Hydraulic conductivity (m/d) by hydrostratigraphic zone

Zone	Geomean K	Zone	Geomean K	Zone	Geomean K
(1) Sand Bench	1.273	(4) Bench's C&D	0.312	(7) Lower Beach	0.137
(2) Bench A	0.208	(5) Toe B	0.390	(8) Upper Beach	0.536
(3) Bench B	0.183	(6) Toe C	0.461	(9) Cont. Beaching	0.322

Table A3. Horizontal hydraulic conductivity references values for tailings sand (Price, 2005)

K (m/d)	Location	Description of Test	Data Source	Report
0.1097	SWSS, cell 46	Rising Head Bail Tests (cell 46), n = 21 ,Kh/Kv = 1	Price, 2005	Price, 2005
0.1624	SWSS, cell 46	Rising Head Bail Tests (cell 46), n = 21 ,Kh/Kv = 20	Price, 2005	Price, 2005
0.4666	SWSS, cells	Constant or falling head tests, cells, n=23	McKenna, 1996a	AGRA, 1997
0.4061	SWSS, beaches	Constant or falling head tests, beaches, n = 5	McKenna, 1996a	AGRA, 1997
1.7280	SWSS	Seepage analysis, Kh/Kz = 16	Klohn Leonoff, 1991	Klohn Leonoff, 1991
0.2506	various	Falling Head Slug Tests, n= 172	McKenna, 2002	McKenna, 2002
1.8144	MLSB	Field gradients between SP, n=229	McKenna, 2002	McKenna, 2002
0.2419		Intact and reconstituted samples, constant and falling head tests, n= 82	McKenna, 2002	McKenna, 2002
0.5011		Field Pump Test, n= 26	McKenna, 2002	McKenna, 2002
1.9872		Lab Model, n= 6, Kh/Hz=1 assumed	McKenna, 2002	McKenna, 2002
0.6912		Syncrude design values, Kh/Kz = 16	McKenna, 2002	McKenna, 2002
0.8640		Estimated upper end value	Caughill, 1998	Golder, 1998
1.7280	MLSB	Dyke back analysis, Kh/Kz = 17	Terracon, 1992	Golder, 1998
0.622 to 1.296		Falling head tests	Terracon, 1992	Golder, 1998
0.0345 to 3.456	SWSS	Slug tests	AGRA, 1996	Golder, 1998
0.086 to 0.691		Seepage calculations	AGRA, 1996	Golder, 1998

MLSB – Mildred Lake Settling Basin

A2. Hydraulic Conductivity – vertical

Based on McKenna's (2002) research, a K_h/K_v ratio of 16 was generally used for SWSS designs and a K_v geometric mean of 0.084 m/d was reported from laboratory testing of four frozen cores of clean tailings sand from Cell 34. In addition, McKenna (2002) performed finite element back analyses on Cell 31 using SEEP/W (Geo-slope International Limited, 1998) and the October 1999 condition that resulted in 16 being a being a good fit to the phreatic surface, but he also reported values of 1 and 100. Based upon his extensive research he recommended a ratio of 10 (to reflect a less precise value than 16) with an anticipated range of 1 to 20.

Price (2005) used K_h/K_v ratios ranging between 1 and 20, with six out of the nine zones assigned either 10 or 20, following the recommendations from McKenna (2002).

A3. Hydraulic Conductivity – underlying sediments

Based on the measurements of the hydraulic conductivity of the underlying glaciofluvial sediments (Table A4), the lower boundary of the model was a no flow/flux boundary.

Table A4. Horizontal and vertical hydraulic conductivity references values for underlying glaciofluvial sediments (Price, 2005).

K (m/d)	Kh or Kv	Location	Description of Test	Data Source	Report
5.18E-06	Kv	OSLO Lease 31	Consolidation test - OSLO Lease 31	Terracon, 1985	Golder, 1998
3.72E-03	Kv	OSLO Lease 31	Permeameter test - OSLO Lease 31	Terracon, 1990A	Golder, 1998
4.84E-03	Kh	OSLO Lease 31	Slug tests	Terracon, 1990b	Golder, 1998
1.81E-02	Kh	OSLO Lease 31	Slug tests	Terracon, 1990b	Golder, 1998
1.21E-02	Kh	OSLO Lease 31	Slug tests	Hardy BBT, 1988	Golder, 1998
8.64E-03	Kh	MLSB	Calibrated gw model	Terracon, 1992	Golder, 1998
1.73E-03	Kh	SWSS, cell 45	Slug test, OW99-29, PL2/PG3	Barry Esford, 2002,Syncrude	on file at Syncrude
1.73E-04	Kh	SWSS, cell 31	Slug test, OW98-10	Barry Esford, 2002,Syncrude	
5.18E-03	Kh	SWSS, cell 31	Slug test, OW98-11	Barry Esford, 2002,Syncrude	
8.64E-04	Kh	SWSS, cell 31	Slug test, OW98-13	Barry Esford, 2002,Syncrude	
1.04E-04	Kv	SWSS, N of cell 48	Triaxial constant head permeameter tests, BHA-MWA-89-02A -4.75, PG	Klohn Leonoff, 1990	Klohn Leonoff, 1990

MLSB – Mildred Lake Settling Basin

A4. Saturated Water Contents (Porosity) θ_s

There was good agreement amongst the references that porosity of the tailings sand ranges between 0.35 to 0.40 based on experimental data and numerical modeling.

A5. Residual Water Contents θ_r

The residual saturations reported in the references ranged from a low of 0.02 to a high of 0.08 and are summarized in the following Tables A5 (those without charts) and A6 (those with Soil Water Characteristics Charts (SWCC)).

Table A5. Reference residual saturation values (without charts)

Reference		Type	θ_r
Table 3	Carsel and Parrish (1988)	Loamy Sand	0.057
UNSODA database	USDA (1999)	Loamy Sand	0.049
Table 5.2-3	AGRA (1994) in Hunter (2001)	Tailings Sand	0.02
Rosetta Lite	v 1.1 (2003)	82 % Sand	0.0408
		12.6 % Silt	
		4.4 % Clay	
Rosetta Lite	v 1.1 (2003)	82 % Sand	0.0424
		12.6 % Silt	
		4.4 % Clay	
		1.6 g/cm^3	
Regression analyses	Welsh (2015) model	Sand to loamy sand	0.078

Table A6. Reference residual saturation values (with SWCC)

Price (2005) Fig. 3-3 θ_r = 0.07 Predicted by van Genuchten curve for sandy silt	McKenna (2002) Table D-2 θ_r = 0.08 at 55 kPa
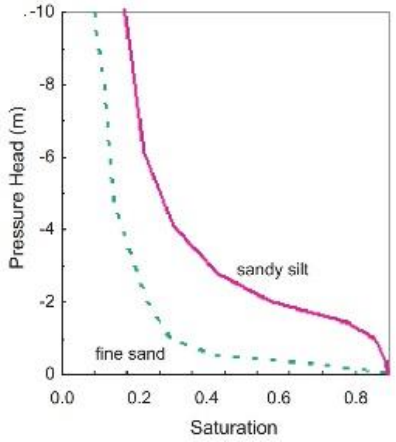	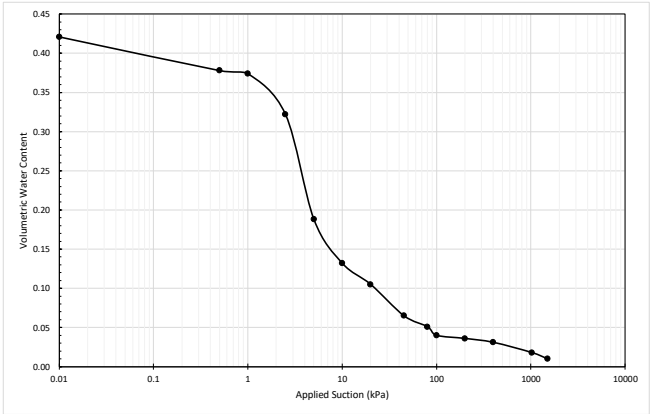

Table A6 cont. Reference residual saturation values (with SWCC)

Hunter (2001) Fig. 5.2-1
Model $\theta_r = 0.05$
Tests values = 0.013, 0.02, & 0.035

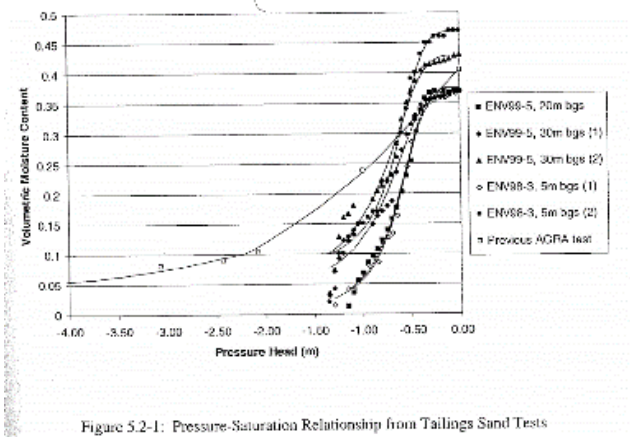

Figure 5.2-1: Pressure-Saturation Relationship from Tailings Sand Tests

Price, J. (2009) Fig. 3

$\theta_r = 0.06$

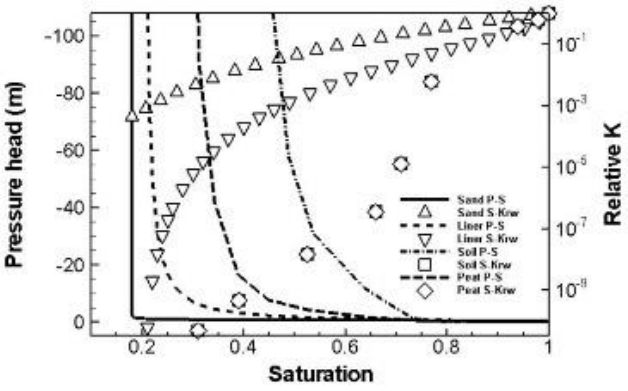

O'Kane (2007) Fig 4.2 & 5.4
Not explicitly stated

Laboratory soil-water characteristic curve Fig 4.2, green line.

Of 3 curves, only 1 had distinct break

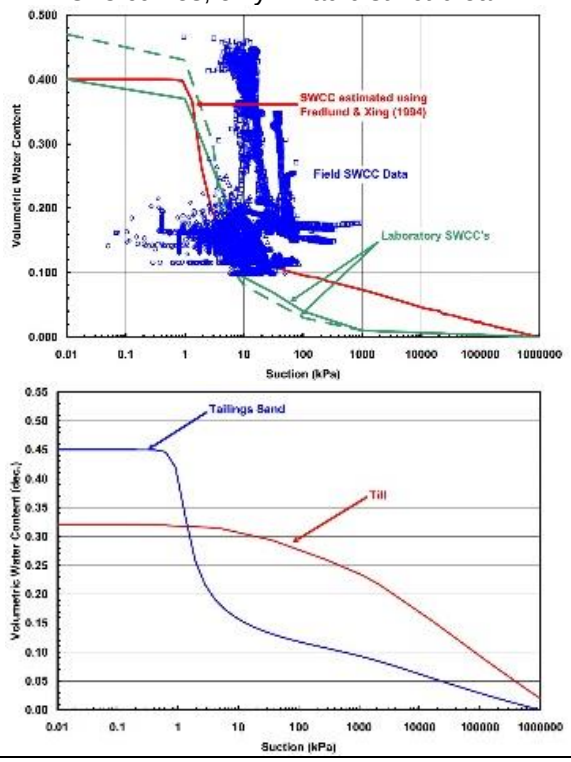

Carrera-Hernandez (2012) Fig. 3

Not explicitly stated

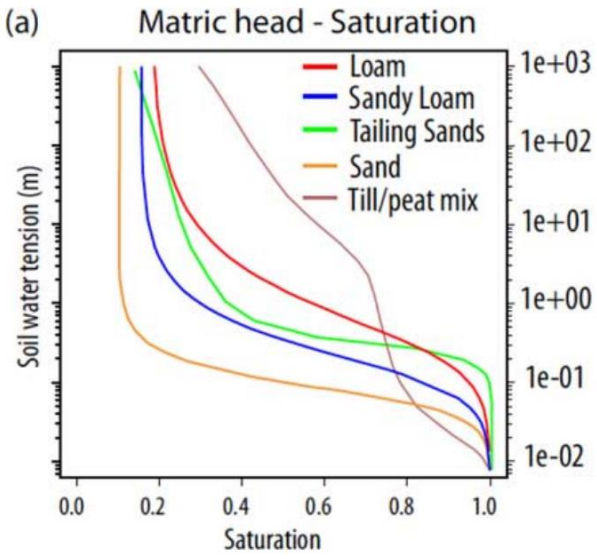

A6. Alpha (α) and N

During review of the references, it became apparent that the published values for alpha and n for standard USDA soil textures and those predicted by Rosetta Lite program were different than those derived by laboratory testing of oil sands tailings (Hunter, 2001) (Table A7). Both alpha and n are empirical coefficients required by the van Genuchten (1980) equation for unsaturated flow. Alpha is related to the inverse of the air entry suction, and n is a measure of the pore size distribution. These values require direct input by the HYDRUS (2D/3D) program. The abundance and behavior of the fines in the tailings material is the key element in it's uniqueness.

Table A7. Reference alpha and n values

Reference	Texture Group	α (m^{-1})	n
Carsel and Parrish (1988)	USDA Loamy sand	12.4	2.28
AGRA (1994) in Hunter (2001)	Dyke sand	1.24	2.44
USDA (1999) UNSODA	USDA Loamy sand	3.48	1.746
Hunter (2001) laboratory	Dyke sand (average)	1.55	3.856
Hunter (2001) model	Sand tailings - beached	1.55	1.746
Rosetta Lite v 1.1 (2003)	82% Sand 12.6% Silt 4.4% Clay (USDA Loamy sand)	4.04	1.833
Rosetta Lite v 1.1 (2003)	82% Sand 12.6% Silt 4.4% Clay 1.6 g/cm^3 (USDA Loamy sand)	4.25	1.88
Price, A. (2005) model	Sandy silt (tailings)	5.11	3.51
Price, J. (2009) model	Sand tailings	1.9	6
Welsh (2015) model	Sand to loamy sand	10.1	1.66

References

Carrera-Hernandez, J.J., Mendoza, C.A., Devito, K.J., Petrone, R.M., Smerdon, B.D. 2012. Reclamation for aspen revegetation in the Athabasca oil sands: Understanding soil water dynamics through unsaturated flow modelling. Can. J. Soil Sci. 92: 103-116.

Carsel, R.F., Parrish, R.S. 1988. Developing joint probability distributions of soil water retention characteristics. Water Resources Research, Vol. 24, No. 5, 755-769. May 1988

Geo-slope International Limited. 1998. SEEP/W Software Package for finite element seepage analysis.

Hunter, G. 2001. Investigation of Groundwater flow within an Oil Sand Tailings Impoundment and Environmental Implications. Masters Thesis, University of Waterloo, Waterloo. 361 p.

Liggett, J. 2004. Water and Salt Budgets for a Sand Tailings Dam. Bachelors Thesis, University of Alberta, Edmonton. 53 p.

McKenna, G.T. 2002. Sustainable mine reclamation and landscape engineering. Doctoral Dissertation, University of Alberta, Edmonton. 661 p.

O'Kane Consultants Inc. 2007. Soil-Atmosphere Field Response Modelling of Southwest Sands Storage Facility Cell 32. Prepared for Syncrude Canada Ltd. OKC Report No. 690/14-01. March 2007.

Price, A.C.R. 2005. Evaluation of groundwater flow and salt transport within an undrained tailings sand dam. Masters Thesis, University of Alberta, Edmonton. 129 p.

Price, J.S., McLaren, R.G., Rudolph, D.L. 2009. Landscape restoration after oil sands mining: conceptual design and hydrologic modelling for fen reconstruction. International Journal of Mining, Reclamation and Environment, 24:2, 109-123.

Rosetta Lite. 2003. Version 1.1 embedded within HYDRUS (2D/3D) v. 2.05.0250. Schaap, M.G., Leij, F.J., van Genuchten, M.T., Rosetta: a compute program for estimating soil hydraulic parameters with hierarchical pedotransfer functions,. J. of Hydrol., 251, 163-176, 2001.

United States Department of Agriculture. 1999. UNSODA database, maintained by U.S. Salinity Laboratory.

van Genuchten, M. Th. 1980. A closed-form equation for predicting the hydraulic conductivity of unsaturated soils, Soil Sci. Soc. Am. J., 44, 892-898.

Welsh, R.B. 2015. Simulation of variably saturated groundwater flow and the effects of weeping tile drains at a partially reclaimed oil sands coarse tailings facility. Masters project, University of Waterloo, Waterloo. 67 p.

APPENDIX B – PRECIPITATION RECORDS

The precipitation records for the years 2003 to 2009 (Chart B1) were gathered either from the local weather station in Cell 32 or from the Environment Canada (EC) Mildred Lake weather station[30] when data from the weather station was missing, incomplete, or suspect erroneous (Table B1). The EC data was considered reliable, however it should be noted that thunderstorms in this region can produce very localized precipitation meaning that the EC records could under or over-report precipitation. Snow depth and density surveys were conducted every March from 2004 to 2009 along the A' to A transect to provide an measure of the available melt water in April. The annual geomean precipitation was 0.366 m with about 26 % falling as snow and about 73 % falling as rain. Precipitation ranged between a low of 0.255 m to a high of 0.497 m.

Chart B1. Yearly snow water equivalents and rain totals, 2003 to 2009

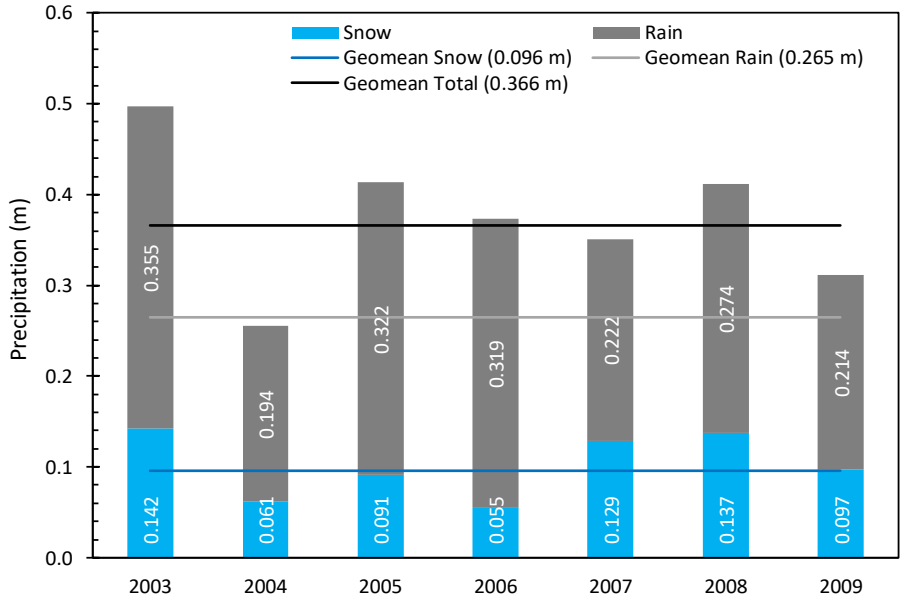

[30] Station # 3064528, located 12 km northeast at 310 m elevation

Table B1. Monthly precipitation data sources, timing, and rates (m)

	2003	2004	2005	2006	2007	2008	2009
January							
February							
March							
April (snow)	0.142	0.061	0.091	0.055	0.129	0.137	0.097
April (rain)	0	0	0.039	0.006	0.022	0	0.022
May	0.049	0.045	0.029	0.047	0.014	0.014	0.016
June	0.063	0.011	0.069	0.036	0.027	0.073	0.075
July	0.071	0.035	0.108	0.146	0.042	0.045	0.034
August	0.021	0.021	0.068	0.043	0.094	0.106	0.077
September	0.100	0.083	0.008	0.040	0.018	0.019	0.012
October	0.052		0.001	0.005	0.006	0.017	
November							
December							
Total	0.497	0.255	0.413	0.373	0.351	0.411	0.311

Color Key	Cell 32 weather station	EC Mildred Lake weather station	Snow[31]	Snow survey

EC – Environment and Climate Change Canada

References

Environment and Climate Change Canada. Historical Climate Data, Government of Canada, Ottawa, Ontario. [online]. http://climate.weather.gc.ca/. Accessed March 8, 2016.

[31] Month where precipitation fell as snow. Snow was assumed to accumulate during the winter and was accounted for in the snow survey. Some snow was assumed to be lost to sublimation.

APPENDIX C – DEPTH TO GROUNDWATER

The fourteen monitoring wells used to calibrate the simulation are listed in Table C1 along with the averaged simulated pressure heads for both steady state and transient boundary conditions.

Table C1. Averaged measured and simulated groundwater elevations 2003-2009 for transient and steady state boundary conditions.

Well ID	Averaged Measured Groundwater Elevation	Transient BC		Steady State BC	
		Averaged Simulated Groundwater Elevation	Elevation Difference (measured-simulated)	Averaged Simulated Groundwater Elevation	Elevation Difference (measured-simulated)
	m	m	m	m	m
GW01-1.5wt	353.35	353.50	-0.151	353.51	-0.165
GW02-2.5wt	355.88	356.07	-0.187	356.08	-0.209
GW03-3wt	358.43	357.83	0.600	357.85	0.571
GW04-1.75wt	359.62	359.42	0.199	359.45	0.175
GW05-2.2wt	360.89	361.30	-0.410	361.31	-0.418
GW06-3.8wt	362.74	363.11	-0.372	363.11	-0.377
GW07-5wt	365.44	365.43	0.009	365.41	0.015
GW08-2.5wt	368.06	367.80	0.265	367.79	0.274
GW09-1.5wt	369.67	369.93	-0.255	369.91	-0.240
GW10-2.5wt	373.04	372.61	0.429	372.52	0.503
GW11-4wt	375.94	375.25	0.688	375.12	0.817
GW12-1.5wt	379.17	378.29	0.880	378.16	1.030
GW13-2.5wt	380.63	380.54	0.093	380.31	0.340
GW15-6.8wt	384.51	384.22	0.285	383.97	0.513

APPENDIX D – SENTIVITY ANALYSES ADDITIONAL INFORMATION

A sensitivity analyses was performed (using the SS BC) to evaluate the chosen parameters in comparison to the other values given in the references. The following Table D1 lists the percentage change along with the value for horizontal hydraulic conductivity, anisotropy, residual saturation, porosity, alpha, n, and infiltration flux used in the analyses.

Table D1. Sensitivity analyses values

Parameters	Model Value	Decreased Value	Increased Value	Rational
Kh (m/d)		(-50%)	(+50%)	Based on approximation error in field data
Sand Bench - 1	1.27	0.635	2.54	
Bench A - 2	0.50	0.250	1.00	
Bench B - 3	0.183	0.092	0.366	
Bench C&D - 4	0.150	0.075	0.30	
Toe B – 5	0.390	0.195	0.78	
Toe C – 6	0.461	0.231	0.922	
Lower Beach - 7	0.137	0.069	0.274	
Upper Beach – 8	0.322	0.161	0.644	
Contained Beaching - 9	0.536	0.268	1.072	
Kh/Kv (global)		(-50%)	(+50%)	Based on values reported by references
				Based on calibration experience
Sand Bench – 1	20	10	30	
Bench A - 3				
Bench B – 2	16	8	24	
Contained Beaching - 9				
Lower Beach – 7	10	5	15	
Upper Beach - 8				
Bench C&D – 4	5	2.5	7.5	
Toe C - 6				
Toe B - 5	1	0.5	1.5	
Residual Sat (global)	0.13, 0.15, 0.18, 0.2	0.065, 0.075, 0.09, 0.1 (-50%)	0.16, 0.19, 0.23, 0.25 (-25%)	Based on values reported by references
Porosity (global)	0.35, 0.40	0.33 (-5%)	0.42 (+5%)	
Alpha (m^{-1}) (global)	1.24	1.1 (-13%)	4.25 (+343%)	Based on values reported by references
n (global)	1.70	1.3 (-25%)	3.86 (+127%)	HYDRUS lower limit is 1.2 Based on value reported by references

APPENDIX E – TRANSIENT BC CALIBRATION

Chart E1. Left: Measured groundwater elevations (m) (black) and simulated groundwater elevations (m) (blue) vs. time. Right: Measured groundwater elevations (m) (black) and simulated pressure head (m) (orange) vs. time plotted on same scale using different values and axis. The measured Average Depth to Water (ADTW) from the ground surface.

GW01-1.5wt, Slope A, ADTW 0.520 m

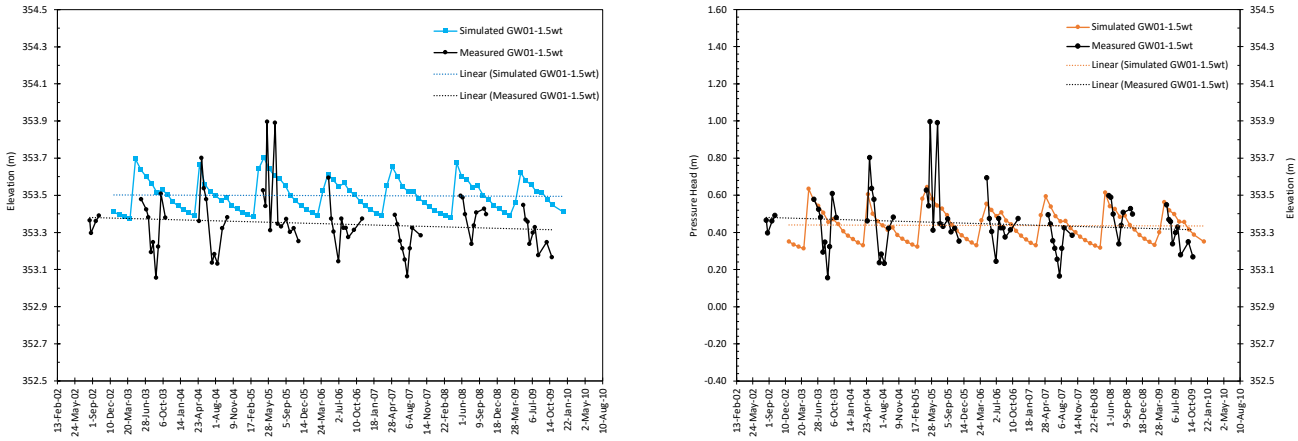

GW02-2.5wt, Slope A, ADTW 1.768 m

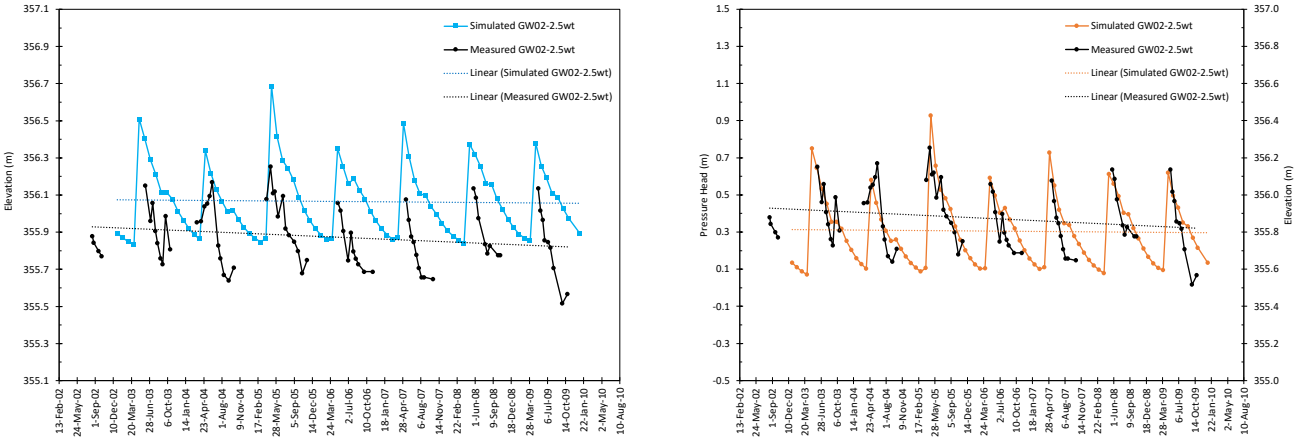

GW03-3wt, Bench A, ADTW 2.233 m

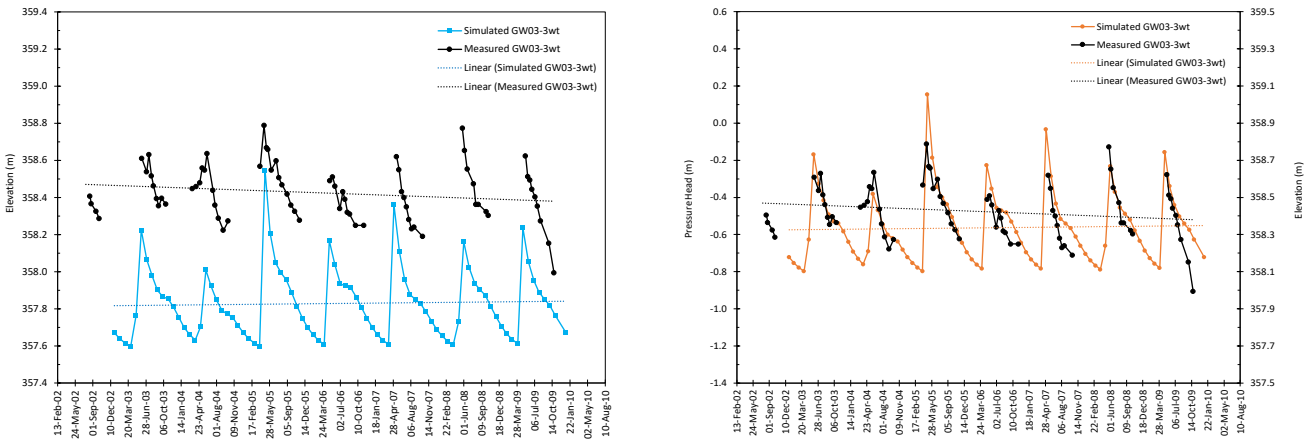

GW04-1.75wt, Bench A, ADTW 1.169 m

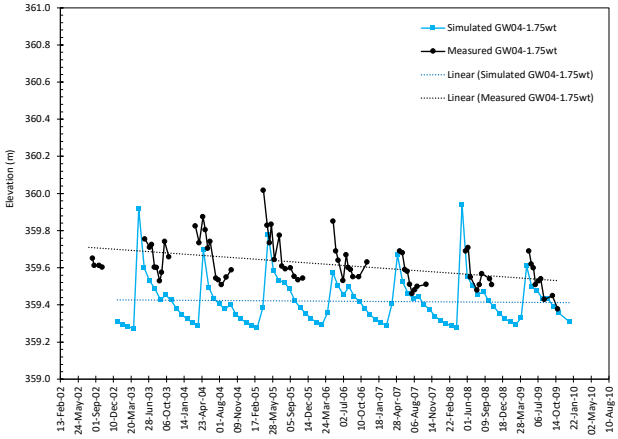

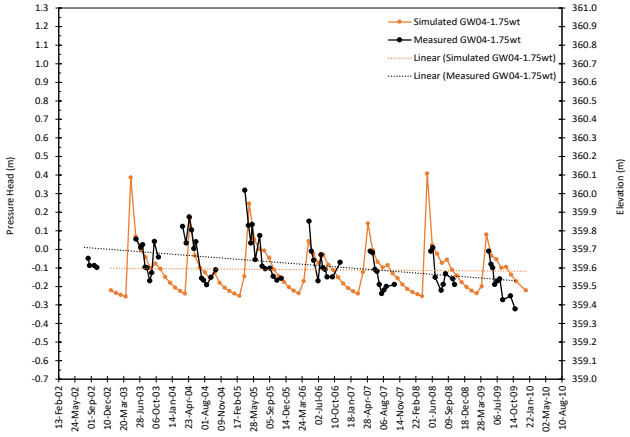

GW05-2.2wt, Slope B, ADTW 1.193 m

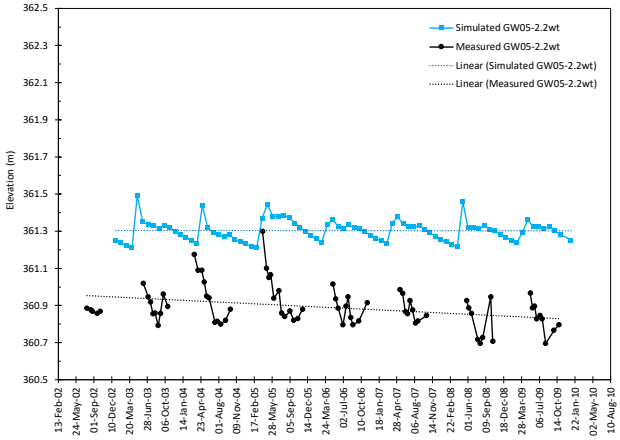

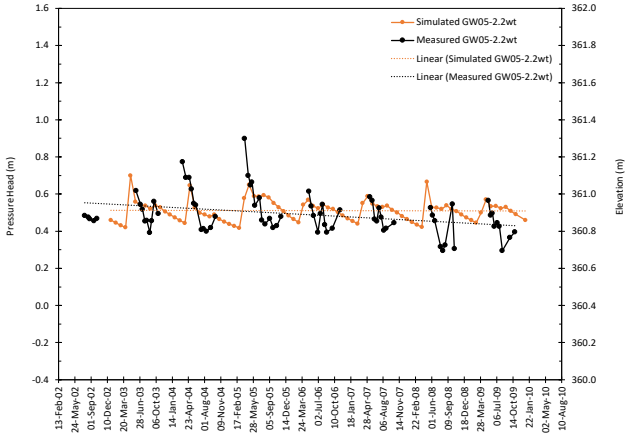

GW06-3.8wt, Slope B, ADTW 2.965 m

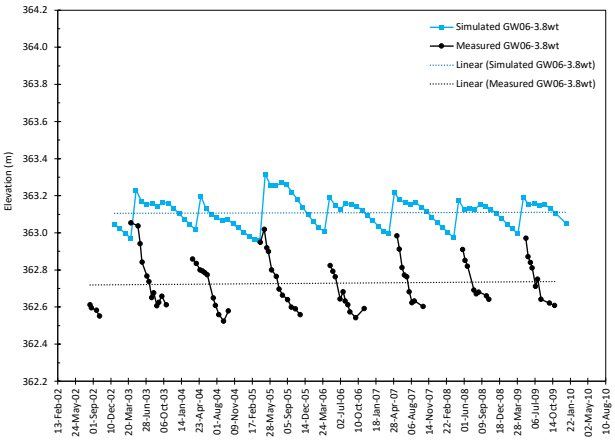

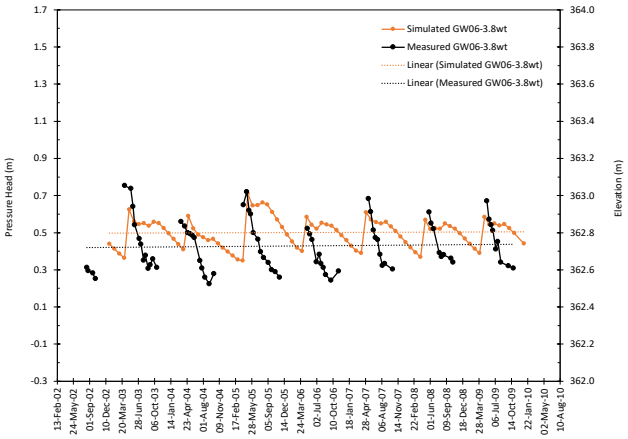

GW07-5wt, Bench B, ADTW 4.192 m

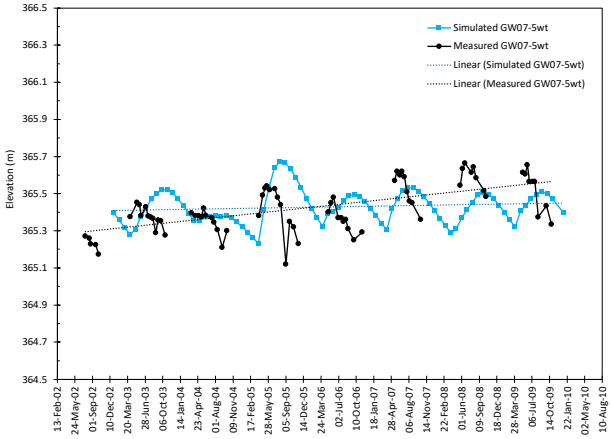

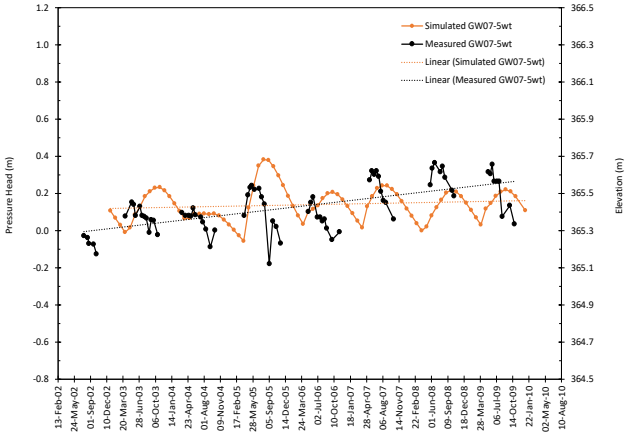

GW08-2.5wt, Bench B, ADTW 1.535 m

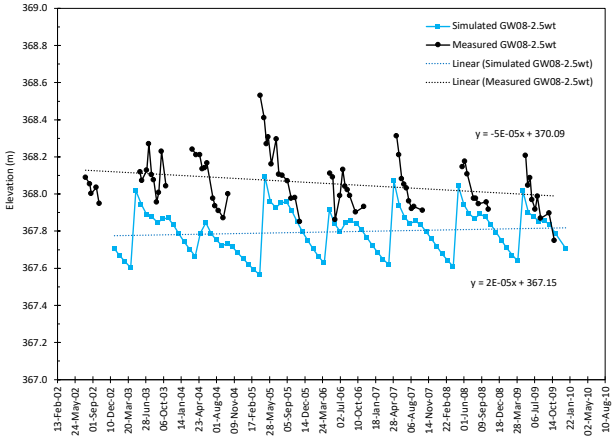

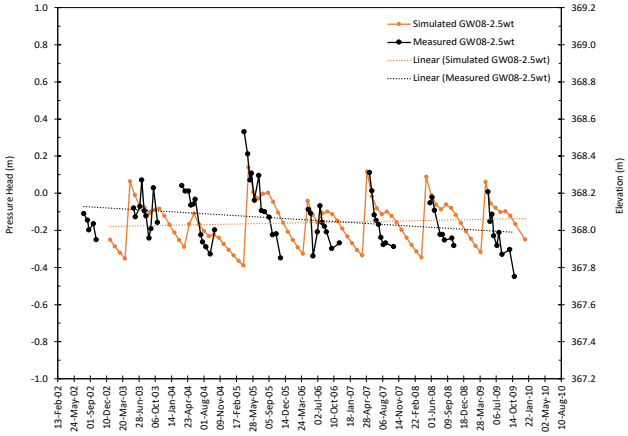

GW09-1.5wt, Slope C, ADTW 0.780 m

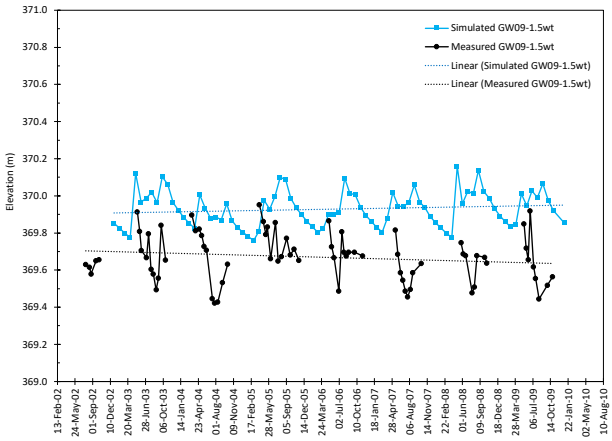

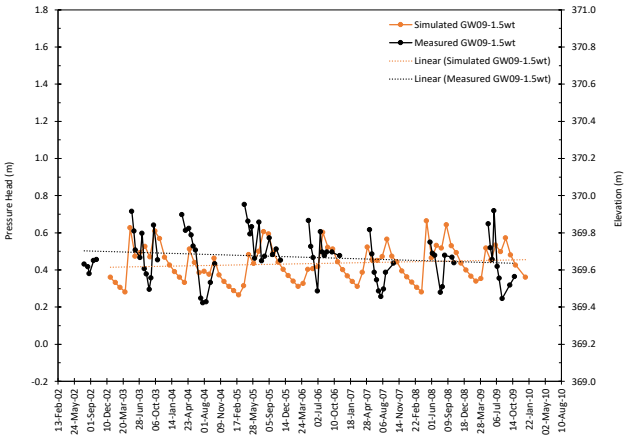

GW10-2.5wt, Slope C, ADTW 1.376 m

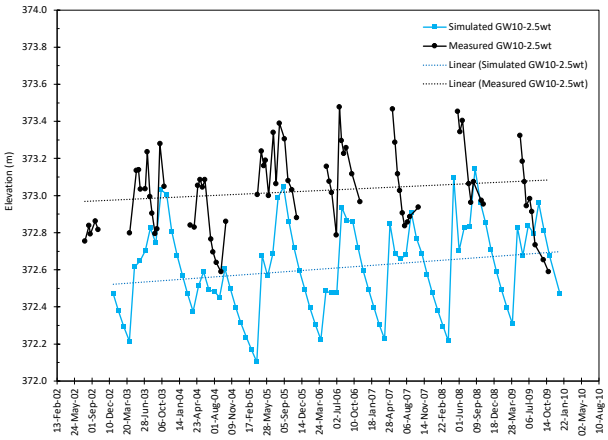

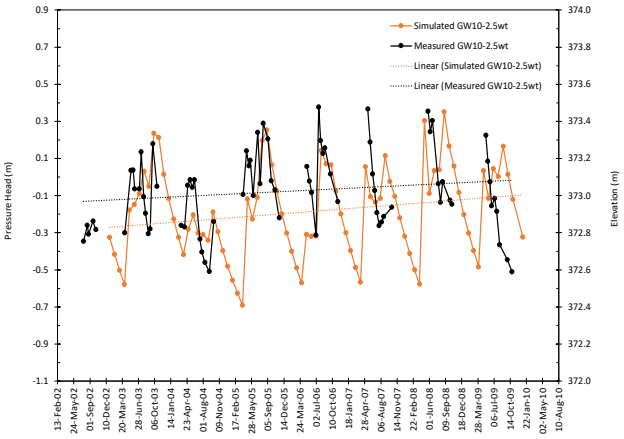

GW11-4wt, Bench C, ADTW 2.912 m

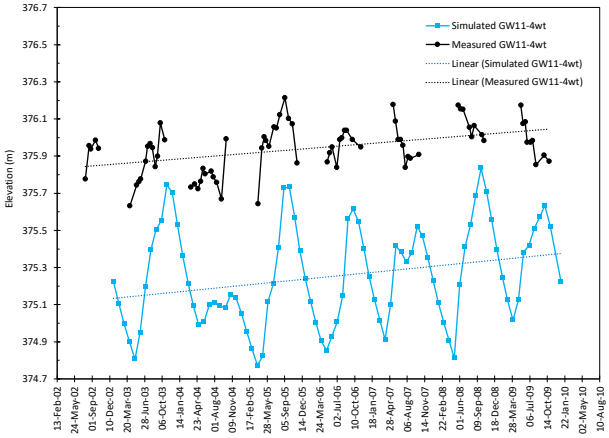

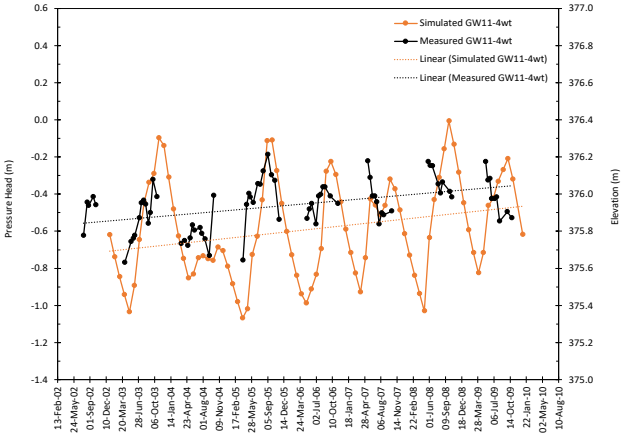

GW12-1.5wt, Bench C, ADTW 0.891 m

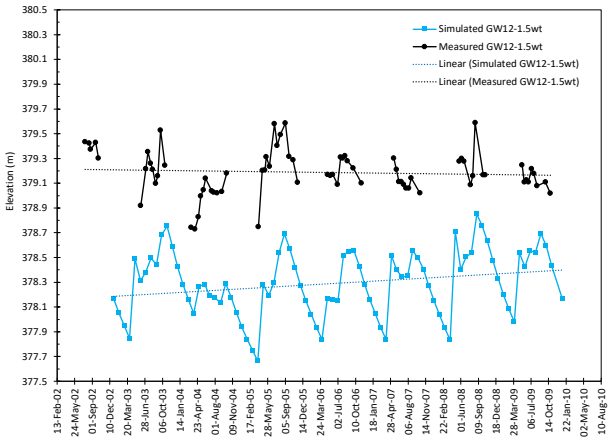

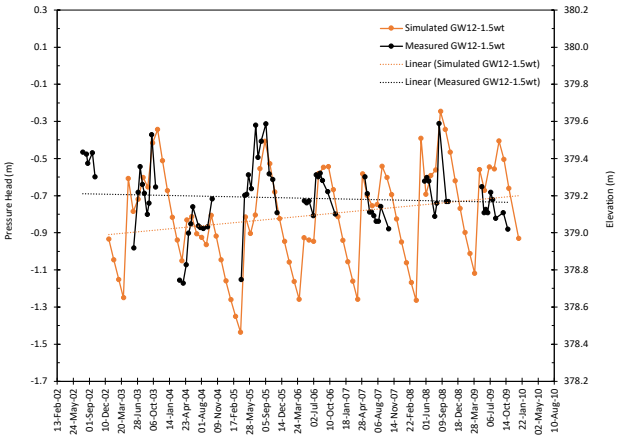

GW13-2.5wt, Bench C, ADTW 1.007 m

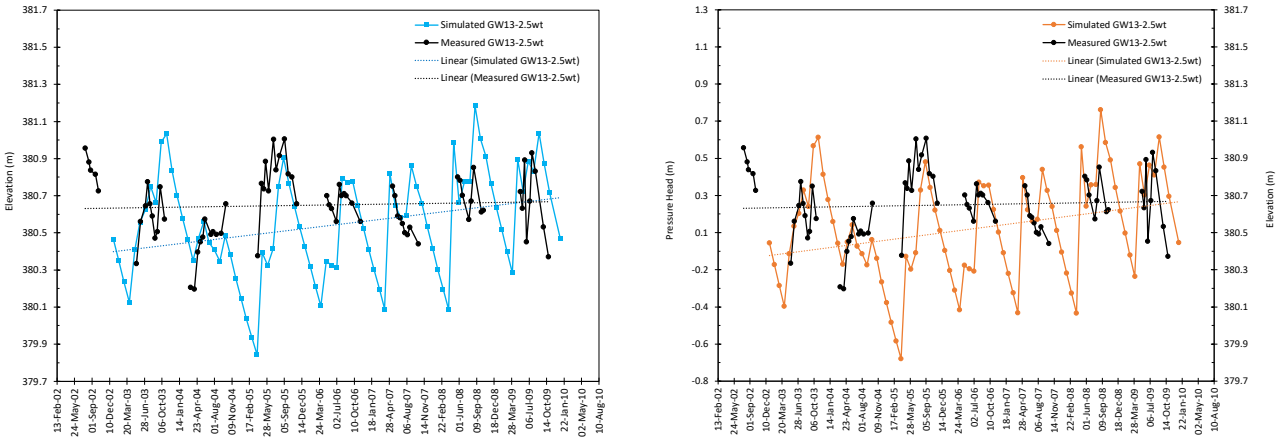

GW15-6.8wt, Bench D, ADTW 4.958 m

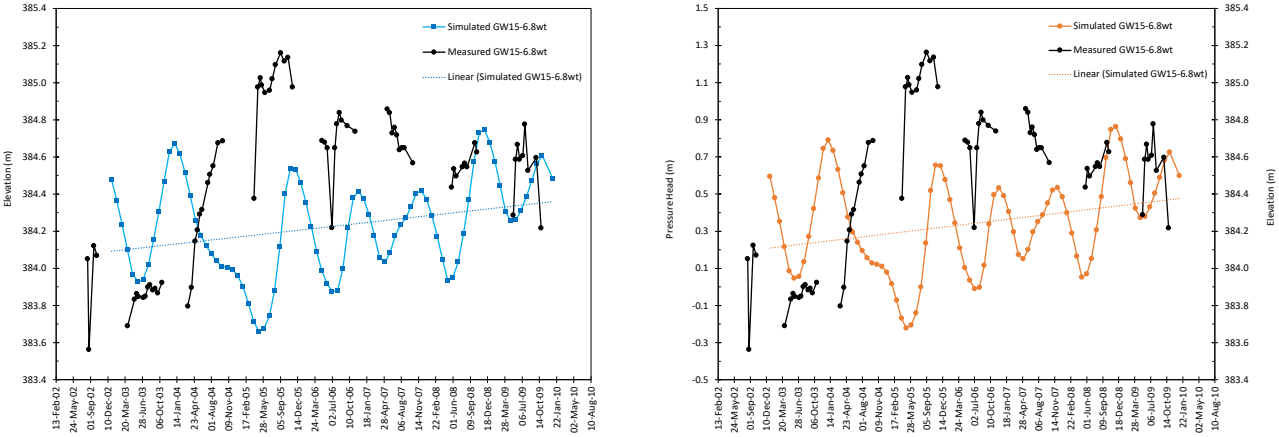

Table E1. Average measured depth to groundwater, 2003 to 2009

Depth	< 1 m	1 to 4 m		4 to 5 m
Well ID	GW1-1.5wt	GW2-2.5wt	GW6-3.8wt	GW7-5wt
	GW9-1.5wt	GW3-3wt	GW8-2.5wt	GW15-6.8wt
	GW12-1.5wt	GW4-1.75wt	GW10-2.5wt	
		GW5-2.2wt	GW11-4wt	
		GW13-2.5wt		

All the simulated pressure heads were converted into geodetic elevations (NAD83) based on the elevation of a fixed reference point. This reference elevation was inserted into the mesh of the model as an observation point at the elevation of the groundwater on August 28, 2003. It did not differ significantly from the mid-screen elevation, which is more traditionally used (Table E2).

Table E2. Observation point elevations

Well ID	Observation point elevation
	m
GW01-1.5wt	353.06
GW02-2.5wt	355.76
GW03-3wt	358.39
GW04-1.75wt	359.53
GW05-2.2wt	360.79
GW06-3.8wt	362.61
GW07-5wt	365.29
GW08-2.5wt	369.49
GW09-1.5wt	369.49
GW10-2.5wt	372.79
GW11-4wt	375.84
GW12-1.5wt	379.10
GW13-2.5wt	380.47
GW15-6.8wt	383.88

Table E3. Comparison of the measured and simulated groundwater elevations trends over the calibration period. The magnitude of the slope give next to the description. Color code: Pink – mismatched trends; Orange – trends in the same direction; Green – matched trends.

Well ID	Measured Trend	Simulated Trend
GW1-1.5wt	Decreasing 10^{-5}	Decreasing 10^{-6}
GW2-2.5wt	Decreasing 10^{-5}	Decreasing 10^{-6}
GW3-3wt	Decreasing 10^{-5}	Increasing 10^{-6}
GW4-1.75wt	Decreasing 10^{-5}	Decreasing 10^{-6}
GW5-2.2wt	Decreasing 10^{-5}	Decreasing 10^{-6}
GW6-3.8wt	Increasing 10^{-6}	Increasing 10^{-6}
GW7-5wt	Increasing 10^{-4}	Increasing 10^{-5}
GW8-2.5wt	Decreasing 10^{-5}	Increasing 10^{-5}
GW9-1.5wt	Decreasing 10^{-5}	Increasing 10^{-5}
GW10-2.5wt	Increasing 10^{-5}	Increasing 10^{-5}
GW11-4wt	Increasing 10^{-5}	Increasing 10^{-5}
GW12-1.5wt	Decreasing 10^{-5}	Increasing 10^{-5}
GW13-2.5wt	Increasing 10^{-5}	Increasing 10^{-4}
GW15-6.8wt	None	Increasing 10^{-4}

APPENDIX F – FUTURE FLOW AND TRANSPORT DATA TABLES

Table F1. Future I TDS concentration g/m^2 at Seepage Boundaries

Date	Toe C Trans	Toe B Trans	Toe A Trans	PD Trans	Toe C SS	Toe B SS	Toe A SS	PD SS
July 24, 2004	3064.1	2814.4	15132.1	2732.0	2974.9	2819.0	15602.4	2735.7
February 14, 2006	2774.9	2713.9	14740.1	2622.4	2823.4	2766.4	15027.5	2635.4
September 7, 2007	2763.9	2746.8	14502.6	2516.6	2672.0	2771.4	14336.4	2524.2
March 31, 2009	3303.1	3025.1	17704.2	2381.6	2532.9	2767.6	13559.6	2393.3
October 22, 2010	2490.6	2710.7	13070.4	2266.1	2403.8	2733.8	12880.7	2266.0
May 14, 2012	2374.4	2703.0	10856.1	2174.1	2284.6	2674.9	12385.3	2169.2
December 6, 2013	2143.9	2573.9	12047.0	2109.2	2174.1	2602.2	12067.3	2104.7
June 29, 2015	2144.4	2534.4	11239.6	2076.6	2072.3	2523.2	11847.1	2061.7
January 19, 2017	1946.0	2417.6	11586.5	2036.3	1977.9	2440.5	11657.5	2027.6
August 13, 2018	1959.3	2372.7	11488.3	2009.7	1892.2	2359.0	11449.5	1993.5
March 5, 2020	1774.1	2255.5	11097.1	1965.8	1812.8	2276.3	11204.9	1954.1
September 26, 2021	1804.7	2200.8	11202.3	1925.9	1740.7	2196.0	10923.5	1907.5
April 20, 2023	1768.8	2177.4	9188.8	1872.7	1673.7	2117.1	10617.7	1855.5
November 10, 2024	1607.7	2037.0	10416.7	1820.3	1611.6	2040.6	10287.5	1799.9
June 3, 2026	1613.2	1992.5	9191.4	1771.9	1554.5	1966.7	9957.2	1742.7
December 26, 2027	1479.7	1888.5	9694.3	1708.0	1501.1	1896.5	9620.8	1684.8
July 18, 2029	1504.1	1849.0	9172.5	1656.4	1451.5	1828.8	9284.4	1626.7
February 8, 2031	1380.2	1755.0	8967.4	1593.6	1404.3	1764.9	8960.2	1569.7
August 31, 2032	1410.8	1712.2	8934.9	1542.5	1359.6	1703.4	8642.2	1514.0
March 25, 2034	1737.7	1825.9	11219.7	1484.3	1317.4	1645.8	8330.3	1459.8
October 16, 2035	1326.5	1598.4	8304.0	1433.6	1276.4	1591.9	8036.7	1407.9
May 8, 2037	1289.8	1573.2	6928.9	1383.6	1237.8	1540.5	7749.2	1358.0
November 30, 2038	1187.1	1489.3	7583.9	1332.8	1200.3	1490.3	7480.1	1310.5
June 22, 2040	1208.2	1464.1	6940.9	1292.7	1164.1	1444.0	7223.2	1265.1
January 13, 2042	1113.7	1394.2	7026.1	1243.2	1129.3	1398.8	6978.6	1222.1
August 7, 2043	1137.6	1373.4	6848.9	1206.2	1095.5	1356.2	6746.2	1181.2
February 27, 2045	1042.5	1308.0	6536.0	1163.0	1062.8	1314.9	6526.0	1142.5
September 20, 2046	1072.1	1282.8	6548.2	1128.9	1031.2	1274.8	6318.0	1105.6
April 13, 2048	1060.7	1277.3	5311.9	1090.8	1000.5	1237.0	6116.2	1070.5
November 4, 2049	970.4	1201.9	6045.6	1057.0	970.8	1200.2	5927.2	1036.8
May 28, 2051	979.8	1184.6	5327.5	1026.8	941.9	1164.5	5744.3	1004.7
December 19, 2052	902.8	1128.9	5635.9	991.8	914.0	1130.0	5568.8	973.8
July 12, 2054	921.8	1111.7	5367.0	966.6	886.8	1096.6	5400.0	944.2
February 2, 2056	847.3	1061.1	5262.6	933.4	860.3	1064.2	5237.3	915.7
August 25, 2057	868.4	1040.8	5270.2	908.1	834.6	1032.8	5080.7	888.3
March 19, 2059	1071.1	1116.8	6653.4	879.1	809.7	1002.3	4929.1	861.8
October 9, 2060	817.9	979.4	4959.6	854.2	785.4	972.7	4782.9	836.1
May 2, 2062	796.6	966.5	4162.0	829.4	761.9	944.0	4641.0	811.4
November 24, 2063	732.7	917.0	4581.2	804.2	738.9	916.0	4504.0	787.4
June 16, 2065	745.9	903.4	4212.0	783.2	716.7	888.8	4370.6	764.1
January 7, 2067	687.4	861.9	4280.9	756.3	695.1	862.4	4241.6	741.5
July 31, 2068	702.1	849.3	4189.3	736.6	674.0	836.8	4116.2	719.6
February 21, 2070	643.2	810.1	4013.3	713.2	653.6	811.9	3994.5	698.3
September 14, 2071	660.9	794.7	4023.3	693.2	633.7	787.5	3875.8	677.7
April 7, 2073	653.6	790.2	3280.7	672.4	614.5	764.0	3761.5	657.6
October 29, 2074	597.7	744.2	3728.4	651.8	595.9	741.0	3649.5	638.0
May 21, 2076	603.0	732.8	3296.0	634.8	577.8	718.7	3540.7	619.0
December 13, 2077	555.3	698.6	3487.1	613.5	560.2	697.2	3435.5	600.6
July 6, 2079	566.6	687.0	3322.0	597.6	543.3	676.1	3332.7	582.6
January 26, 2081	520.4	655.8	3257.3	577.4	526.8	655.8	3233.0	565.3
August 19, 2082	533.3	642.8	3259.4	561.9	510.9	636.0	3135.8	548.4
March 12, 2084	658.0	689.2	4115.8	543.8	495.5	616.7	3041.6	531.9
October 3, 2085	502.1	604.3	3064.6	528.2	480.6	598.1	2950.5	516.0
April 26, 2087	489.0	596.1	2569.8	512.7	466.2	580.1	2861.2	500.4
November 17, 2088	449.9	565.1	2829.5	496.6	452.3	562.5	2774.9	485.3
June 10, 2090	458.3	555.5	2607.0	483.7	438.8	545.6	2691.7	470.6
January 1, 2092	422.5	530.6	2644.9	467.4	425.8	529.2	2610.4	456.4
July 25, 2093	431.7	522.8	2588.5	454.8	413.2	513.4	2531.5	442.6
February 15, 2095	395.9	498.5	2473.8	440.0	401.2	498.0	2455.0	429.4
September 7, 2096	407.4	488.7	2479.6	427.2	389.4	483.2	2381.0	416.5
April 1, 2098	403.3	486.4	2022.8	414.0	378.1	468.8	2309.5	403.9
October 23, 2099	369.1	458.1	2297.0	401.6	367.1	454.9	2240.4	391.7
May 16, 2101	373.2	451.5	2030.3	390.6	356.6	441.5	2173.1	379.9

Table F1. Cont.

December 8, 2102	344.3	430.7	2146.7	377.8	346.5	428.6	2108.3	368.6
June 30, 2104	352.0	424.4	2042.3	368.0	336.7	416.0	2045.3	357.7
January 21, 2106	324.2	405.3	2006.2	355.6	327.2	404.0	1984.1	346.9
August 14, 2107	332.9	397.6	2007.6	346.1	318.1	392.3	1925.4	336.7
March 7, 2109	411.5	427.6	2538.9	335.0	309.3	381.0	1869.1	326.6
September 28, 2110	314.9	374.9	1890.5	325.7	300.7	370.1	1814.1	317.1
April 20, 2112	307.4	370.4	1588.2	316.5	292.5	359.6	1760.9	307.8
November 12, 2113	283.7	352.0	1748.3	306.7	284.6	349.5	1710.1	298.9
June 5, 2115	289.7	347.2	1609.8	299.0	276.9	339.7	1660.6	290.2
December 26, 2116	267.9	331.9	1638.7	289.3	269.6	330.3	1612.8	281.8
July 20, 2118	274.7	327.5	1606.2	282.2	262.4	321.1	1566.4	273.8
February 10, 2120	252.6	313.3	1537.4	273.1	255.5	312.4	1522.3	266.0
September 2, 2121	260.7	308.1	1544.9	266.0	248.8	303.8	1478.9	258.5
March 27, 2123	258.8	307.8	1262.3	258.0	242.4	295.6	1437.9	251.2
October 17, 2124	237.8	290.3	1436.5	251.0	236.2	287.7	1397.6	244.2
May 10, 2126	241.1	286.9	1273.5	244.8	230.1	280.0	1359.0	237.4
December 2, 2127	223.1	274.4	1350.1	237.3	224.2	272.6	1321.7	230.9
June 24, 2129	228.9	271.2	1286.6	231.7	218.6	265.5	1285.6	224.6
January 15, 2131	211.3	259.8	1267.0	224.5	213.2	258.6	1250.8	218.5
August 7, 2132	217.8	255.8	1273.4	219.2	208.0	251.9	1217.1	212.6
March 1, 2134	270.0	275.4	1611.9	212.7	202.9	245.4	1184.7	206.9
September 22, 2135	207.4	242.6	1204.7	207.3	197.9	239.2	1153.5	201.5
April 14, 2137	203.2	240.4	1011.8	202.0	193.1	233.1	1123.5	196.1
November 6, 2138	188.0	229.1	1120.8	196.5	188.5	227.2	1094.2	190.9
May 29, 2140	192.6	226.7	1034.8	192.2	184.0	221.6	1065.4	186.1
December 20, 2141	178.6	217.5	1056.4	186.3	179.5	216.2	1038.5	181.2
July 14, 2143	183.7	215.4	1038.1	182.1	175.3	210.8	1011.6	176.6
February 3, 2145	169.4	206.5	997.2	176.9	171.2	205.8	986.5	172.2
August 27, 2146	175.4	203.7	1006.5	173.0	167.2	200.8	961.5	167.8
March 20, 2148	174.6	203.8	822.7	168.4	163.4	195.9	937.6	163.6
October 11, 2149	160.9	193.2	941.1	164.2	159.7	191.3	914.4	159.6
May 4, 2151	163.6	191.5	836.1	160.6	156.1	186.8	891.7	155.7
November 25, 2152	151.8	183.7	889.3	156.2	152.5	182.4	870.3	151.9
June 18, 2154	156.1	182.0	851.0	153.0	149.1	178.1	849.5	148.2
January 9, 2156	144.6	174.8	839.9	148.7	145.8	174.0	828.7	144.6
August 1, 2157	149.3	172.6	846.4	145.5	142.5	170.0	809.2	141.2
February 23, 2159	185.4	186.3	1074.3	141.7	139.4	166.1	790.2	137.8
September 15, 2160	143.0	164.7	806.3	138.7	136.3	162.3	771.3	134.6
April 8, 2162	140.3	163.6	680.9	135.5	133.3	158.7	753.5	131.4
October 31, 2163	130.1	156.4	753.7	132.0	130.5	155.1	735.8	128.4
May 23, 2165	133.7	155.1	698.0	129.5	127.6	151.7	718.7	125.4
December 14, 2166	124.2	149.1	714.3	125.9	124.9	148.3	702.8	122.5
July 7, 2168	128.0	148.2	703.7	123.5	122.2	145.0	686.2	119.7
January 28, 2170	118.3	142.4	678.3	120.2	119.6	141.9	670.9	117.0
August 21, 2171	122.7	140.7	686.3	117.8	117.1	138.8	655.7	114.4
March 14, 2173	122.4	141.5	562.1	115.0	114.6	135.7	641.0	111.8
October 5, 2174	113.0	134.1	645.1	112.5	112.2	132.9	626.9	109.3
April 27, 2176	115.2	133.1	574.9	110.3	109.9	130.0	612.8	106.9
November 19, 2177	107.1	128.1	612.8	107.5	107.6	127.2	599.7	104.6
June 12, 2179	110.4	127.2	587.4	105.6	105.4	124.5	586.6	102.3
January 2, 2181	102.4	122.5	581.5	102.8	103.2	121.8	573.8	100.0
July 26, 2182	105.9	121.2	586.9	100.9	101.1	119.3	561.5	97.9
February 17, 2184	131.8	131.1	747.3	98.4	99.0	116.8	549.4	95.8
September 9, 2185	101.7	116.0	561.7	96.5	97.0	114.4	537.7	93.7
April 2, 2187	100.0	115.5	476.7	94.5	95.1	112.0	526.2	91.7
October 24, 2188	92.9	110.6	528.1	92.5	93.1	109.7	515.1	89.8
May 17, 2190	95.6	109.8	491.1	90.8	91.3	107.4	504.3	87.9
December 8, 2191	89.0	105.9	502.3	88.5	89.5	105.2	493.7	86.0
July 1, 2193	91.8	105.2	496.6	86.9	87.7	103.1	483.4	84.2
January 22, 2195	85.0	101.4	478.7	84.8	85.9	101.0	473.4	82.5
August 14, 2196	88.3	100.4	485.1	83.3	84.2	99.0	463.6	80.8
March 8, 2198	88.3	100.9	401.2	81.4	82.6	97.0	454.1	79.1
September 29, 2199	81.6	95.9	457.7	79.8	81.0	95.0	444.8	77.5
April 22, 2201	83.2	95.5	408.1	78.4	79.4	93.1	435.7	75.9
November 14, 2202	77.5	92.0	435.9	76.5	77.8	91.3	426.9	74.4

APPENDIX G – FUTURE FLOW AND TRANSPORT RESULTS FIGURES

This section summarizes the pressure head distribution figures, the TDS distribution figures, the TDS concentration curves at seepage boundaries and the cumulative TDS charts for the future flow and transport simulations.

Figure G1. Future pressure heads (m) at 10, 25 and 50 years' time, transient boundary condition

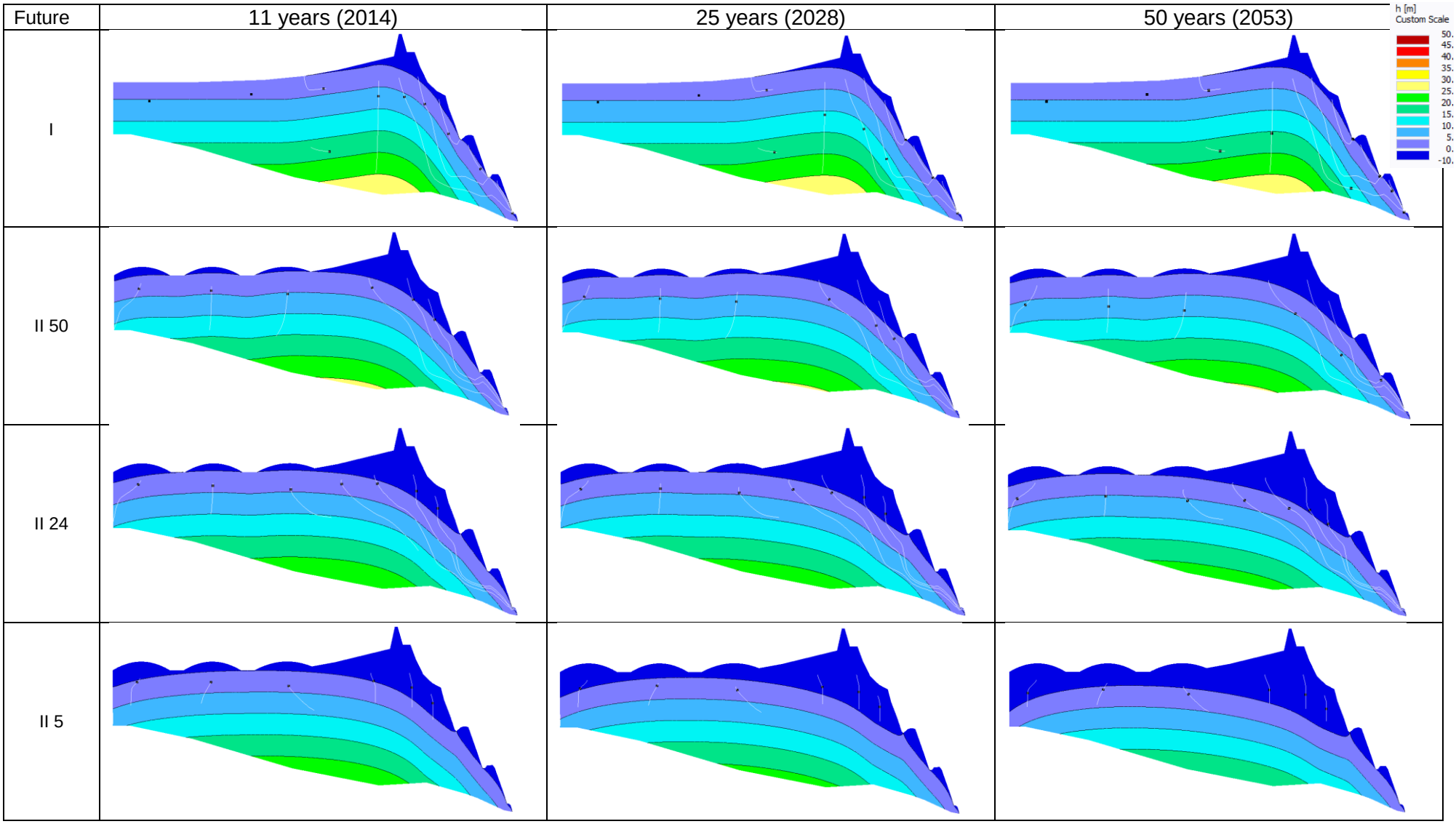

Figure G2. Future pressure heads (m) at 75, 100 years, and 200 years' time, transient boundary condition

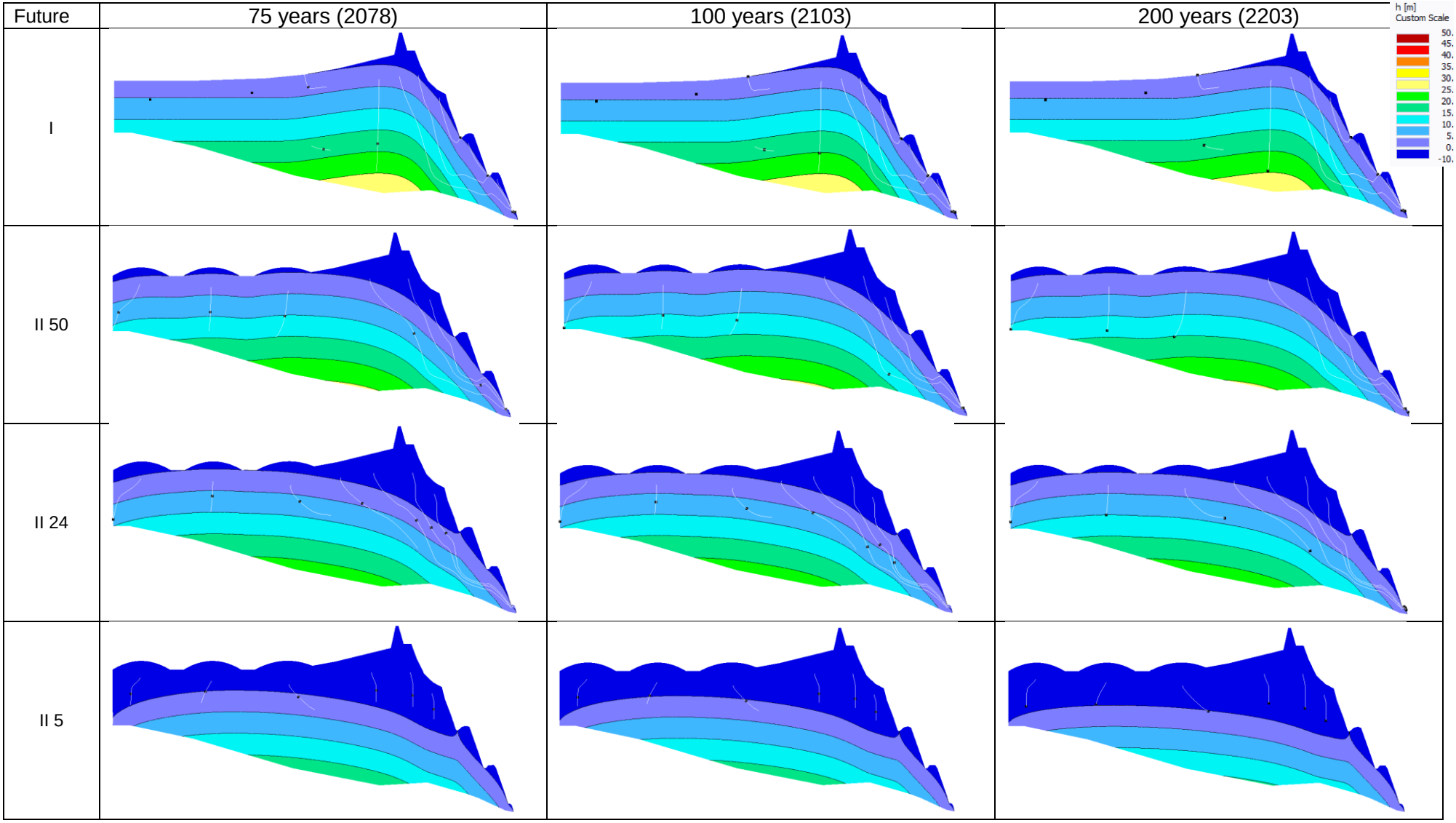

Figure G2. Future TDS distributions (g/m^3) at 11, 25, and 50 years' time, transient boundary condition

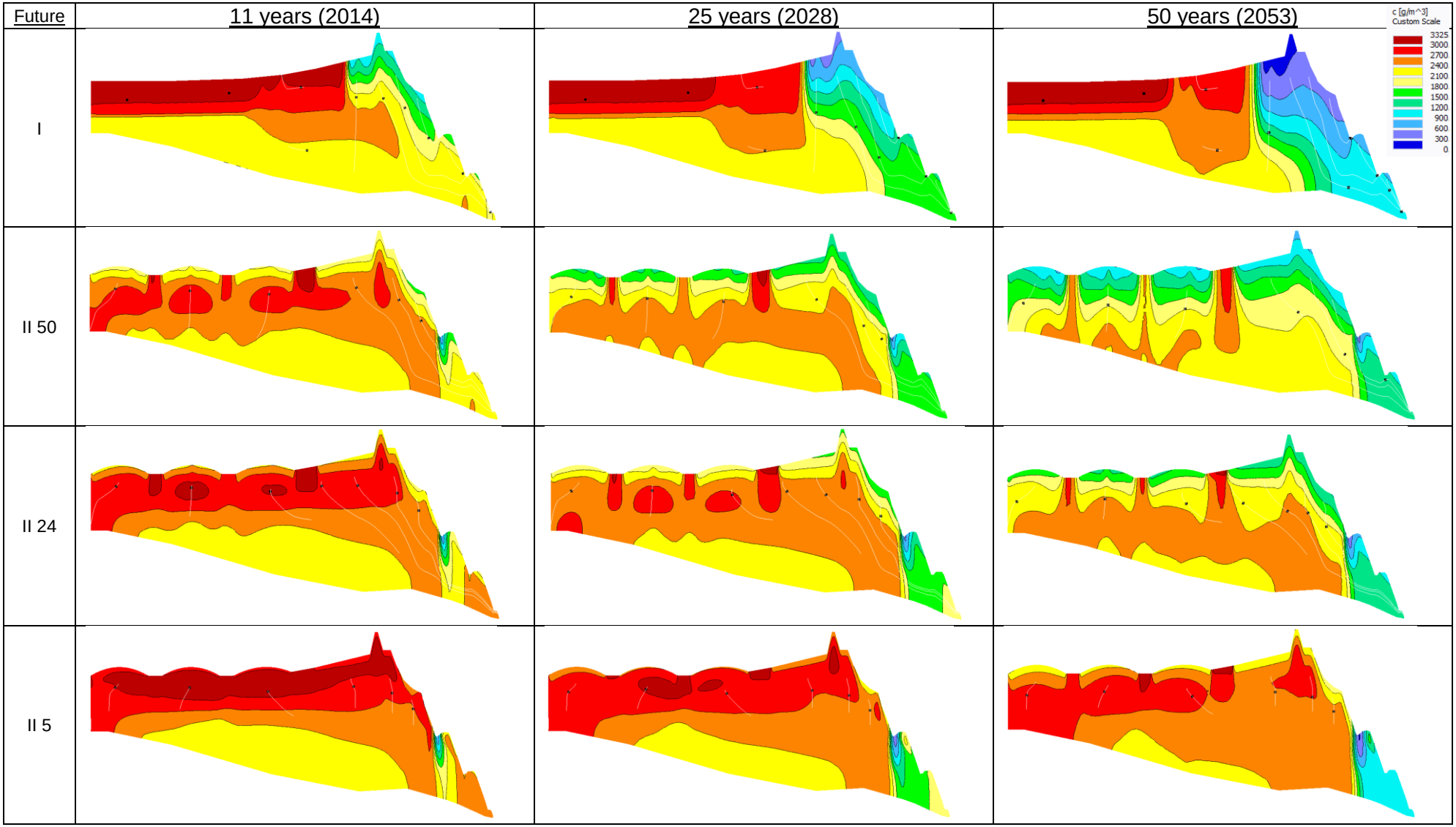

Figure G2. Future TDS distributions (g/m^3) at 75, 100, and 200 years' time, transient boundary condition

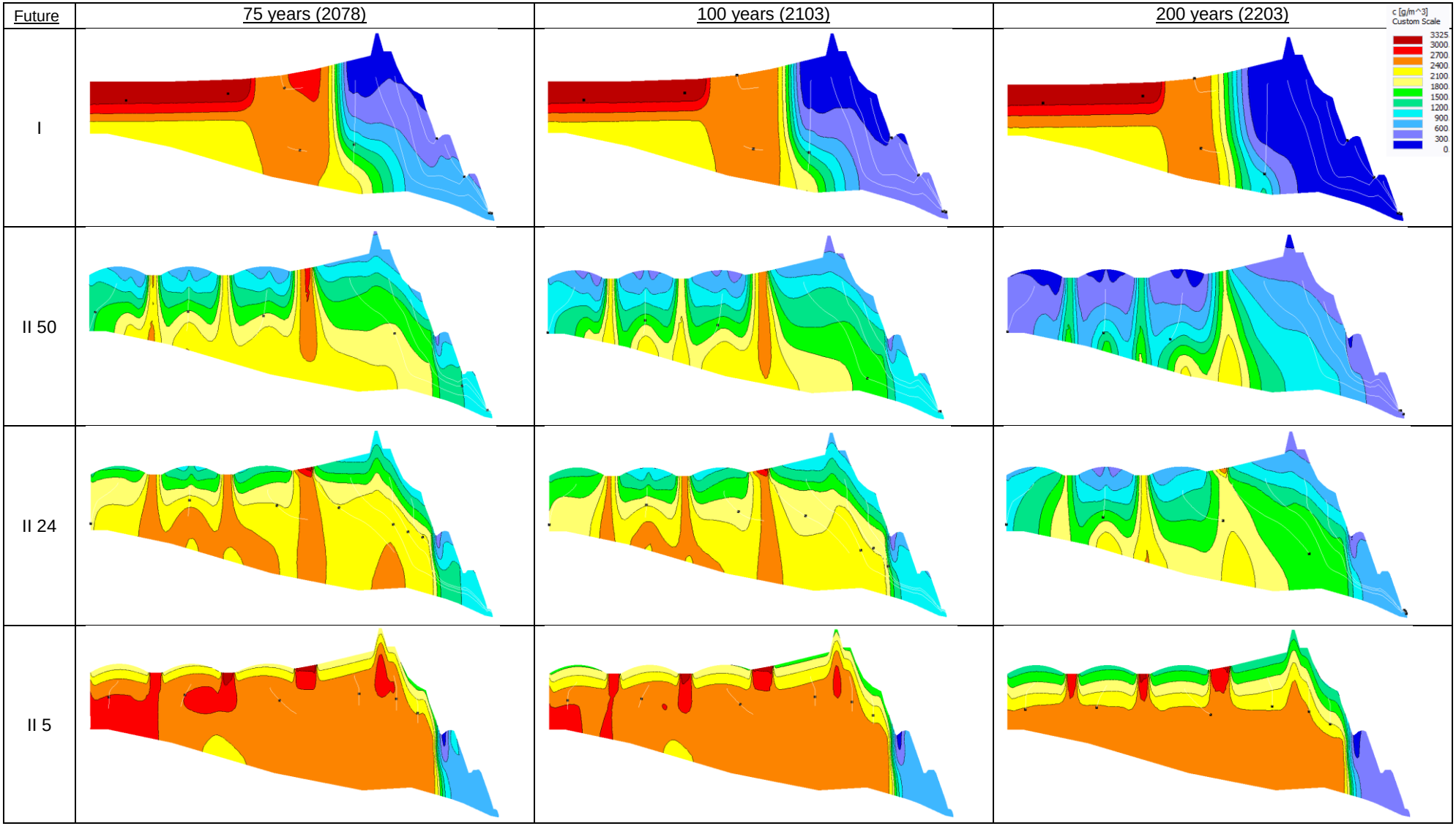

Appendix H

Piezometer Location Plan with Photographs

SWSS Cell 31 Transect
Piezometer Nests

N

L 2007

M 2008

F 2007

B 2007

N 2006

G 2008

H 2008

I 2008

Perimeter Ditch

355

370

380

Sand Bench

Slope A

Bench A

Slope B

Bench B

Slope C

Bench C

Slope D

Bench D

Slope E

SG01

GW 32

GW 30

GW 01

GW 27

GW 02

GW 03

GW 25

GW 26

GW 04

GW 05

GW 24

GW 06

GW 07

GW 08

GW 28

GW 09

GW 29

GW 33

GW 10

GW 11

GW 12

GW 13

GW 15

SG03

SG02

A

B

C

D

E

F

G

H

I

J

K

L

M

N

A 2006

C 2007

D 2008

E 2008

J 2008

K 2008

contour interval =1m

Piezometer Cell 31
Staff Gague
Met Station
Photo direction & year

0 25 50 100 Meters

M. Goddard, 2017. Evaluation of cover options and climate change scenarios for a large undrained sand tailings dam in northern Alberta, Canada. Universiteit Utrecht MSc. Photograph credits C. Mendoza, pers. comm., 2016.